Organic chemistry around young high-mass stars

Allen, Veronica Amber

Chapter 2

Chemical segregation in hot cores with disk candidates

V. Allen, F. F. S. van der Tak, Á. Sánchez-Monge, R. Cesaroni, M. T. Beltrán (A&A 603, A133, 2017)

Abstract

Context: In the study of high-mass star formation, hot cores are empirically defined stages where chemically rich emission is detected toward a massive YSO. It is unknown whether the physical origin of this emission is a disk, inner envelope, or outflow cavity wall and whether the hot core stage is common to all massive stars.
Aims: We investigate the chemical makeup of several hot molecular cores to determine physical and chemical structure. We use high spectral and spatial resolution submillimeter observations to determine how this stage fits into the formation sequence of a high-mass star.
Methods: The submillimeter interferometer ALMA (Atacama Large Millimeter Array) was used to observe the G35.20-0.74N and G35.03+0.35 hot cores at 350 GHz in Cycle 0. We analyzed spectra and maps from four continuum peaks (A, B1, B2 and B3) in G35.20-0.74N, separated by 1000-2000 AU, and one continuum peak in G35.03+0.35. We made all possible line identifications across 8 GHz of spectral windows of molecular emission lines down to a 3σ line flux of 0.5 K and determined column densities and temperatures for as many as 35 species assuming local ther-

modynamic equilibrium (LTE).
Results: In comparing the spectra of the four continuum peaks, we find each has a distinct chemical composition expressed in over 400 different transitions. In G35.20, B1 and B2 contain oxygen- and sulfur-bearing organic and inorganic species but few nitrogen-bearing species whereas A and B3 are strong sources of O-, S-, and N-bearing organic and inorganic species (especially those with the CN bond). Column densities of vibrationally excited states are observed to be equal to or greater than the ground state for a number of species. Deuterated methyl cyanide is clearly detected in A and B3 with D/H ratios of 8 and 13%, respectively, but is much weaker at B1 and undetected at B2. No deuterated species are detected in G35.03, but similar molecular abundances to G35.20 were found in other species. We also find co-spatial emission of isocyanic acid (HNCO) and formamide (NH_2CHO) in both sources indicating a strong chemical link between the two species.
Conclusions: The chemical segregation between N-bearing organic species and others in G35.20 suggests the presence of multiple protostars surrounded by a disk or torus.

2.1 Introduction

Studying the formation of high-mass stars (> 8 $M_\odot$) is important because they drive the chemical evolution of their host galaxies by injecting energy, through UV radiation, strong stellar winds, and supernovae, and heavy elements into their surroundings (Zinnecker & Yorke 2007). In the study of high-mass star formation, several models have been proposed to explain the earliest processes involved. In particular, the work of McKee & Tan (2003) describes a process similar to that of low-mass stars including a turbulent accretion disk and bipolar outflows (see also Tan et al. (2014)), the model by Bonnell and Smith (2011) proposes that matter is gathered competitively from low-turbulence surroundings between many low-mass protostars funneling more material to the most massive core, and the model by Keto (2007) uses gravitationally trapped hypercompact HII regions to help a massive protostar to acquire more mass. All of these models predict the existence of disks as a mechanism to allow matter to accrete onto the protostar despite high radiation pressure (Krumholz et al. 2009). However, until recently only a few candidate disks around B-type protostars were known. Several disks have been detected through the study of complex organic molecules (COMs), molecular species bearing carbon and at least six atoms, allowing for the detection of more disks (Cesaroni et al. 2006; Kraus et al. 2010; Beltrán & de Wit 2016).

While the earliest stages of high-mass star formation have not yet been clearly determined, it is well known that a chemically rich stage exists, known as a hot molecular core (HMC; see Tan et al. (2014) for a review of high-mass star formation). In this stage COMs are released from the icy surfaces of dust grains or formed in the hot circumstellar gas (Herbst & van Dishoeck 2009). These hot cores are dense ($n_H > 10^7$ cm^{-3}), warm (100-500 K), and compact (< 0.05 pc) and are expected to last up to 10^5 years. The signpost of the hot core stage is a rich molecular emission spectrum including many COMs like methanol (CH_3OH) and methyl cyanide (CH_3CN). These species may be formed on dust grain surfaces in a cooler place (or time) and released from grain surfaces as the forming star heats the grains. Alternatively, they may form in the hot gas surrounding these massive young objects as the higher temperature allows for endothermic reactions to take place more

readily. In reality, it is likely that both formation paths are necessary to achieve the molecular abundances seen around hot cores. High spatial and spectral resolution observations can help us to disentangle the different COMs and their spatial distribution during this phase. Disks candidates have been discovered in a few HMC sources, suggesting a link between disks and HMC chemistry. Studying the chemistry of such regions can help us to understand the process of high-mass star formation as chemical differences across small physical scales provide clues to the different evolutionary stages involved.

With the advent of the Atacama Large Millimeter Array (ALMA), it is now possible to make highly sensitive, high spectral, and spatial resolution observations of less abundant molecular species. The search continues for the precursors of life, such as the simplest amino acid, glycine (H_2NCH_2COOH), but complex organic species with up to 12 atoms have already been detected[1]. These include important precursors to amino acids, such as aminoacetonitrile (H_2NCH_2CN), detected by Belloche et al. (2008); the simplest monosaccharide sugar glycolaldehyde (CH_2OHCHO), first observed in a hot molecular core outside the Galactic center by Beltrán et al. (2009); and formamide (NH_2CHO) extensively studied by López-Sepulcre et al. (2015). With ALMA we have the ability to detect hot cores and study their properties in detail to determine how the spatial distribution of COMs influences the formation of massive stars. Despite advances in technology, astronomers have yet to determine whether the emission from the hot core arises from the inner envelope (spherical geometry) or from a circumstellar disk (flat geometry). It is also possible that these hot cores could be outflow cavity walls as has been recently modeled for low-mass stars by Drozdovskaya et al. (2015).

In this paper we study the chemical composition and spatial distribution of species in two high-mass star-forming regions, G35.20-0.74N and G35.03+0.35 (hereafter G35.20 and G35.03 respectively), which have been shown to be strong disk-bearing candidates. We present a line survey of the hot core in G35.03 and in four continuum peaks in the G35.20 hot core containing $\sim$ 18 different molecular species (plus 12 vibrationally excited states and 22 isotopologues) of up to 10 atoms and >400 emission lines per source. We also present our analysis of the chemical segregation

[1] https://www.astro.uni-koeln.de/cdms/molecules

within core B of G35.20 depicting a small-scale (<1000 AU) separation of nitrogen chemistry and temperature difference. A chemical separation on the scale of a few 1000s of AU within a star-forming region has been seen before in Orion KL (Caselli et al. 1993a), W3(OH) and W3(H_2O) (Wyrowski et al. 1999b), and AFGL2591 (Jiménez-Serra et al. 2012).

The distance to both sources has been estimated from parallax measurements to be 2.2 kpc for G35.20 (Zhang et al. 2009) and 2.32 kpc for G35.03 (Wu et al. 2014). G35.20 has a bolometric luminosity of 3.0×10^4 $L_\odot$ (Sánchez-Monge et al. 2014) and has been previously studied in Sánchez-Monge et al. (2013a) and Sánchez-Monge et al. (2014) in which they report the detection of a large (r∼2500 AU) Keplerian disk around core B and a tentative Keplerian disk in core A. The bolometric luminosity of G35.03 is 1.2×10^4 $L_\odot$ and was reported to have a Keplerian disk (r∼1400-2000 AU) around the hot core A in Beltrán et al. (2014).

Table 2.1: Source continuum characteristics

Continuum peak	Right ascension	Declination	Size[a] ($''$)	S_ν^b (Jy)	$T_{\rm kin}^c$ (K)	$N(H_2)$ [d] (cm^{-2})	Mass [e] ($M_\odot$)
G35.20 A	18:58:12.948	+01:40:37.419	0.58	0.65	285	2.4×10^{25}	13.0
G35.20 B1	18:58:13.030	+01:40:35.886	0.61	0.19	160	6.4×10^{24}	3.8
G35.20 B2	18:58:13.013	+01:40:36.649	0.65	0.12	120	3.3×10^{24}	2.2
G35.20 B3	18:58:13.057	+01:40:35.442	0.58	0.08	300	2.5×10^{24}	1.4
G35.03 A	18:54:00.645	+02:01:19.235	0.49	0.21	275	1.1×10^{25}	4.4

[a]: Deconvolved average diameter of the 50% contour of the 870 μm continuum.
[b]:Integrated flux density within the 10σ contour of the 870 μm continuum.
[c]:Average kinetic temperature based on CH_3CN line ratios as calculated using RADEX. For details, see § 2.3.3.
[d]:Calculated from source size, continuum flux density, and kinetic temperature (§ 2.3.3).
[e]:Sources mass calculated as in Sánchez-Monge et al. (2014) using the average kinetic temperatures.

2.2 Observations and methods

2.2.1 Observations

G35.20 and G35.03 were observed with ALMA in Cycle 0 between May and June 2012 (2011.0.00275.S). The sources were observed in Band 7 (350 GHz) with the 16 antennas of the array in the extended configuration (baselines in the range 36-400 m) providing sensitivity to structures

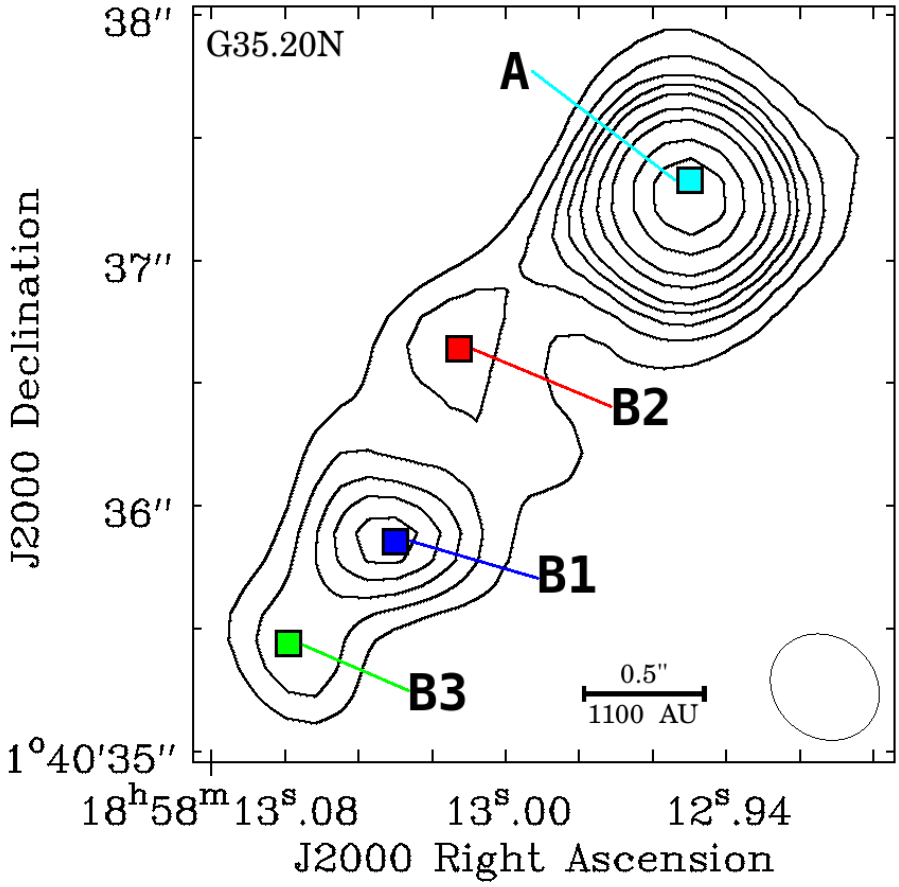

Figure 2.1: Image of the 870 μm continuum emission from Cycle 0 ALMA observations of G35.20. Contour levels are 0.03, 0.042, 0.055, 0.067, 0.08, 0.10, 0.13, 0.18, and 0.23 Jy/beam (σ = 1.8 mJy/beam). The pixel-sized colored squares indicate each of the spectral extraction points. Ellipse denotes the synthesized beam.

0.4″ - 2″. The digital correlator was configured in four spectral windows (with dual polarization) of 1875 MHz and 3840 channels each, providing a resolution of ∼0.4 km s^{-1}. The four spectral windows covered the frequency ranges [336 849.57-338 723.83] MHz, [334 965.73-336 839.99] MHz, [348 843.78-350 718.05] MHz, and [346 891.29-348 765.56] MHz. The rms noise of the continuum maps are 1.8 mJy/beam for G35.20 and 3 mJy/beam for G35.03. For full details, see Sánchez-Monge et al. (2014)

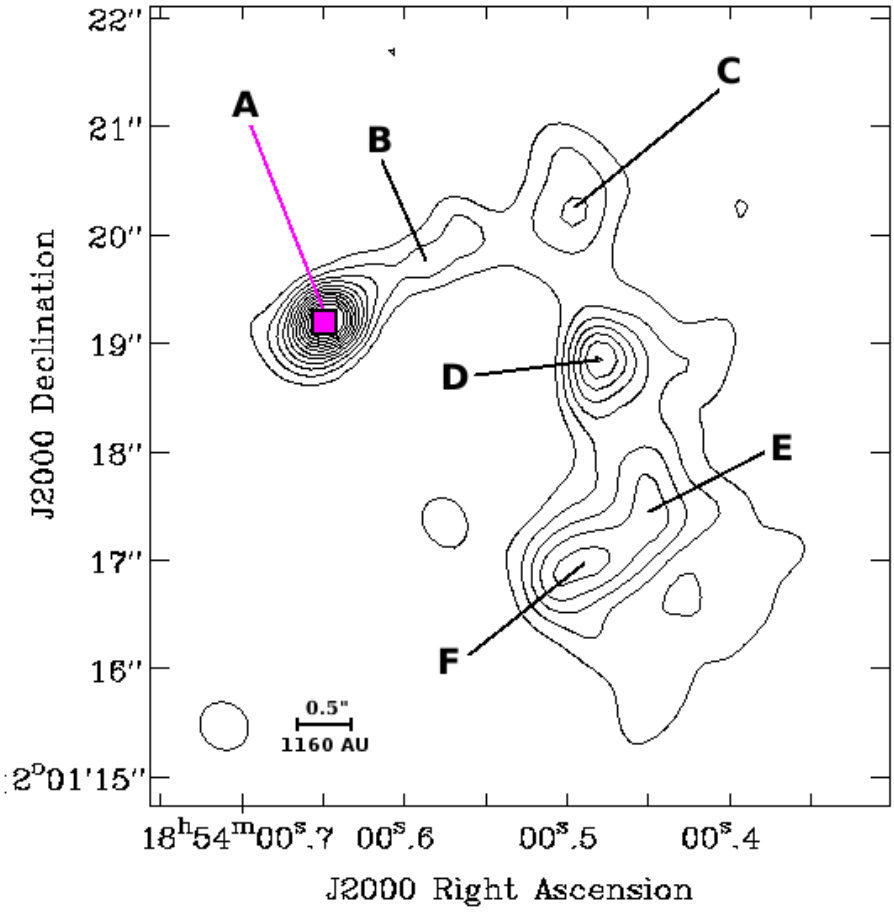

Figure 2.2: Image of the 870 μm continuum emission from Cycle 0 ALMA observations of G35.03. Contour levels are 8.6, 16.8, 24.9, 33, 41.2, 49.3, 57.4, 65.5, 73.6, 81.8, and 89.9 mJy/beam (σ = 3.0 mJy/beam). The pixel-sized colored square indicates the spectral extraction point. The cores identified in Beltrán et al. (2014) are labeled A-F. Ellipse denotes the synthesized beam.

and Beltrán et al. (2014).

2.2.2 Line identification process

Spectra were extracted from the central pixel of the continuum peak in core A and the three continuum peaks in core B (B1, B2, B3) in

G35.20 and the continuum peak in core A in G35.03 using CASA[2] (see Figures 2.1 and 2.2 for spectra extraction positions and continuum levels and Table 2.1 for the J2000 coordinates and a summary of statistics). The other peaks (B-F in G35.03 and C-G in G35.20) were not analyzed because they do not show hot core chemistry, i.e., little or no emission from COMs. The three continuum peaks in G35.20 B were chosen to investigate the chemical structure across the disk shown in Sánchez-Monge et al. (2014) (who analyzed B as a single core); however, the disk in G35.03 A only has a single continuum point associated with the hot core, so analysis for this source was from this peak. G35.20 A was analyzed as the strongest continuum source in the region with hot core chemistry and was also analyzed at the single continuum peak. Line parameters (listed in Appendix B) were determined using Gaussian profile fits to spectral lines from each continuum peak via Cassis[3], primarily using the Cologne Database for Molecular Spectroscopy (CDMS; Müller et al. (2001)) database and Jet Propulsion Laboratory (JPL; Pickett et al. (1998)) database for deuterated methanol (CH_2DOH), ethanol (C_2H_5OH), NH_2CHO, acetaldehyde (CH_3CHO), and CH_3OH (ν=2) transitions.

The process of identifying all species present in these spectra consisted of several parts. Bright lines ($T_B > 5$ K) from known species were identified first (i.e., those from Sánchez-Monge et al. (2014): CH_3OH, methyl formate (CH_3OCHO), CH_3CN, simple molecules) numbering ∼100 lines per source. The remaining bright lines (> 5 K) were identified by choosing the most likely molecular candidate, namely the transition with the higher Einstein coefficient that is limited to a minimum of about 10^{-7} s^{-1}, or with a upper level energy (E_{up}) within the expected range, generally less than 500 K, composed of C,H,O and/or N and within 2 km s^{-1} (∼2 MHz) of the rest frequency of the transition. This brings the total to about 200 per source. Finally, for any remaining unidentified lines > 3σ (∼ 0.5 K) a potential species was selected, then the entire spectrum was checked for nondetections of expected transitions of this species. The total number of identified lines was over 400 for each source, including partially blended and blended transitions for which it was ev-

[2]Common Astronomy Software Applications is available from http://casa.nrao.edu/

[3]CASSIS has been developed by IRAP-UPS/CNRS (http://cassis.irap.omp.eu).

Table 2.2: Line detections and measurements for H_2CS with errors in parentheses.

Transition	Frequency (MHz)	G35.20 A FWHM (km s^{-1})	G35.20 A T_{peak} (K)	G35.20 B1 FWHM (km s^{-1})	G35.20 B1 T_{peak} (K)	G35.20 B2 FWHM (km s^{-1})	G35.20 B2 T_{peak} (K)
H_2CS ν=0							
$10_{1,10}$-$9_{1,9}$	338083	5.9 (0.1)	51.7 (0.9)	2.7 (0.1)	27.3 (1.0)	2.4 (0.1)	28 (1)
$10_{1,9}$-$9_{1,8}$	348532	5.8 (0.1)	59.2 (1.3)	2.6 (0.1)	31 (1)	2.3 (0.1)	31 (1)
$H_2C^{33}S$							
$10_{1,10}$-$9_{1,9}$	335160	7.5 (0.2)	3.91 (0.09)	1.6 (0.5)	0.4 (0.1)	1.5 (0.6)	0.4 (0.2)
$H_2C^{34}S$							
$10_{0,10}$-$9_{0,9}$	337125	blended		1.2 (0.7)	0.7 (0.4)	1.5 (0.2)	1.0 (0.1)
$10_{4,6}$-$9_{4,5}$	337460	blended		in abs. feature		1.5 (0.4)	0.55 (0.09)
$10_{2,9}$-$9_{2,8}$	337475	6.3 (0.3)	16.0 (0.3)	1.66 (0.08)	3.8 (0.2)	1.7 (0.1)	3.8 (0.2)
$10_{3,8}$-$9_{3,7}$	337555	blended		2.0 (0.2)	0.78 (0.05)	1.7 (0.5)	0.6 (0.2)
$10_{3,7}$-$9_{3,6}$	337559	blended		2.16 (0.09)	1.55 (0.04)	1.3 (0.1)	0.54 (0.04)
$10_{2,8}$-$9_{2,7}$	337933	blended		1.2 (0.5)	0.8 (0.2)	1.8 (0.5)	0.7 (0.1)

Transition	Frequency (MHz)	G35.20 B3 FWHM (km s^{-1})	G35.20 B3 T_{peak} (K)	G35.03 A FWHM (km s^{-1})	G35.03 A T_{peak} (K)
H_2CS ν=0					
$10_{1,10}$-$9_{1,9}$	338083	2.54 (0.06)	44.3 (0.9)	6.6 (0.1)	21.0 (0.3)
$10_{1,9}$-$9_{1,8}$	348532	2.58 (0.04)	52.1 (0.7)	6.33 (0.09)	21.3 (0.3)
$H_2C^{33}S$					
$10_{1,10}$-$9_{1,9}$	335160	2.5 (0.2)	1.47 (0.08)	$< 3\sigma$	
$H_2C^{34}S$					
$10_{0,10}$-$9_{0,9}$	337125	1.9 (0.1)	2.5 (0.1)	$< 3\sigma$	
$10_{4,6}$-$9_{4,5}$	337460	blended		blended	
$10_{2,9}$-$9_{2,8}$	337475	3.1 (0.2)	4.9 (0.2)	blended	
$10_{3,8}$-$9_{3,7}$	337555	2.03 (0.04)	2.35 (0.03)	$< 3\sigma$	
$10_{3,7}$-$9_{3,6}$	337559	2.37 (0.06)	2.26 (0.03)	$< 3\sigma$	
$10_{2,8}$-$9_{2,7}$	337933	2.3 (0.1)	2.4 (0.1)	$< 3\sigma$	

ident or implied by the line shape that another transition was present. It is noted in Appendix 2.B if the line identity is uncertain in case of strong blending or multiple probable candidates.

The remaining total of unidentified and unclear identity (where there is more than one potential species) lines is about 80 for the peaks in B and G35.03 with an additional 30 in G35.20 A. These unknown transitions could be either species whose transitions for this frequency regime have not yet been measured/calculated or species whose likely identity was not clear. The peak intensities of the unknown lines were all less than 5 K. Line parameters were measured by fitting a Gaussian profile to the emission line with the Cassis line spectrum tool. In some cases, partially blended lines were fit together with one or more extra Gaussians

for a more accurate measurement, although in those cases the errors were larger. The full line survey can be found in Appendices A and B, but an example is given in Table 2.2, where the parameters obtained for thioformaldehyde (H_2CS) are listed. The line identities are first presented ordered by frequency, and then, to emphasize the chemistry of these objects, the tables of measured line parameters are sorted by molecular species.

To validate the line identifications, fits were made simultaneously to all identified species via the XCLASS software Möller et al. (2017)[4]. This program models the data by solving the radiative transfer equation for an isothermal object in one dimension, taking into account source size and dust attenuation. The residuals between the fitted lines and observed spectra are between 5 and 25%, validating the XCLASS fits and our line identifications. The observed spectra and the XCLASS fits can be found in Appendix 2.E and further information about the XCLASS analysis is detailed in § 2.3.4.

2.2.3 Image analysis

To confirm our identifications of several complex organic species, maps were made of unblended transitions. Similar spatial distributions and velocity profiles of transitions with similar upper energy levels are consistent with these being the same species. Figure 2.3 shows integrated intensity (moment zero) maps of CH_3OCHO ν=0 and ν=1 transitions, H_2CS, $(CH_2OH)_2$, CH_3CHO ν=0, and ν=2 transitions in G35.20 and Figure 2.4 shows the same transitions in G35.03. During this process, we discovered a difference in spatial extent between N-bearing species and O-bearing species in G35.20 core B. The N-bearing species peak at the location of continuum peak B3 and are generally not found at the other side of the disk near continuum peak B2. We comment on this difference in detail in § 2.4.2. Channel maps were made in CASA for 20 different species for interesting isolated lines with a range of upper energy levels (see Table 2.3) to determine the spatial distribution of various species. Zeroth (integrated intensity), first (velocity), and second (dispersion) moment maps were also made for these species. A selection of integrated intensity maps can be found in Figures 2.3 and 2.4.

[4]The software can be downloaded from here: https://xclass.astro.uni-koeln.de/

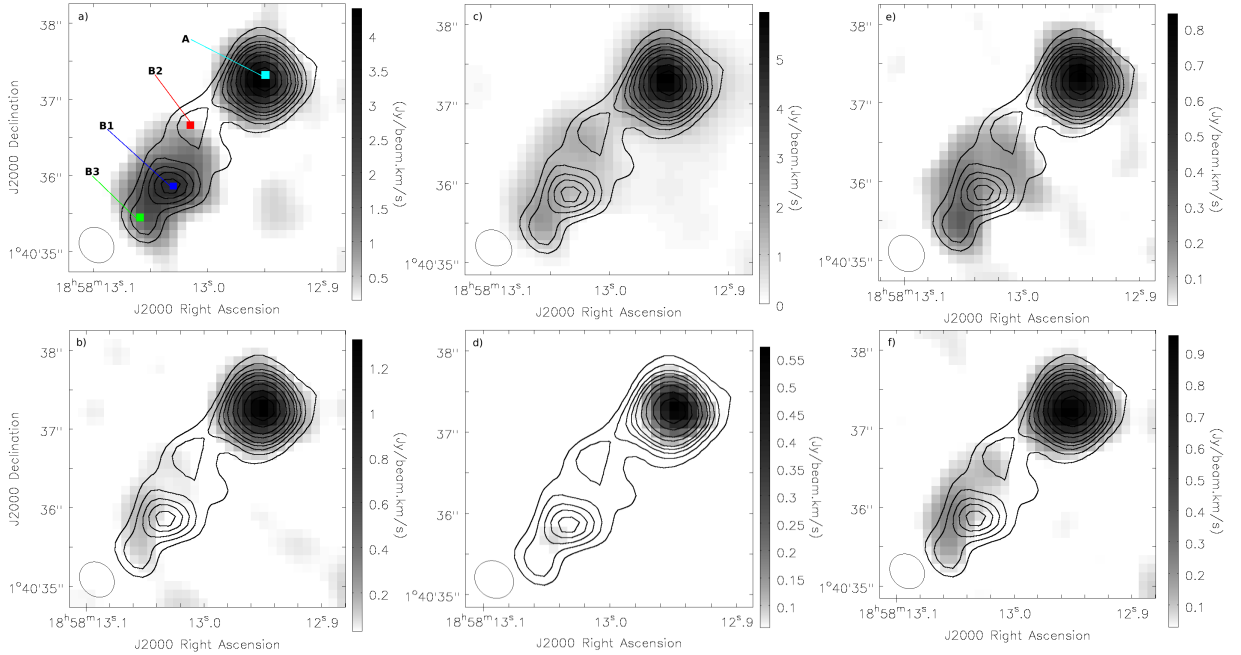

Figure 2.3: Integrated intensity maps of six species across G35.20, where the contours are the 870 μm continuum with the same levels as Figure 2.1. Panel a) shows the CH_3OCHO ν=0 emission at 336.086 GHz integrated from 18.5 to 38 km s^{-1}. Panel b) shows the CH_3OCHO ν=1 emission at 348.084 GHz integrated from 26 to 38.5 km s^{-1}. Panel c) shows the H_2CS emission at 338.083 GHz integrated from 24.5 to 38.5 km s^{-1}. Panel d) shows ethylene glycol ($(CH_2OH)_2$) emission at 335.030 GHz integrated from 25-36.5 km s^{-1}. Panel e) shows CH_3CHO ν=0 emission at 335.318 GHz integrated from 22.5 to 37 km s^{-1}. Panel f) shows CH_3CHO ν=2 emission at 349.752 GHz integrated from 24 to 29 km s^{-1}. It can clearly be seen between panels a) and b) and between e) and f) that vibrationally excited states have a much smaller emitting region. It is also clear in panel d) that $(CH_2OH)_2$ is only seen in core A. The ellipse denotes the synthesized beam.

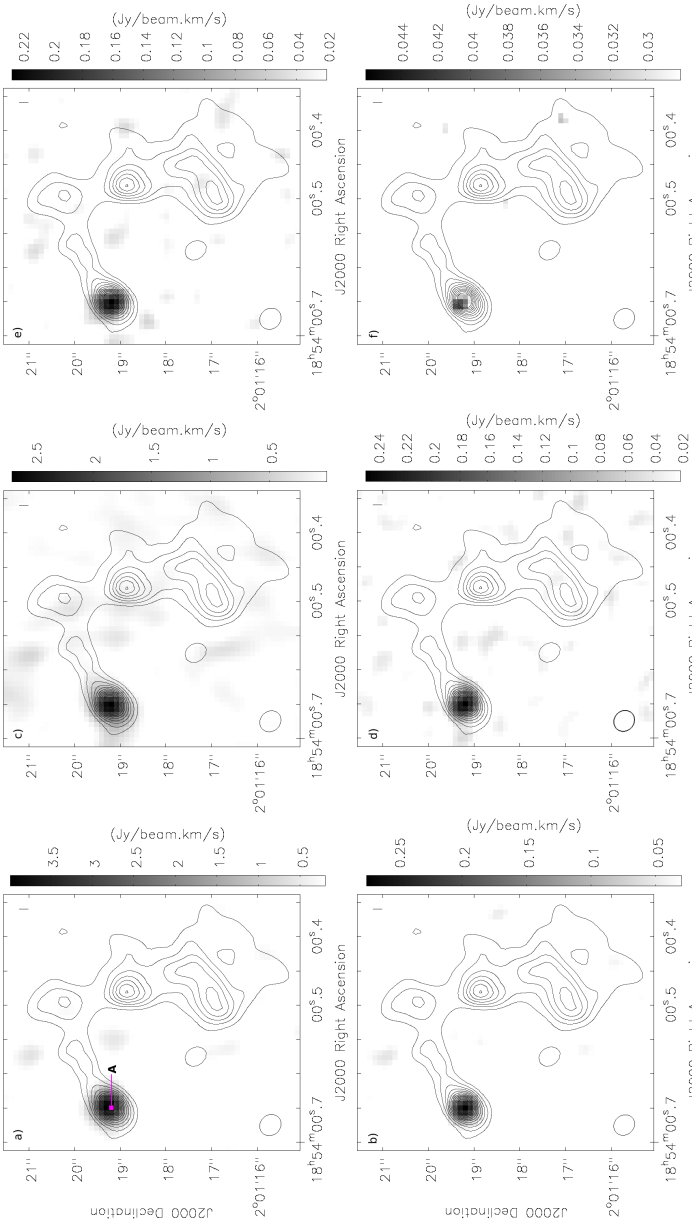

Figure 2.4: Integrated intensity maps of six species across G35.03, for which the contours are the 870 μm continuum with the same levels as Figure 2.2. Panel a) shows the CH_3OCHO ν=0 emission at 336.086 GHz integrated from 37 to 57 km s^{-1}. Panel b) shows the CH_3OCHO ν=1 emission at 348.084 GHz integrated from 42 to 50 km s^{-1}. Panel c) shows the H_2CS emission at 338.083 GHz integrated from 37 to 52 km s^{-1}. Panel d) shows $(CH_2OH)_2$ emission at 335.030 GHz integrated from 38.5 to 48.5 km s^{-1}. Panel e) shows CH_3CHO ν=0 emission at 335.318 GHz integrated from 39.5 to 48.5 km s^{-1}. Panel f) shows CH_3CHO ν=2 emission at 349.752 GHz integrated from 42 to 47 km s^{-1}. It is clear between panels a) and b) and between e) and f) that vibrationally excited states have a much smaller emitting region. It is also clear in panel d) that $(CH_2OH)_2$ is observed in this source.The ellipse denotes the synthesized beam.

Table 2.3: Table of source line characteristics. Column 1 lists the name of the peak. Column 2 shows the number of molecular species with one or more transition detected. The total in parentheses indicates the number of XCLASS catalog entries including isotopologues and vibrationally excited transitions separately. Column 3 gives the range of upper level energies observed. Column 4 is the average line width for each peak. Column 5 is the average velocity of the lines at each peak. Averages are calculated from all Gaussian line measurements as listed in Appendix B.

Continuum peak	Species (total)	E_{up} (K)	<FWHM> (km s^{-1})	<v_{LSR}> (km s^{-1})
G35.20 A	23 (52)	17-1143	5.2	32.2
G35.20 B1	21 (42)	17-1074	2.1	29.2
G35.20 B2	21 (41)	17-973	1.9	32.3
G35.20 B3	22 (50)	17-1143	2.4	28.5
G35.03 A	22 (46)	17-1143	4.7	45.3

2.3 Results and analysis

2.3.1 Line detections

A total of 431 different transitions were identified in 52 different catalog entries (18 "regular" ν=0 main isotopes species plus 34 vibrationally excited states and isotopologues). Table 2.3 shows the number of species detected per source and Figures 2.4 and 2.5 show the number of unblended and partially blended transitions detected per species in each source. In addition, a few species were identified from a single transition and are listed in Figure 2.7.

The peak with the most transitions is the weakest continuum source, B3. The strongest continuum source, G35.20 A, suffers greatly from blending and therefore has fewer unblended transitions, but is also chemically diverse (containing 23 identified species versus 22 in B3). G35.03 A, the second strongest continuum source, contains the third most molecular species, mainly because deuterated species are not present. Regarding line flux, B3 generally has the brightest emission of core B except in a few cases where B1 has slightly brighter lines. Overall B2 has the weakest emission, but still has a diverse range of species. The lines in G35.03 A are less bright than G35.20 A and are generally brighter than B3. The line fluxes from continuum peak G35.20 A are higher than any of the peaks in B except in a few cases in which B3 has higher line fluxes.

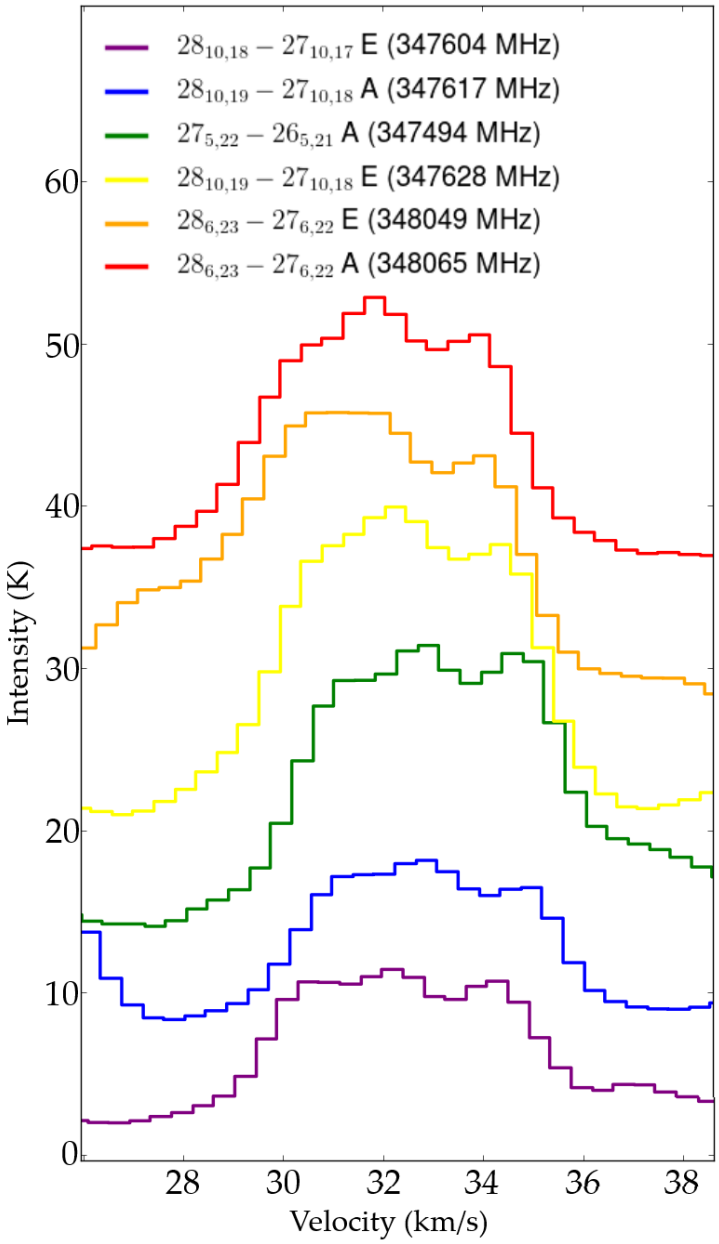

Figure 2.5: Profiles of CH_3OCHO transitions toward source G35.20 A showing double peaked emission lines. Features at the edge of the frame are separate lines. If the source is more compact than the beam, this could indicate rotation.

2.3.2 Line profiles

Most lines are fit by single Gaussians, but some profiles are more complex. Table 2.3 shows a summary of line properties at each peak. The average measured line width for G35.20 A was 5.2 km s^{-1} with an average v_{LSR} of 32.2 km s^{-1}. In G35.20 A, 23% of identified unblended lines are double peaked and nearly all of the rest are broad (FWHM in A is 5-8 km s^{-1} compared to 1-3 km s^{-1} at the B peaks; see below) suggesting that rotation of an unresolved structure is present (See Figure 2.5). As the double peaked transitions tend to have higher upper energies (typically ∼300 K), we propose that these originate in a warmer region closer to the central source, therefore indicating Keplerian-type rotation. This effect is especially prominent in the CH_3OCHO, C_2H_5OH, and CH_2DOH lines. Fits were made to each of the two components for CH_3OCHO using Cassis and the peaks were found to be separated by about 2.5 km s^{-1}. Double peaked lines are indicated in the line property tables in Appendix B. Line blending is prominent for G35.20 A, possibly because the object is more compact and therefore less resolved than core B. This could also be a consequence of G35.20 A being more chemically rich or having intrinsically broader line widths. There are a number of emission lines that are weakly detected in A and undetected at any other continuum peak. This is possibly because A is the brightest source in both line and continuum emission, so these species may also be present at the continuum peaks in B, but are lost in the noise. The emission lines from G35.20 A were fit with a single Gaussian for consistency, even where double peaked lines appeared, as the goal was chemical not kinematic analysis.

The average line widths for the emission lines from continuum peaks B1, B2, and B3 were 2.1, 1.9, and 2.4 km s^{-1}, respectively. The v_{LSR} of each of the continuum peaks in core B corresponds well with the velocity gradient of the disk observed in Sánchez-Monge et al. (2014). At B3 in the southeast of the core, the average measured v_{LSR} is 28.5 km s^{-1}, at B1, the brightest in continuum in the center of the core, the average v_{LSR} is 29.2 km s^{-1}, and at B2 in the northernmost part of core B the average v_{LSR} is 32.3 km s^{-1}. For the continuum peaks B1, B2, and B3, only the emission component was measured and taken into account for LTE modeling.

The spectra of sources B1, B2, and B3 show apparent absorption fea-

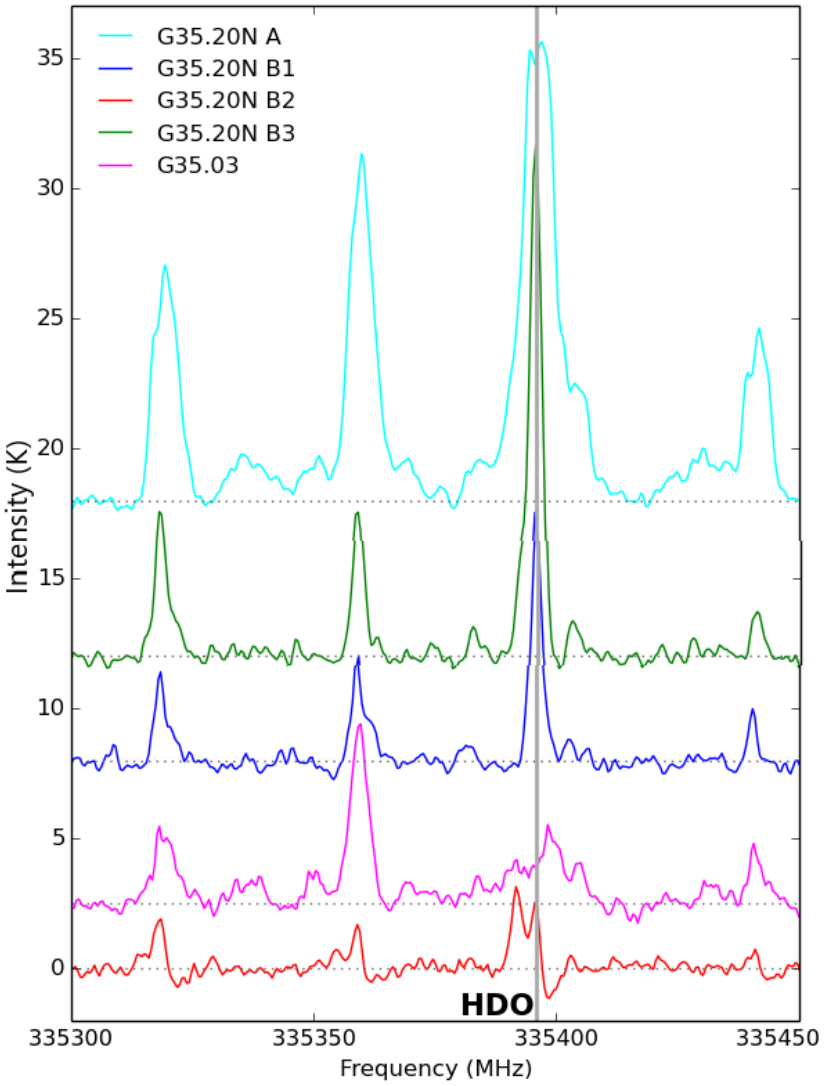

Figure 2.6: Sample spectrum for the frequency range 335.3-335.45 GHz in the rest frame of each peak to indicate the diversity of these sources. G35.03 and G35.20 A do not appear to have any absorption features (in this range), but it is notable that the lines for these two sources are broader. The deuterated water (HDO) emission line at 335.396 is especially strong in B3, double peaked in G35.20 A, possibly has two velocity components in B2, and is either very weak or offset by several km s^{-1} in G35.03.

tures, which originate in gaps in the observations due to emission larger than about 2″ being resolved out. In the spectra from B1, apparent redshifted absorption features are seen in every bright line except SO_2 and SO. In CH_3CN, the absorption is less pronounced, but the emission lines are asymmetrically blue. In the spectra of B2, the apparent absorption features are blueshifted and are obvious in all lines and are especially deep (∼2.5 K) for CH_3CN. In B3, the apparent absorption features can be seen weakly in all species but are strong (∼ 5 K) for CH_3OH ν=0 transitions.

G35.03 A generally has weaker lines than the brightest sources in G35.20 (A and B3) and broader lines than those in B1, B2, and B3 with an average FWHM of 4.7 km s^{-1}. The measured average v_{LSR} of the emission lines from this continuum peak was 45.3 km s^{-1}. There are no strong absorption features or double peaked emission lines. Figure 2.6 shows the different properties of each source in example spectra.

2.3.3 Kinetic gas temperatures

To estimate the kinetic temperature (T_{kin}) for each region without assuming local thermodynamic equilibrium (LTE), we use RADEX (van der Tak et al. 2007), which is a radiative transfer code that assumes an isothermal and homogeneous medium, treats optical depth with a local escape probability, and uses collisional rate coefficients from the LAMDA database (Schöier et al. 2005; Green 1986). We use this software to calculate line intensity ratios across a range of kinetic temperatures and densities and determine whether it is reasonable to assume LTE.

	G35.20 A				G35.20 B1			
Species	Lines	Size	T_{ex}	N_{col}	Lines	Size	T_{ex}	N_{col}
CH_3OH (ν=0)	29	0.6	164	3.5×10^{18}	28	0.3	234	6.9×10^{17}
CH_3OH (ν_{12}=1)	21	0.5	218	4.8×10^{18}	24	0.36	153	1.2×10^{18}
CH_3OH (ν_{12}=2)	14	0.4	227	3.8×10^{18}	18	0.18	154	2.2×10^{18}
$^{13}CH_3OH$	5	1.0	121	1.6×10^{17}	6	0.3	113	3.9×10^{16}
$CH_3\ ^{18}OH$	4	1.1	121	4.4×10^{16}	6	0.3	82	1.4×10^{16}
$H_2C^{18}O$	3	0.6	188	8.5×10^{14}	4	0.3	41	5.7×10^{14}
CH_3OCHO (ν=0)	28	0.98	103	8.1×10^{16}	38	0.5	285	4.5×10^{16}
CH_3OCH_3	10	0.34	229	3.7×10^{17}	11	0.22	156	3.8×10^{17}
CH_3CHO (ν=0)	14	0.4	234	1.7×10^{16}	19	0.33	206	7.0×10^{16}
CH_3CHO (ν_{15}=1)	7	1.1	278	5.5×10^{15}	7	0.2	300.0	2.3×10^{14}
CH_3CHO (ν_{15}=2)	4	0.7	295	4.3×10^{15}	1	⋆		
HCOOH	5	0.6	103	1.4×10^{16}	4	0.3	156	1.1×10^{15}
C_2H_5OH	30	0.8	281	7.1×10^{16}	33	0.7	78	6.0×10^{15}
$(CH_2OH)_2$	23	0.6	172	3.5×10^{16}	0	⋆		
NH_2CHO	3	0.7	98	7.6×10^{15}	3	0.3	50	5.7×10^{15}
$NH_2{}^{13}CHO$	2	†		1.4×10^{14}	2	†		1.0×10^{14}
CH_3CN (ν=0)	10	0.45	208	3.9×10^{16}	9	0.32	129	7.2×10^{15}
CH_3CN (ν_8=1)	11	0.6	359	3.2×10^{16}	5	0.29	283	3.5×10^{15}
$CH_3\ ^{13}CN$	2	1.0	263	5.0×10^{14}	4	0.7	262	2.0×10^{14}
CH_2DCN	4	0.5	82.3	4.1×10^{15}	7	0.1	180	3.0×10^{13}
C_2H_5CN	13	0.9	125	1.5×10^{16}	8	⋆		
$CH_3{}^{13}CH_2CN$	2	†		6.9×10^{14}	0	⋆		
$^{13}CH_3CH_2CN$	1	†		6.9×10^{14}	0	⋆		
CH_3CHDCN	13	0.6	97	2.9×10^{15}	0	⋆		
C_2H_3CN	6	0.6	77	1.3×10^{16}	0	⋆		
HCCCN (ν = 0)	1	1.2	176	1.7×10^{15}	1	0.9	119	9.2×10^{14}
$HC^{13}CCN$ (ν = 0)	1	†		3.4×10^{13}	0	⋆		
$HCC^{13}CN$ (ν = 0)	0	†		3.4×10^{13}	0	⋆		
HCCCN (ν_6=1)	1	0.6	200	3.1×10^{15}	0	⋆		
$HCC^{13}CN$ (ν_6 = 1)	1	†		6.2×10^{13}	0	⋆		
HCCCN (ν_7=1)	2	0.37	251	5.3×10^{15}	3	0.8	219	5.8×10^{14}
$H^{13}CCCN$ (ν_7 = 1)	2	†		1.0×10^{15}	0	⋆		
$HC^{13}CCN$ (ν_7 = 1)	1	†		1.0×10^{15}	0	⋆		
$HCC^{13}CN$ (ν_7 = 1)	1	†		1.0×10^{15}	1	⋆		
HCCCN (ν_7 = 2)	1	0.20	350	2.2×10^{15}	0	⋆		
H_2CS	2	1.3	165	1.4×10^{16}	2	2.0	230	3.3×10^{15}
$H_2C^{34}S$	1	†		5.3×10^{14}	5	†		1.9×10^{14}
SO_2	5	1.4	260	1.7×10^{16}	5	1.44	279	3.3×10^{16}
$^{33}SO_2$	1	†		1.7×10^{14}	1	†		2.5×10^{14}
$^{34}SO_2$	1	†		1.2×10^{14}	1	†		1.2×10^{14}
CH_2DOH ‡	18		150	5.0×10^{16}	35		140.0	9.0×10^{15}
CH_3OCHO (ν=1) ‡	8		120	1.9×10^{17}	6		140.0	9.0×10^{15}

Table 2.4: Results of XCLASS LTE modeling for each of our sources. Four columns are shown under each source name: 1) Number of unblended or partially blended transitions per species detected, 2) modeled source size ($''$), 3) excitation temperature (K), and 4) column density (cm^{-2}). The errors on each value are shown in Appendix 2.C.

G35.20 B2				G35.20 B3				G35.03 A			
Lines	Size	T_{ex}	N_{col}	Lines	Size	T_{ex}	N_{col}	Lines	Size	T_{ex}	N_{col}
24	0.36	136	5.3×10^{17}	33	0.35	155	6.2×10^{17}	29	0.40	142	1.8×10^{18}
23	0.32	145	6.2×10^{17}	24	0.36	189	9.8×10^{17}	21	0.30	239	2.6×10^{18}
18	0.15	152	1.0×10^{18}	19	0.20	172	1.8×10^{18}	14	0.20	192	5.1×10^{18}
6	1.1	97	8.0×10^{15}	7	1.20	89	1.6×10^{16}	5	0.6	120	5.0×10^{16}
4	0.9	75	1.4×10^{15}	5	1.20	111	5.8×10^{15}	4	1.2	130	1.0×10^{16}
4	0.32	29	1.5×10^{15}	4	1.09	125	4.2×10^{14}	1	0.50	62	2.1×10^{14}
33	0.5	64	2.0×10^{16}	31	0.59	67	2.7×10^{16}	28	0.2	100	2.3×10^{15}
8	0.4	67	1.3×10^{16}	19	0.49	97	1.7×10^{17}	10	0.7	150	8.3×10^{16}
18	0.26	88	2.3×10^{15}	20	1.16	170	2.1×10^{15}	14	0.5	120	1.3×10^{15}
4	⋆			13	0.56	224	1.4×10^{15}	7	0.5	220	1.3×10^{15}
0	⋆			3	0.12	102	8.1×10^{14}	0	⋆		
2	⋆			7	0.4	173	3.8×10^{15}	5	0.7	100	5.0×10^{15}
33	0.12	297	1.0×10^{15}	32	0.43	178	1.3×10^{16}	30	0.4	150	4.9×10^{16}
0	⋆			0	⋆			34	0.70	100	2.8×10^{16}
2	0.6	45	2.3×10^{14}	4	0.3	53	1.6×10^{15}	3	0.8	43	4.7×10^{15}
2	†		5.1×10^{12}	2	†		5.1×10^{13}	2	†		8.5×10^{13}
9	0.62	132	1.3×10^{15}	10	0.35	208	6.5×10^{15}	10	0.30	186	3.0×10^{16}
4	⋆			13	0.8	213	1.3×10^{15}	11	0.30	216	3.6×10^{16}
3	0.44	55	1.4×10^{14}	9	0.7	118	5.4×10^{14}	2	0.35	70	1.4×10^{15}
1	⋆			6	0.8	90	1.1×10^{15}	1	⋆		
3	⋆			18	0.8	160	4.5×10^{14}	13	0.5	78	5.0×10^{15}
0	⋆			0	⋆			0	⋆		
0	⋆			0	⋆			0	⋆		
0	⋆			0	⋆			0	⋆		
0	⋆			11	0.8	207	7.3×10^{14}	0	⋆		
1	0.8	122	2.0×10^{14}	1	1.2	251	1.8×10^{15}	1	0.6	140	2.3×10^{15}
1	⋆			1	†		3.8×10^{13}	1	⋆		
0	⋆			1	†		3.8×10^{13}	0	⋆		
0	⋆			2	0.4	256	2.4×10^{15}	0	⋆		
0	⋆			1	†		5.4×10^{13}	0	⋆		
2	⋆			3	0.98	288	2.1×10^{15}	2	0.8	194	5.9×10^{15}
0	⋆			2	†		4.6×10^{13}	0	⋆		
0	⋆			1	†		4.6×10^{13}	0	⋆		
0	⋆			2	†		4.6×10^{13}	0	⋆		
0	⋆			4	0.35	473	1.3×10^{15}	0	⋆		
2	1.0	50	1.2×10^{15}	2	0.9	87	6.1×10^{15}	2	1.7	96	3.7×10^{15}
6	†		8.9×10^{13}	5	†		6.1×10^{14}	0	⋆		
5	2.42	114	6.6×10^{15}	5	1.3	288	3.9×10^{16}	5	1.2	281	7.5×10^{16}
1	†		1.4×10^{14}	2	†		1.9×10^{15}	1	†		3.4×10^{15}
1	†		1.6×10^{14}	1	†		1.3×10^{15}	1	⋆		
31		240.0	6.0×10^{15}	32		160.0	1.5×10^{16}	1			
4				8				4			

Table 2.5: Star (⋆) symbols indicate that a species was not modeled in XCLASS for this peak. † indicates that this species was coupled to the main isotopologue for fitting and the isotope ratio was calculated keeping the source size and excitation temperature the same as the main isotope. The column density indicated in these cases reflects the best-fit isotope ratio. To improve the fits for various HC_3N states, the $^{12}C/^{13}C$ isotope ratio was fixed at 50. ‡ these species were analyzed using Cassis because they were not yet incorporated in the XCLASS database.

We used the CH_3CN line ratios for these sources as this species is a known tracer (Wang et al. 2013) of kinetic temperature as a near-symmetric top molecule where transitions with different energy levels have similar critical densities. We consider as input parameters the ratios of the peaks of unblended CH_3CN lines. The transitions used were 19_8-18_8, 19_6-18_6, 19_5-18_5, 19_4-18_4, 19_3-18_3, and 19_2-18_2 with a column density of 5×10^{15} cm^{-2}. The line ratios were modeled for kinetic temperatures between 100 and 500 K and for H_2 densities between 10^6 and 10^9 cm^{-3}. Errors were calculated from the measured error on the Gaussian fit of each spectral line.

We find that B2 is the coolest region with an average T_{kin} of 120 K and a range from 90-170 K. Next hottest is B1 with an average T_{kin} of 160 K and a range from 120-220 K. G35.20 A is significantly hotter than these with an average T_{kin} of 285 K and a range from 150-450 K. B3 is consistently the hottest, ranging from 175-490 K with an average T_{kin} of 300 K. The kinetic temperatures in G35.03 are also very high, ranging from 100-450 K with an average T_{kin} of 275 K.

The varying temperatures for different transition ratios may indicate a temperature gradient within the sampled gas, which requires advanced methods such as RATRAN (Hogerheijde & van der Tak 2000) or LIME (Brinch & Hogerheijde 2010) to model. The K=6/K=4 ratio consistently traces the lowest temperature. The K=8/K=3 ratio traces the highest temperature for A, B3, and G35.03, while the highest temperatures for B1 and B2 are traced by the K=6/K=3 and K=6/K=5 ratios, respectively.

These average kinetic temperatures were used in calculating the mass of the core and H_2 column density based on the 870 μm continuum flux as in Sánchez-Monge et al. (2014). Using a dust opacity of 1.75 cm^2 g^{-1} and a gas-to-dust ratio of 100, core A has a mass of 13.0 $M_\odot$, B1 has a mass of 3.8 $M_\odot$, B2 has a mass of 2.2 $M_\odot$, B3 has a mass of 1.4 $M_\odot$, and G35.03 has a mass of 4.4 $M_\odot$. G35.20 A generally has a lower kinetic temperature than B3, but higher energy transitions are observed and it is also much more massive with a continuum flux density that is 10 times higher.

2.3.4 Molecular column densities

To estimate the column densities of each detected species, we used the XCLASS software. For any given set of parameters (source size, temperature, column density, velocity, and line width) XCLASS determines the opacity for each spectral channel for each species, and these opacities are added to produce a spectrum of the opacity changing with frequency. In a last step, the opacity is converted into brightness temperature units to be directly compared with the observed spectrum. The fitting process compares the synthetic spectrum to the observed spectrum, and minimizes the χ^2 by changing the five parameters indicated above. As input parameters, we limited the line width and v_{LSR} to $\pm$ 1 km s^{-1} from the measured values so the transitions could easily be identified by the fitting algorithm. Source size, excitation temperature (T_{ex}), and column density (N_{col}) were allowed to vary widely to begin with and then were better constrained around the lowest χ^2 fits per parameter per species. For species that were observed to be located only in the regions of the hot cores (mostly complex organic molecules), the source size was varied from 0.1-1.5″ to be comparable with the observed emission extent and the T_{ex} was allowed to vary from 50-500 K. The column density was allowed to vary from 10^{13}-10^{19} cm^{-2}. For species that were observed to emit over a more extended region (H_2CS and SO_2), the source size input range was varied between 1.0-3.5″, the T_{ex} input range was 20-200 K, and the column density input range was 10^{12}-10^{16} cm^{-2}.

For a few species (SiO, $H^{13}CO^+$, $C^{17}O$, $H^{13}CN$, and $C^{34}S$) only one transition was observed, so we kept the source size fixed at the measured extent of the emission at 3σ and the excitation temperature fixed at 50 K and 100 K to determine the column densities at these two possible temperatures. The results for the single line transitions are given in Table 2.7.

Figure 2.7 presents a summary of the abundances observed per core as modeled via XCLASS. The excitation temperatures ranged from about 100-300 K generally with a few species outside this range. The H_2 column densities used were based on the 870 μm continuum emission (values shown in Table 2.1) as determined in section 4.1 of Sánchez-Monge et al. (2014). These mass and column density estimates are lower limits as Sánchez-Monge et al. (2014) determined that in our observations we recover 30% of the flux compared to SCUBA 850 μm observations.

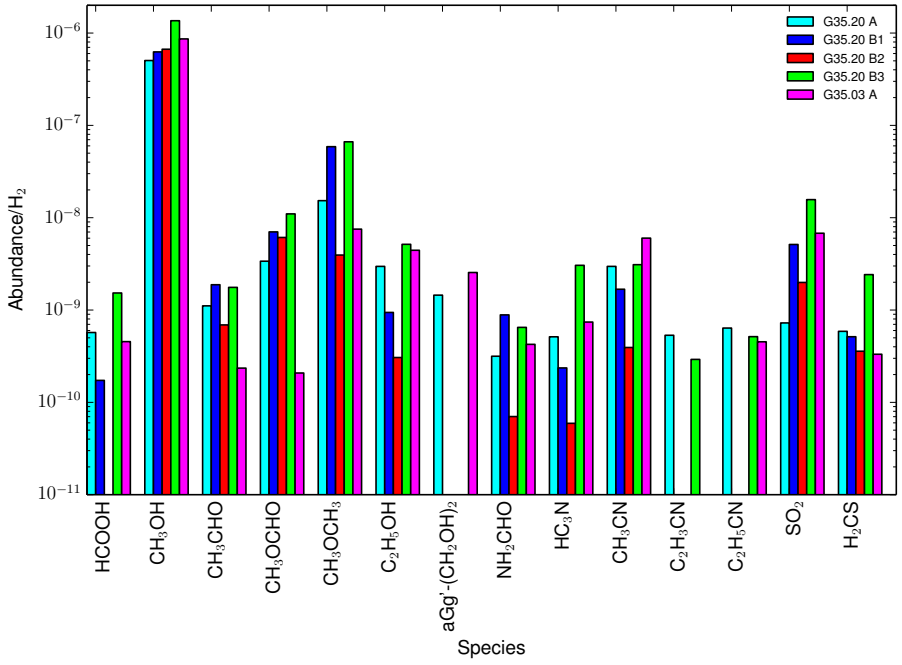

Figure 2.7: Abundances vs. H_2 as determined using the XCLASS software package for each of the cores modeled. All main isotope species modeled from more than one transition are shown. The column densities for vibrationally excited states were added to the ν=0 state for CH_3OH, CH_3CHO, CH_3CN, and cyanoacetylene (HC_3N) to determine abundances. The CN-bearing species in both plots clearly indicate the missing emission in B1 and B2 for vinyl cyanide (C_2H_3CN) and ethyl cyanide (C_2H_5CN) and reduced abundances in B2 for CH_3CN and HC_3N. We stress that as these species do not always trace the same gas, these abundances are lower limits.

The modeled values for column density and excitation temperature were checked against rotational diagrams from Cassis and found to be in agreement. The column densities determined using Cassis are lower than those from XCLASS, but this is an effect of a less robust optical depth analysis and assuming the source size fills the beam.

Uncertainties on excitation temperatures tend to be 10-20%, but for some species the fit results are upper or lower limits. For entries that are not upper or lower limits, the range of errors is 1-160 K with an average temperature error of 40 K (or 37%). Source size uncertainties are generally 0.1-0.3″ with an average error of 0.2″, but range from 0.01-

1.0″. Error ranges for column densities were typically less than 1 order of magnitude (with an average error of 0.7 orders of magnitude) with a range between 0.2 and 2.8 orders of magnitude. For species where only one transition is modeled uncertainties for the column densities of these species are up to two orders of magnitude. Tables 2.4 and 2.5 show the full list of detected species and isotopologues with the number of transitions detected in each core and indicates whether the listed species or isotopologue was modeled in XCLASS. The resulting synthetic spectra are shown together with the observed spectra in Appendix 2.E and can be seen to be very good fits of the data. The results of the XCLASS analysis are summarized in Appendix 2.D.

In the following subsections, we outline any special considerations used in modeling specific molecules. Section 2.3.4 outlines the treatment of most complex organic molecules and their isotopologues and excited states. Section 2.3.4 details the special treatment of the observed HC_3N emission. Section 2.3.4 explains the fitting methods for SO_2 and H_2CS. Section 2.3.4 shows how simple molecules with only one transition are modeled. Section 2.3.4 summarizes how the few species not included in the XCLASS database are handled.

Complex organic molecules

We modeled 10 different species containing 6 or more atoms: methanol (CH_3OH), ethanol (C_2H_5OH), methyl formate (CH_3OCHO), acetaldehyde (CH_3CHO), dimethyl ether (CH_3OCH_3), formamide (NH_2CHO), ethylene glycol ($(CH_2OH)_2$), methyl cyanide (CH_3CN), vinyl cyanide (C_2H_3CN), and ethyl cyanide (C_2H_5CN).

Several species with ^{13}C isotopologues were detected, along with many cases of deuteration. The ^{18}O isotopologue for methanol and formaldehyde were detected in all cores, but in no other species. This is due, in part, to limited laboratory data where the properties of these transitions have not yet been measured or calculated.

High energy transitions in our sources are observed to emit from a much smaller area than lower energy transitions (see Figures 2.3 and 2.4) and many are not observed in B1 or B2. Because these vibrationally excited states emit from a smaller region, we assume that this emission originates from a denser and possibly hotter region and therefore, the continuum derived H_2 column density is a lower limit. For this rea-

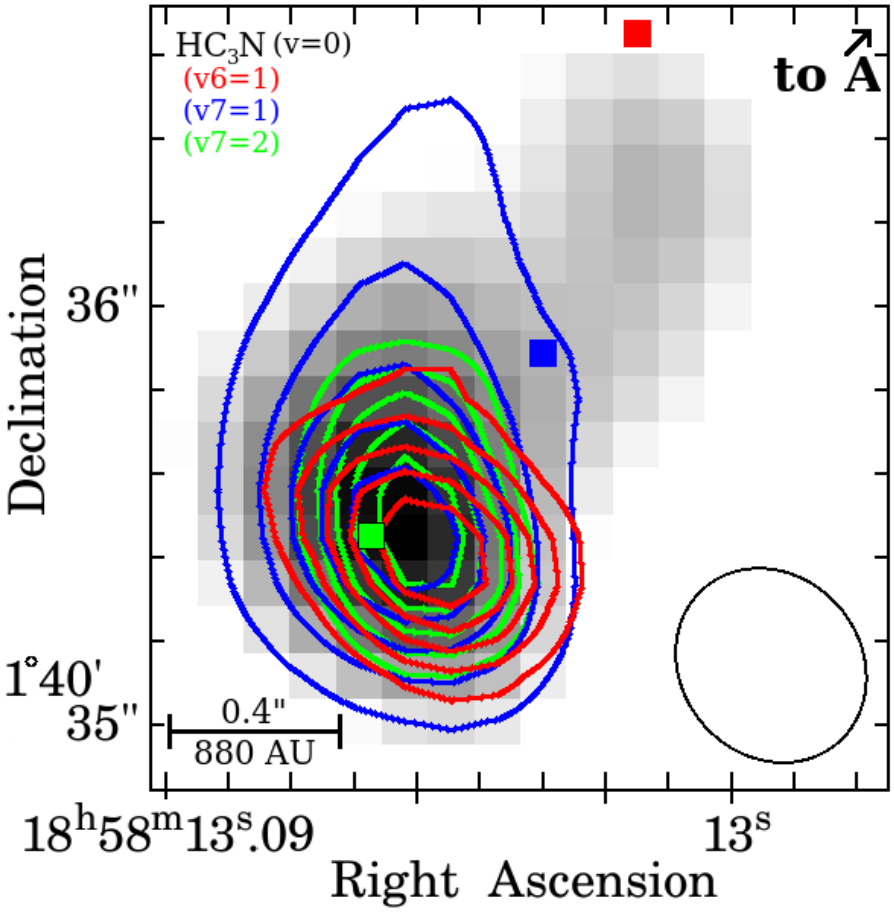

Figure 2.8: Integrated intensity of HC_3N J = 37-36 emission is shown: (ν=0) (grayscale), ν_7=1 (blue contours), ν_6=1 (red contours), and ν_7=2 (green contours) The green contours are 0.05, 0.069, 0.088, 0.106, and 0.125 Jy/beam km s^{-1}. Blue contours are 0.2, 0.422, 0.644, 0.866, and 1.088 Jy/beam km s^{-1}. Red contours are 0.043, 0.067, 0.092, 0.117, and 0.141 Jy/beam km s^{-1}. Sources B1, B2, and B3 are indicated with colored boxes as in Figure 2.1.

son the column densities for these species cannot be easily converted to abundances, and cannot be precisely compared to their ν=0 states. Nevertheless, noting their derived excitation temperatures and densities is useful in comparing the properties of the different regions of gas.

Table 2.6: Columns 2 and 3 list vibrational temperatures for HC_3N with corresponding column densities. Fluxes for ^{13}C isotopologues were multiplied by 50 to be comparable to Galactic isotope ratios. Columns 4 and 5 correspond to the kinetic temperatures (from RADEX) and the average excitation temperatures (from all XCLASS modeled HC_3N vibrational states) and column 6 is the total column density from the XCLASS fits.

Source	T_{vib} (K)	N_{col} (vib) (cm^{-2})	T_{kin} (K)	T_{ex} (K)	N_{col} (XCLASS) (cm^{-2})
G35.20 A	210±80	$4^{+11}_{-3} \times 10^{15}$	285^{+165}_{-135}	280	1.2×10^{16}
G35.20 B1	160±20	$6.2^{+340}_{-6.0} \times 10^{14}$	160^{+60}_{-40}	210	1.6×10^{15}
G35.20 B2	120±60	$5^{+27}_{-4} \times 10^{14}$	120^{+50}_{-30}	130	2×10^{14}
G35.20 B3	160±20	$2.4^{+1.4}_{-0.9} \times 10^{15}$	300^{+190}_{-125}	310	8.4×10^{15}
G35.03 A	n/a	n/a	275±175	170	8.1×10^{15}

2

Cyanoacetylene (HC_3N) and vibrational temperature

Between 2 and 10 different states were detected in each source for this species, but with only a few transitions, so the isotopologues were coupled to the main isotopologue for each vibrational state and fixed at a $^{12}C/^{13}C$ isotope ratio of 50. The ν=0 state was modeled for all regions and the isotopologue $HC^{13}CCN$ ν=0 was coupled with HC_3N ν=0 to improve the uncertainty (from fitting one transition to fitting two). The fit for $HCC^{13}CN$ ν=0 was also coupled with HC_3N ν=0 for B3, as this is the only location where this species was detected.

Each of the vibrational states (ν_6=1, ν_7=1, ν_7=2) were modeled separately due to their differing spatial extent (Figure 2.8) and the source size was observed to be more compact with higher excitation. No vibrationally excited states were modeled for B2, as they were not detected in the observations and only the ν_7=1 state was modeled for B1 and G35.03. HC_3N ν_6=1 was modeled for A and B3 and was coupled with $HCC^{13}CN$ ν_6=1 with the $^{12}C/^{13}C$ isotope ratio fixed at 50. HC_3N ν_7=1 was also modeled coupled with the three different ^{13}C isotopologues of

	G35.20 A			G35.20 B1			G35.20 B2		
Species	Size	50 K	100 K	Size	50 K	100 K	Size	50 K	100 K
$HN^{13}C$	1.5	3.1×10^{13}	4.1×10^{13}	0.8	1.7×10^{13}	1.6×10^{13}	1.0	1.6×10^{13}	1.6×10^{13}
SO	1.5	3.6×10^{13}	3.6×10^{13}	1.4	3.7×10^{17}	3.6×10^{17}	1.2	3.7×10^{16}	1.7×10^{16}
$H^{13}CO+$	1.5	1.6×10^{13}	5.3×10^{12}	0.8	8.3×10^{12}	8.2×10^{12}	1.0	3.1×10^{13}	3.1×10^{13}
SiO	1.4	7.1×10^{13}	7.2×10^{13}	1.1	9.0×10^{13}	8.7×10^{13}	1.1	6.2×10^{12}	6.2×10^{12}
$C^{34}S$	1.7	2.8×10^{15}	1.2×10^{15}	1.2	3.4×10^{14}	2.9×10^{14}	1.0	4.6×10^{14}	3.5×10^{14}
HNCO	1.3	2.3×10^{16}	7.5×10^{16}	1.0	1.2×10^{16}	6.9×10^{15}	1.0	2.2×10^{15}	9.4×10^{14}
HDCO	1.5	1.6×10^{15}	2.6×10^{13}	1.2	4.5×10^{14}	1.0×10^{15}	1.0	1.7×10^{14}	2.6×10^{14}
HDO	1.3	1.8×10^{18}	4.8×10^{17}	0.9	5.6×10^{17}	3.3×10^{16}	0.7	1.8×10^{17}	7.8×10^{15}

	G35.20 B3			G35.03 A		
Species	Size	50 K	100 K	Size	50 K	100 K
$HN^{13}C$	1.5	1.1×10^{14}	1.2×10^{14}	1.2	2.5×10^{12}	5.8×10^{12}
SO	1.2	3.7×10^{16}	1.1×10^{17}	1.3	2.4×10^{17}	1.1×10^{17}
$H^{13}CO+$	1.5	6.5×10^{12}	2.8×10^{13}	1.5	1.7×10^{13}	2.1×10^{13}
SiO	0.8	1.2×10^{11}	2.8×10^{11}	1.1	5.7×10^{13}	1.1×10^{14}
$C^{34}S$	1.1	5.3×10^{14}	6.8×10^{14}	1.5	8.1×10^{14}	7.1×10^{14}
HNCO	1.1	2.3×10^{16}	8.4×10^{15}	1.1	1.8×10^{16}	7.7×10^{15}
HDCO	1.5	1.6×10^{15}	1.5×10^{15}		N/A	
HDO	1.0	9.2×10^{17}	7.6×10^{16}		N/A	

Table 2.7: Table of column densities (cm^{-2}) determined via XCLASS for species with single transition detections. Each peak was modeled with the excitation temperatures fixed at 50 K and 100 K. The source sizes are the measured diameter of the 3σ emission in arcseconds ($''$).

HC_3N ν_7=1 for A and B3 with the isotope ratio fixed at 50. HC_3N ν_7=2 was only modeled for A and B3 where the emission becomes very compact.

We determined vibrational temperatures from all of the observed HC_3N lines for each peak and found them to be in agreement with our RADEX and XCLASS results (see Table 2.6 and Figure 2.9). The temperatures ranged from 120-210 K, which indicates that our assumption of LTE is reasonable, even where species are vibrationally excited. The vibrational temperature for peak B3 is smaller than the kinetic temperature, but is consistent within errors (see Table 2.6).

The ratio of intensities of HC_3N ν_7 and ν_0 transitions indicates the proportion of vibrationally excited to ground-state molecules in the region (Wyrowski et al. 1999a). For G35.20 B1 and B2 this ratio is $\sim$0.15 and for A and B3 it is $\sim$0.3. Our sources are all similar to the other hot cores studied in Wyrowski et al. (1999a), where G35.20 A is similar to

SgrB2N, B1 and B2 similar to Orion KL and W3(H_2O), and B3 similar to G29.96-0.02. Vibrational temperature analysis for G35.03 A could not be completed as the only unblended HC_3N lines detected were from the vibrational state ν_7=1.

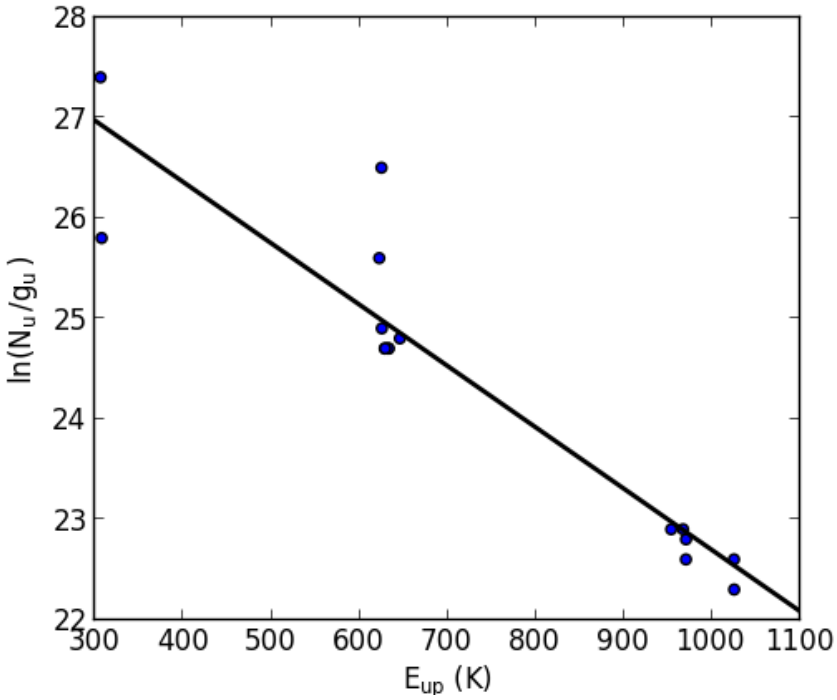

Figure 2.9: Vibrational diagram for all of the HC_3N transitions from G35.20 B3 including ground and vibrationally excited states with J=37-36 and J=38-37. Fluxes for ^{13}C isotopologues were multiplied by 50 to be comparable to Galactic isotope ratios. The vibrational temperature calculated for peak B3 is 160 ± 20 K

Sulfur bearing molecules

Sulfur bearing molecules SO_2 and H_2CS were modeled with their detected isotopologues coupled to the main isotopologue varying the isotope ratio. Sulfur isotope ratios in the ISM have been shown to be 15-35 for $^{32}S/^{34}S$ and 4-9 for $^{34}S/^{33}S$ (Chin et al. 1996). Solar isotope ratios

are 22.6 for $^{32}S/^{34}S$ and 5.5 for $^{34}S/^{33}S$ (Anders & Grevesse 1989). Our best-fit isotope ratio for $^{32}SO_2/^{33}SO_2$ was between 16 and 100. The ratio of $^{32}SO_2/^{33}SO_2$ in space has been reported for Orion KL in Esplugues et al. (2013), with varying ratios for different parts of the region ranging from 5.8-125 reporting a ratio of 25 in the Orion hot core. The best-fit isotope ratio for our observations of $^{32}SO_2/^{34}SO_2$ was around 33. The main isotopologue fit of H_2CS was made based on three transitions and was modeled with $H_2C^{34}S$ coupled (only the abundance ratio was varied). The best-fit isotopic ratio for $H_2C^{32}S/H_2C^{34}S$ was 11, where the ratio reported for SgrB2 by Belloche et al. (2013) was 22.

Simple molecules

For the following simple species (those with less than six atoms), only a single transition was observed, so to estimate their column densities, the source size and excitation temperatures were fixed. The temperatures were modeled at 50 K and 100 K for all but $C^{17}O$, which was modeled at 20 K and the source size was fixed at the measured extent of the 3σ emission. Several species were previously demonstrated to have quite extended emission ($H^{13}CO^+$, $C^{17}O$, SiO) in Sánchez-Monge et al. (2014); Beltrán et al. (2014). A summary of the results for these species is given in Table 2.7.

- Formyl cation ($H^{13}CO^+$ 4-3) - Only the emission component of this species was modeled. Extended emission shown in Sánchez-Monge et al. (2014); Beltrán et al. (2014).
- Carbon monoxide ($C^{17}O$ 3-2) - At the location of our pixel sources there was a lot of uncertainty in identifying of this line owing to severe line blending at this frequency. For G35.20 A this could not be modeled owing to line confusion. Extended emission indicates that this species is seen in the surrounding cloud, so a larger source size and a lower temperature were used.
- Heavy (Deuterated) water (HDO $3_{3,1}$-$4_{2,2}$) - This transition, along with all other deuterated species, was not clearly detected in G35.03, so HDO $3_{3,1}$-$4_{2,2}$ was not modeled there. For the other peaks, the emission was fairly extended and the best-fit source sizes were between 0.6″ (at B2) and 1.5″ (at B3).

Species analyzed with Cassis

Some species could not be modeled with XCLASS as they were not yet included in its database. These species were measured and analyzed with Cassis.

- Deuterated methanol (CH_2DOH) - Rotational diagrams were created using Cassis for all peaks in G35.20. The rotational temperatures ranged from 140-240 K and column densities were 0.6-5.0 x 10^{16} cm^{-2}. The CH_3OH ν=0 rotational diagrams were made using Cassis to compare to these values to determine deuteration fraction.

- Vibrationally excited methyl formate (CH_3OCHO ν=1) - Rotational diagrams were made from all CH_3OCHO transitions and the high energy ν=1 transitions continued the trend of the rotational diagrams well. Therefore the reported rotational temperatures and column densities are those of all transitions for that peak.

- Doubly deuterated formaldehyde (D_2CO) - This species was not modeled because only a single partially blended transition was detected.

2.4 Discussion

2.4.1 Overall chemical composition

Despite originating from different clouds, G35.03 and G35.20 have similar (within an order of magnitude) abundances of all modeled species except deuterated isotopologues (see § 2.4.4). We find peak B3 shows the highest abundances within G35.20 B versus H_2 of all species except for NH_2CHO and CH_3CHO, for which peak B1 has the highest abundance and H_2CO, for which peak B2 has the highest abundance.

It is possible that comparing the column densities of various complex organic molecules to that of H_2 is a less effective method of comparing abundances between these sources. The value for H_2 column density derived from the continuum (and therefore the dust) does not necessarily reflect the density of the warm dense gas where COMs are formed. Given the uncertainty of the H_2 column densities, we also estimated

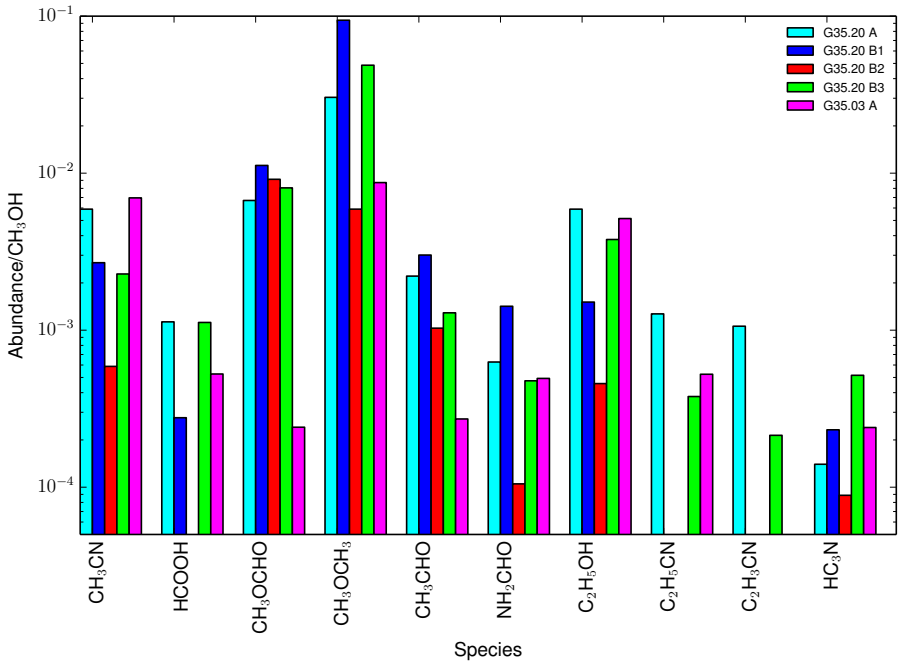

Figure 2.10: Plot of molecular abundances vs. CH_3OH. The column densities for vibrationally excited states were added to the ν=0 state for CH_3OH, CH_3CHO, CH_3CN, and HC_3N to determine abundances.

the abundances of some molecules relative to CH_3OH, whose emission is less resolved than the continuum emission. Figure 2.10 shows the relative abundance for several species. This figure confirms the main result of Figure 2.7 namely that abundances in B3 are higher than the other continuum peaks in G35.20 B except in NH_2CHO and CH_3CHO. We thus conclude that B3 appears to be the most chemically rich of the three sources in G35.20 B. The ratio versus methanol for our sources are less than any of the different types of objects reviewed in Herbst & van Dishoeck (2009). Comparing the ratio of CH_3CN to CH_3OH in our sources to those in Öberg et al. (2013), we see that to reach a similar ratio in NGC 7538 IRS9, the gas would be over 7000 AU from the center.

In Öberg et al. (2014), it is suggested that the ratio of abundances of CH_3CHO + CH_3OCHO (X-CHO) and CH_3OCH_3 + C_2H_5OH (X-CH_3) is related to the temperature and type of source. Laboratory experiments

have shown that higher abundance of CHO-bearing molecules indicates the importance of cold ice COM chemistry. If X-CHO/X-CH_3 is near 1, then the source is a cooler, lower mass source and a ratio much less than 1 corresponds to a hotter and more massive source. In line with their observation, we also see a higher ratio of X-CHO/X-CH_3 at the coolest peak, G35.20 B2, where the ratio is 1.6, and low ratios at the hottest peaks, G35.20 A, B1, B3, and G35.03 A (0.25, 0.15, 0.18, and 0.04, respectively). From figure 1 in Öberg et al. (2014), peak G35.20 B2 could be a massive hot core, but it could also be low mass, whereas peaks G35.20 A, B1, B3, and G35.03 A definitely fall into the massive hot core regime, where warm ice chemistry becomes more important.

Our XCLASS model fits show higher or nearly equal column densities for several vibrationally excited states versus their ground states. The XCLASS analysis is satisfactory as long as the energy of the lines span a relatively small range, but a single temperature model is inadequate to fit lines with very different excitation energy. Because of the presence of temperature gradients in these sources, the ground state lines and vibrationally excited lines can be fitted with significantly different temperatures since they trace gas originating from smaller areas with equal or higher column densities.

2.4.2 Chemical segregation in G35.20

Sánchez-Monge et al. (2013a) show evidence for a Keplerian disk in core B of G35.20. When analyzing the chemical structure of this core at continuum peaks B1, B2, and B3, we see a striking chemical difference within this disk, which argues against a simple axisymmetric disk scenario. Our data show clear evidence for chemical segregation of the G35.20 core on a scale of 100s of AU. Nitrogen-bearing species, especially those containing the cyanide (CN) group (HC_3N, C_2H_5CN, etc.), are only observed in A and the southern part of B (peak B3) except for CH_3CN ν=0, which appears in all four locations, although the abundance compared to CH_3OH at B3 is four times that at B2; $HN^{13}C$, where the abundance versus CH_3OH at B3 is six times more than at B2; and HC_3N ν=0, where the abundance compared to CH_3OH at B3 is 7.5 times that at B2 (see Figure 2.10). The linear scale for this separation of chemistry is less than 1000 AU, which is the smallest observed chemical separation in a star-forming region to date. Figures 2.8 and 2.11 show that cyanides

(HC_3N, C_2H_5CN, etc.) are only observed toward A and the southern part of B with higher abundances at peak B3 and low abundances or missing emission toward B1 and B2.

There are three plausible scenarios to explain this chemical differentiation. First, core B could be a disk in the process of fragmenting on scales that are not well resolved in this dataset, where each of the fragments are developing their own chemistry. Second, there could also be two or three distinct sources within core B, each uniquely influencing the chemistry of their surroundings, which could be due to evolutionary age and/or physical conditions. If the higher kinetic temperature of this region is driving the nitrogen enrichment, Crockett et al. (2015) showed that cyanides can also be made more easily in the hot gas phase than other COMs. If the age is a factor, then an age difference between sources would affect the chemistry of the surroundings. With enhanced abundances of almost all species, it is possible that B3 contains the hottest source in a multicore system sharing a circumcluster disk with sources at B1 and B2.

Third, G35.20B could be a disrupted disk, where it is possible that there are chemical changes within the rotation period of the disk, which is 9700-11100 years (based on the observed radial velocity 3.5-4 km s^{-1} and minimum linear diameter of 2500 AU and assuming an edge-on circular orbit). This is quite a short period of time chemically, although warm-up chemical models like those seen in Crockett et al. (2015) show a sharp increase in abundance from 10^{-10} to 10^{-8} over about 5000 years for CH_3CN. Although N-bearing species are limited to the east side of the disk, N- and O- bearing species formamide (NH_2CHO) and isocyanic acid (HNCO) have a more extended range but show significantly reduced emission at B2 as seen in Figure 2.12. These chemical relationships will be further investigated in a following paper using chemical models.

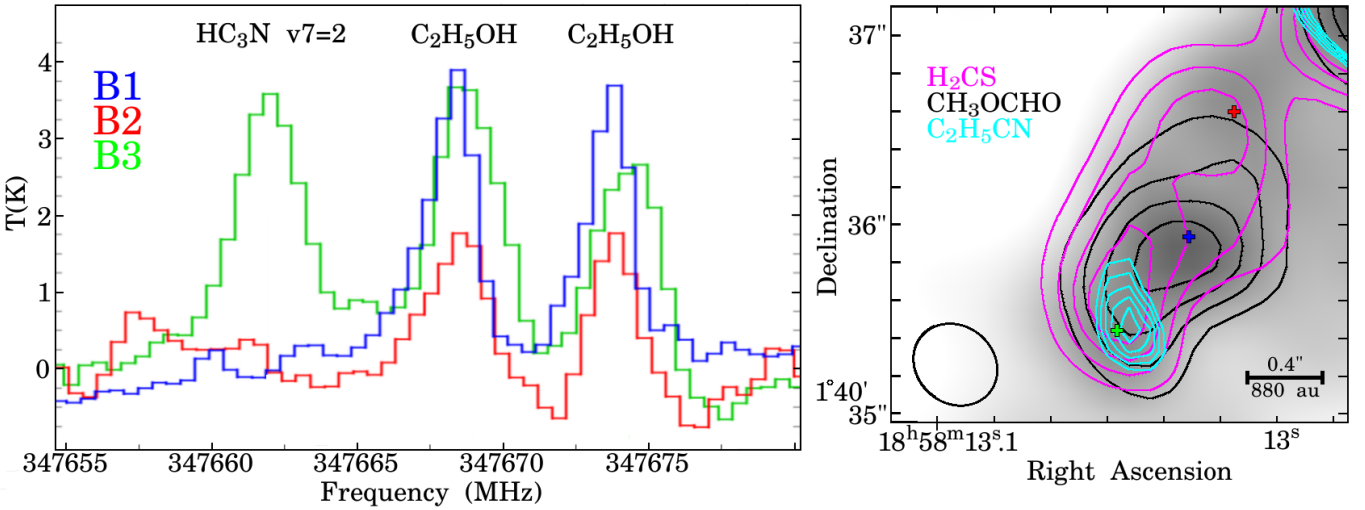

Figure 2.11: G35.20 core B shows clear evidence for small-scale chemical segregation. On the left are spectra extracted from each continuum peak in core B (corresponding to the red, blue, and green crosses in the map to the right). It can clearly be seen in the spectra that the N-bearing species (HC_3N) is only strong in B3, where the O-bearing species (C_2H_5OH) is strong in all 3 regions. On the right, the integrated intensity contours of H_2CS $10_{1,9}$-$9_{1,8}$ (0.55, 0.94, 1.34, and 1.73 Jy/beam km s^{-1}), CH_3OCHO $27_{9,18}$-$26_{9,17}$ (0.70, 1.28, 1.85, and 2.43 Jy/beam km s^{-1}), and C_2H_5CN $40_{1,39}$-$39_{1,38}$ (0.085, 0.100, 0.115, 0.130, and 0.145 Jy/beam km s^{-1}) are shown overlaid on the continuum (grayscale) for core B of G35.20. While the O- and S-bearing organics are distributed across core B, the N-bearing species is only found toward the southwestern part.

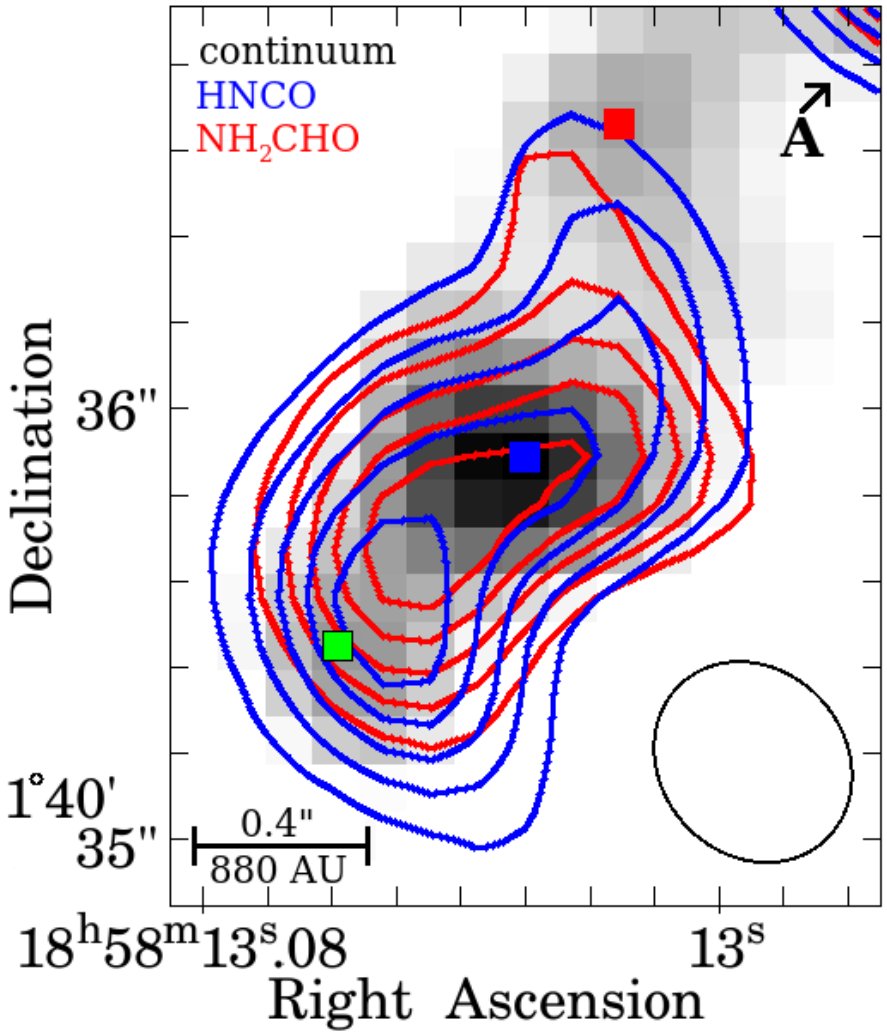

Figure 2.12: Formamide $16_{2,15}$-$15_{2,14}$ (red contours) and HNCO $16_{1,16}$-$15_{1,15}$ (blue contours) emissions are shown overlaid on the dust continuum (grayscale) for core B. These N- and O- bearing species are present in B3 and B1, but B2 is just outside the outermost contour (indicating 1 σ). The red contours are 0.20, 0.33, 0.47, 0.61, and 0.74 Jy/beam km s^{-1} and the blue contours are 0.40, 0.75, 1.10, 1.45, and 1.80 Jy/beam km s^{-1}. B1, B2, and B3 are denoted with colored boxes as in Figure 2.1.

2.4.3 HNCO and Formamide co-spatial emission

It has previously been proposed (Bisschop et al. 2007; Mendoza et al. 2014; López-Sepulcre et al. 2015) based on single dish observations that formamide (NH_2CHO) forms through the hydrogenation of HNCO because there appears to be a constant abundance ratio across a large range of source luminosities and masses. Figure 2.12 shows that these two species have almost the same spatial extent in G35.20 B and their emission peaks are only 0.15″ (or ∼300 AU) apart in G35.20 B. The separation is less than 0.11″ (240 AU) in G35.20 A. The velocity intervals spanned by the line peak velocities in each pixel differ by only 0.5 - 1 km s^{-1}. Our modeled abundance values show N(HNCO)/N(NH_2CHO) is between 2 and 8 for HNCO at 50 K and between 1 and 10 for HNCO modeled at 100 K.

In G35.03, the HNCO and formamide emissions have a separation of less than 0.11″ (255 AU), with the velocity peak differences between 0.5 and 1.0 km s^{-1}. The striking physical connection between these two species makes a strong case for the formation of formamide predominantly through the hydrogenation of HNCO. Coutens et al. (2016) has also recently observed co-spatial emission in HNCO and formamide in the low-mass protobinary system IRAS16293.

2.4.4 Deuteration

We detect seven deuterated species in G35.20, four of which we detect with only one or two observed transitions. We determined the deuterium fractionation of the other three, i.e., CH_2DCN, CH_2DOH, and CH_3CHDCN, using rotation diagrams in Cassis for consistency because CH_2DOH was not in the XCLASS database. From these rotation diagrams, we calculated the D/H values based on the best-fit column densities obtained using the opacity function in Cassis. Relatively little has previously been written about the D/H ratio in methyl cyanide (CH_3CN). In its place of first discovery, Orion KL, the D/H ratio is 0.4-0.9% (Gerin et al. 1992). In a recent paper by Belloche et al. (2016), CH_2DCN was detected in Sgr B2 with a D/H of 0.4%. A D/H for methyl cyanide of 1.3% was also reported in Taquet et al. (2014) in low-mass protostar IRAS 16293-2422. Our values for G35.20 are significantly higher and the varying deuterium fractionation across core B is

quite pronounced for this species. The D/H range in methyl cyanide for each continuum peak is 1-11% at A, 0.3-6% at B1, and 7-21% at B3. Only one unblended transition of CH_2DCN was detected at continuum peak B2, so the D/H could not be determined. The D/H percentages for methyl cyanide determined using the XCLASS fits were 10% at A, 0.4% at B1, and 15% at B3, which fall within the ranges determined using Cassis. We are therefore justified in using Cassis to determine D/H for methanol.

Table 2.8: Deuterium fractionation percentages (%) at continuum peaks in G35.20 as calculated using Cassis. Deuterated ethyl cyanide is only detected at peak A and determining deuterium fractionation for methyl cyanide was not possible for B2.

Source	CH2DCN / CH3CN	CH2DOH / CH3OH	CH3CHDCN / CH3CH2CN
A	6 ± 5	4^{+4}_{-2}	13^{+13}_{-10}
B1	$3^{+3}_{-2.7}$	4^{+3}_{-2}	x
B2	x	5^{+3}_{-2}	x
B3	12^{+9}_{-5}	6^{+4}_{-3}	x

Deuteration in methanol has been more widely studied. In low-mass star-forming regions the CH_2DOH/CH_3OH abundance fraction has been observed to be about 37% (Parise et al. 2002) in IRAS 16293, and in prestellar core L1544 it was close to 10% (Bizzocchi et al. 2014). For G35.20, the D/H ratio was 3-9% at peaks B1 and B2, 4-12% at B3, and 7-17% at A. These values are very similar across core B, although they are slightly enhanced at B3. It is possible that because the methanol emission is more extended, it is more homogeneous. The extra few percent at B3 could be linked to the high temperature and the possibility that this region has heated up recently allowing any deuterium enhancement on the grain surfaces to be released in the gas phase.

Deuterated ethyl cyanide was detected at A with five unblended transitions, eight partially blended transitions, and two identifiable blended transitions. The errors are larger for this species owing to the line blending, but the D/H value for ethyl cyanide using Cassis was found to be between 3 and 26% with a best-fit value of 12% and the D/H from the XCLASS fit is 19%. A summary of these results is shown in Table 2.8 and Figure 2.13.

In contrast, there is almost no sign of deuteration in G35.03. The

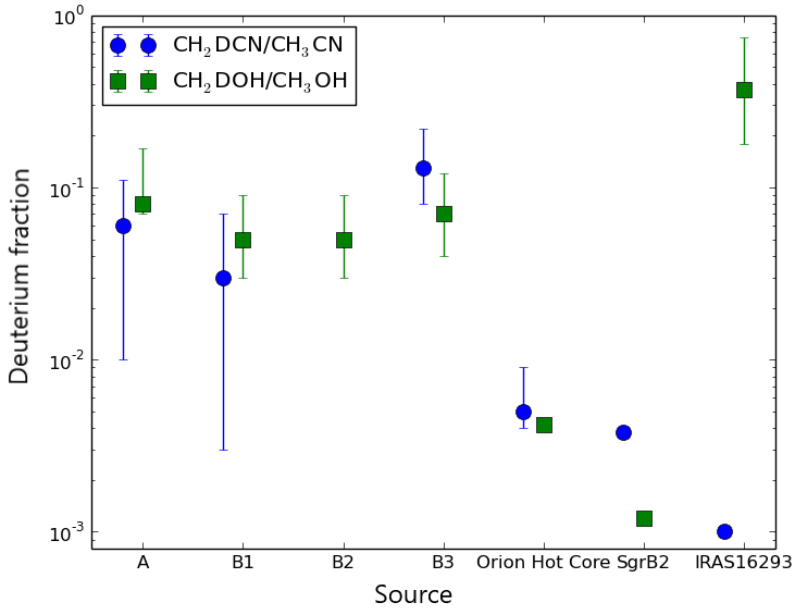

Figure 2.13: D/H fractions for the four continuum peaks in G35.20 compared to the Orion hot core (HC), Sgr B2, and IRAS 16293-2422. The deuterium fractionation in G35.20 is higher than that of other high-mass star-forming regions in Orion and the Galactic center, but lower (for methanol) than in the low-mass star-forming region IRAS 16293. The methyl cyanide D/H value for IRAS 16293 is from an unpublished analysis reported in Taquet et al. (2014).

presence of CH_2DOH is shown through a single line with a brightness temperature of less than 1 K, and HDO is not clearly present as it is either blended with other transitions or offset from v_{LSR} by more than 3 km s^{-1}. HDCO may be present, but is blended with other lines. Our RADEX analysis indicates that the kinetic temperature of the gas around peaks B3 and G35.03 is over 300 K, so the deuterium fraction is unlikely to be tied to the kinetic temperature in these hot cores. From our results there is no clear trend with either mass or temperature and deuterium fraction.

A high fraction of deuterium can indicate that an object is very young ($< 10^5$ years) as deuterated species are formed in cold environments where CO has been depleted onto dust grains (Millar et al. 1989). Once CO returns to the gas phase, deuterated species are destroyed, so a high

deuterium fraction indicates that CO has only sublimated recently. We conclude that B3 is a much younger region than the hot core in G35.03, and in the case of multiple sources within the disk of core B, sublimation of CO from ice grains has happened at different times or rates across the core.

2.4.5 Comparison to other hot cores

The hot core and compact ridge in Orion KL (separation ∼5000 AU) show a chemical difference between N-bearing and O-bearing species. In Caselli et al. (1993a), the authors use a time-dependent model to explain the chemistry of both regions. In this model, shells at different distances were collapsing toward the nearby object IRc2, but when accretion stopped the regions heated up and the grain mantles sublimated showing different chemistry. The model does not perfectly replicate the Orion KL region, but is still a reasonable explanation. In G35.20, there is no clear nearby accreting (or formerly accreting) object that could have caused this same scenario.

The chemical differentiation between W3(OH) and W3(H_2O) shows that the latter is a strong N-bearing source with various complex organics, but the former only contains a handful of O-bearing species (both contain CH_3CN) (Wyrowski et al. 1999b). In Qin et al. (2016), they conclude that this region is undergoing global collapse, but W3(OH) contains an expanding HII region, whereas W3(H_2O) contains a young stellar object that is accreting material but also has an outflow. This is similar to G35.20, but on a larger scale; the separation between these two sources is ∼7000 AU.

Jiménez-Serra et al. (2012) observed that AFGL2591 has a hole in the methanol emission (diameter ∼3000 AU), which is explained using concentric shells where methanol is mainly in a cooler outer shell and S- and N-bearing chemistry are driven by molecular UV photodissociation and high-temperature gas-phase chemistry within the inner shell where the extinction is lower. This differs from G35.20 because the hot N-bearing regions are toward the outer edges of the emission with O- and S-bearing species found between.

Of the three regions where chemical differentiation has been observed, G35.20 core B is most similar to W3(OH) and W3(H_2O). Chemical differences would reasonably be seen if core B contains multiple objects at

different evolutionary stages.

2.5 Conclusions

This work describes the chemical composition of high-mass hot cores in G35.20-0.74N and G35.03+0.35, while providing a template for future chemical study of hot cores in this wavelength regime. Chemical segregation in high-mass star-forming regions is observed on a small scale ($<$ 1000 AU) showing that the high spatial resolution capabilities of ALMA are needed to determine whether such segregation is common. Further observations are needed to determine whether core B in G35.20-0.74N contains a single or multiple sources. While the CH_3CN emission points to Keplerian rotation (Sánchez-Monge et al. 2013a), the continuum implies several protostars and the chemical variation across the proposed disk indicates a complicated source unlike simpler low-mass disks. Both of the regions studied showed co-spatial emission from HNCO and NH_2CHO indicating a chemical link. Various deuterated species were detected at G35.20 peak B3 indicating a very young region. In contrast, G35.03 A shows no obvious deuteration.

Higher spatial resolution ALMA observations of this object will allow us to better resolve the emission from core A and better determine the nature of the velocity gradient there. In addition it may allow us to better determine the origin of the chemical segregation in core B.

The XCLASS software package has a routine that carries out LTE analysis of each point in a map to demonstrate temperature and density differences pixel by pixel. Follow up work will be performed with this LTE analysis and non-LTE map analysis will be carried out with RADEX.

Time-dependent chemical modeling will help to determine if age is a significant factor in the presence of chemical segregation in star-forming regions. A physical chemical model can also help understand the nature of hot cores.

Appendices

Appendix 2.A Properties of detected lines

Table 2.A.1: Detected lines organized by frequency with species, upper energy level (K), and Einstein coefficients (s^{-1}) indicated. Most species are detected in all sources. Ethylene glycol (aGg'$(CH_2OH)_2$) was only detected in G35.20 A and G35.03 A and deuterated ethyl cyanide (CH_3CHDCN) was only detected in G35.20 A. For specific transitions see Appendix B.

Species	**Frequency (MHz)**	**E_{up} (K)**	**A_{ij} (s^{-1})**
CH_3OH ν=0	334970	166.0	3.42E-8
CH_3CHO ν=0	334980	359.9	1.28E-3
CH_3OCHO ν=1	335016	443.5	5.33E-4
aGg'$(CH_2OH)_2$	335030	279.4	9.34E-4
$HC^{13}CCN$ ν=0	335092	305.6	3.01E-3
HDCO	335097	56.2	1.04E-3
CCCS	335109	474.6	2.98E-3
$HCC^{13}CN$ ν=0	335124	305.6	3.01E-3
CH_3OH ν=0	335134	44.7	2.69E-5
CH_3OCHO ν=0	335145	94.9	1.39E-5
CH_3OCHO ν=0	335158	257.1	3.58E-4
$H_2C^{33}S$	335160	101.7	5.53E-4
aGg'$(CH_2OH)_2$	335180	316.7	8.51E-4
CH_3OCHO ν=0	335183	257.1	4.40E-5
t-C_2H_5OH	335192	311.6	5.72E-5
CH_3OCHO ν=0	335208	281.6	3.89E-5
CH_3OH ν=0	335222	336.7	3.85E-8
CH_3CHO ν=2	335224	469.0	8.96E-4
CH_3CHDCN	335229	332.8	3.00E-4
NH_2CDO	335234	170.5	2.61E-3
CH_3CHDCN	335237	332.8	3.20E-3

Table 2.A.1: Detected lines continued.

Species	**Frequency (MHz)**	**E_{up} (K)**	**A_{ij} (s^{-1})**
CH_3CHDCN	335239	332.8	3.20E-3
CH_3CHDCN	335246	332.8	3.00E-4
C_2H_5CN	335274	733.9	1.87E-4
CH_3CHO ν=0	335318	154.9	1.30E-3
aGg'$(CH_2OH)_2$	335357	319.7	8.15E-4
CH_3CHO ν=0	335358	154.8	1.29E-3
CH_3OH ν=0	335363	112.7	8.78E-8
$CH_3^{13}CH_2CN$	335363	386.5	1.74E-4
$CH_3^{13}CH_2CN$	335369	325.9	3.13E-3
CH_3CHO ν=1	335382	361.5	1.31E-3
CH_3OCHO ν=1	335392	453.0	5.66E-3
HDO	335396	335.3	2.61E-5
aGg'$(CH_2OH)_2$	335397	316.7	8.53E-4
CH_3OCHO ν=0	335403	94.9	3.83E-5
$NH_2^{13}CHO$	335403	149.1	2.74E-3
CH_3CHDCN	335427	501.8	2.78E-3
CH_3CHDCN	335430	476.0	2.84E-3
t-C_2H_5OH	335441	293.6	2.17E-4
CH_3OCHO ν=0	335454	94.9	2.44E-5
CH_3CHDCN	335511	330.0	3.18E-3
CH_3CHDCN	335513	430.1	2.95E-3
^{13}CH3OH	335560	192.7	4.04E-4
CH_3OH ν=0	335582	79.0	1.63E-4
t-C_2H_5OH	335631	293.6	2.17E-4
aGg'$(CH_2OH)_2$	335657	288.7	2.98E-4
CH_3OH ν=0	335702	1074.0	5.64E-5
aGg'$(CH_2OH)_2$	335739	304.8	9.77E-4
H^{13}CCCN ν_7=1	335760	632.5	3.01E-3
$CH_3^{18}OH$	335775	218.4	9.61E-4
CH_2DOH	335796	381.1	3.98E-5
$H_2C^{18}O$	335815	60.2	1.05E-3
CH_3OCHO ν=0	335828	225.2	3.95E-5
CH_3OCHO ν=0	335839	225.2	6.97E-4
HC^{13}CCN ν_7=1	335883	622.2	3.01E-3
C_2H_5CN	335895	664.1	1.85E-4
CH_3OCHO ν=0	335900	277.8	2.69E-4
aGg'$(CH_2OH)_2$	335906	308.9	7.63E-4
HCC13CN (v6=1)	335921	1009.6	3.02E-3
HCC^{13}CN ν_7=1	335930	624.7	3.01E-3

Table 2.A.1: Detected lines continued.

Species	**Frequency (MHz)**	**E_{up} (K)**	**A_{ij} (s^{-1})**
t-C_2H_5OH	335950	87.9	1.61E-4
CH_3OCHO ν=1	335961	443.6	5.34E-4
CH_3CHDCN	335989	478.7	1.75E-4
CH_2DOH	335997	94.4	1.12E-4
aGg'$(CH_2OH)_2$	336012	309.6	8.39E-4
CH_3CHO ν=2	336025	535.3	1.31E-3
CH_3OCHO ν=0	336028	277.8	5.14E-4
g-C_2H_5OH	336030	227.3	3.35E-4
CH_3OCHO ν=0	336032	277.8	5.39E-3
CH_3OCHO ν=0	336086	277.9	5.39E-3
SO_2	336089	276.0	2.67E-4
$CH_3^{18}OH$	336100	35.1	1.83E-4
CH_3OCHO ν=0	336111	277.9	5.15E-4
NH_2CHO ν=0	336136	149.7	2.76E-3
t-C_2H_5OH	336158	274.2	2.17E-4
NH_2CHO ν=0	336161	135.5	1.20E-4
CH_3OCHO ν=0	336219	277.9	2.70E-4
aGg'$(CH_2OH)_2$	336223	304.7	7.84E-4
$H^{13}CCCN$ ν_7=1	336227	632.9	3.02E-3
t-C_2H_5OH	336270	274.2	2.17E-4
aGg'$(CH_2OH)_2$	336323	288.4	9.23E-4
CH_2DOH	336325	442.1	1.35E-4
aGg'$(CH_2OH)_2$	336334	301.9	8.63E-4
CH_3OCHO ν=0	336351	249.4	5.49E-4
CH_3OCHO ν=0	336355	230.6	9.84E-3
CH_3OCHO ν=0	336368	249.4	5.49E-4
CH_3OCHO ν=0	336374	230.6	5.57E-4
$HCC^{13}CN$ ν_7=1	336410	625.1	3.03E-3
CH_3CHO ν=1	336416	359.6	1.30E-3
CH_3CHDCN	336425	361.4	3.13E-3
CH_3OH ν=0	336438	488.2	3.63E-5
CH_3CHDCN	336453	361.4	3.13E-3
HC_3N (ν=0)	336520	306.9	3.05E-3
SO	336553	142.9	6.25E-6
g-C_2H_5OH	336572	232.3	3.37E-4
CH_3OH ν=2	336606	747.4	1.63E-4
C_2H_5CN	336614	108.2	1.01E-4
t-C_2H_5OH	336626	162.6	1.34E-4
SO_2	336670	245.1	5.84E-5

Table 2.A.1: Detected lines continued.

Species	**Frequency (MHz)**	**E_{up} (K)**	**A_{ij} (s^{-1})**
$CH_3^{18}OH$	336743	100.9	1.50E-4
aGg'$(CH_2OH)_2$	336756	316.7	9.45E-4
t-C_2H_5OH	336767	255.7	2.16E-4
g-C_2H_5OH	336795	228.0	3.42E-4
aGg'$(CH_2OH)_2$	336828	266.3	8.95E-4
t-C_2H_5OH	336832	255.7	2.16E-4
CH_3OH ν=0	336865	197.1	4.07E-4
CH_3OCHO ν=0	336889	235.5	5.53E-4
CH_3OCHO ν=0	336918	235.5	5.53E-4
aGg'$(CH_2OH)_2$	336939	300.6	8.63E-4
CH_3OH ν=2	336970	1022.7	4.56E-5
CH_3OH ν=2	337022	971.8	1.36E-4
CH_3OH ν=2	337030	941.4	1.55E-4
C_2H_3CN	337040	309.7	3.19E-3
C_2H_3CN	337051	308.4	3.14E-3
C17O	337060	32.0	2.32E-6
CH_3OH ν=2	337066	943.1	1.12E-4
HC_3N ν_6=1	337070	1025.1	3.05E-3
CH_3OH ν=2	337079	901.5	8.38E-5
CH_3CHO ν=2	337082	526.1	1.26E-3
aGg'$(CH_2OH)_2$	337082	309.1	5.46E-4
CH_3OH ν=2	337099	935.2	8.14E-5
CH_3OH ν=2	337114	855.8	1.65E-4
CH_3OH ν=2	337118	932.6	4.41E-5
$H_2C^{34}S$	337125	89.1	5.77E-4
CH_3OH ν=0	337136	61.6	1.58E-5
CH_3OH ν=2	337159	755.0	4.54E-5
CH_3OH ν=2	337175	801.4	1.15E-4
CH_3OH ν=2	337186	791.1	1.68E-4
CH_3OH ν=2	337198	690.2	8.26E-5
CH_3OH ν=2	337252	722.8	1.39E-4
CH_3OH ν=2	337274	679.3	1.13E-4
CH_3OH ν=2	337279	701.8	1.54E-4
CH_3OH ν=2	337284	573.0	2.16E-4
CH_3OH ν=1	337297	390.0	1.65E-4
CH_3OH ν=1	337303	651.0	1.55E-4
CH_3OH ν=2	337312	588.9	1.65E-4
t-C_2H_5OH	337323	238.0	2.15E-4
HC_3N ν_6=1	337335	1025.3	3.06E-3

Table 2.A.1: Detected lines continued.

Species	**Frequency (MHz)**	**E_{up} (K)**	**A_{ij} (s^{-1})**
HC_3N ν_7=1	337344	629.0	3.05E-3
C_2H_5CN	337347	322.4	3.23E-3
CH_2DOH	337349	96.3	1.46E-4
$C^{34}S$	337400	64.8	8.04E-4
CH_3OCH_3	337421	220.1	1.76E-4
t-HCOOH	337429	386.6	2.80E-4
t-HCOOH	337436	446.8	2.43E-4
t-HCOOH	337444	332.8	3.13E-4
C_2H_5CN	337445	322.4	3.23E-3
$H_2C^{34}S$	337460	299.8	4.86E-4
CH_3OH ν=1	337464	357.5	1.69E-4
CH_3OH ν=1	337473	908.0	3.6E-4
$H_2C^{34}S$	337475	141.8	5.56E-4
CH_3OCHO ν=0	337490	267.1	5.34E-4
CH_3OH ν=1	337491	558.2	4.34E-5
t-HCOOH	337492	110.5	2.35E-3
CH_3OCHO ν=0	337504	267.1	5.34E-4
CH_3OH ν=1	337519	482.2	1.38E-4
CH_3OH ν=1	337546	485.4	8.13E-5
$H_2C^{34}S$	337555	207.7	5.27E-4
$H_2C^{34}S$	337559	207.7	5.27E-4
CH_3OH ν=1	337582	428.2	1.13E-4
t-HCOOH	337590	243.9	3.68E-4
CH_3OH ν=1	337605	429.4	1.56E-4
CH_3OH ν=1	337611	387.4	1.37E-4
CH_3OH ν=1	337626	363.5	1.55E-4
CH_3OH ν=1	337636	363.5	1.55E-4
CH_3OH ν=1	337642	356.3	1.65E-4
CH_3OH ν=1	337644	365.4	1.69E-4
CH_3OH ν=1	337646	470.2	1.14E-4
CH_3OH ν=1	337648	611.0	8.23E-5
CH_3OH ν=1	337655	460.9	1.38E-4
CH_3OH ν=1	337671	464.7	1.56E-4
CH_3OH ν=1	337685	545.9	1.14E-4
CH_3OH ν=1	337708	478.2	1.65E-4
CH_3OCH_3	337712	48.0	7.22E-5
CH_3OCH_3	337722	48.0	9.63E-5
t-C_2H_5OH	337727	221.2	2.13E-4
CH_3OCH_3	337731	48.0	1.94E-4

Table 2.A.1: Detected lines continued.

Species	**Frequency (MHz)**	$\mathbf{E}_{up}$ **(K)**	$\mathbf{A}_{ij}$ **(s^{-1})**
CH_3OH ν=1	337749	488.5	1.69E-4
CH_3OCH_3	337770	48.0	1.22E-4
CH_3OCH_3	337779	48.0	1.94E-4
CH_3OCH_3	337787	48.0	1.94E-4
CH_3OCH_3	337790	48.0	7.22E-5
g-C_2H_5OH	337801	223.1	3.45E-4
aGg'$(CH_2OH)_2$	337816	294.6	9.74E-4
HC_3N ν_7=1	337825	629.0	3.07E-3
CH_3OH ν=0	337838	675.9	6.04E-5
CH_3OH ν=2	337878	747.7	1.65E-4
$H_2C^{34}S$	337933	141.9	5.58E-4
$CH_3^{13}CH_2CN$	337951	332.2	3.21E-3
CH_3OH ν=1	337969	390.1	1.66E-4
CH_2DOH	337977	202.5	5.47E-5
D_2CO	338016	342.8	1.04E-6
H_2CS	338083	102.4	5.77E-4
t-C_2H_5OH	338099	205.2	2.11E-4
t-C_2H_5OH	338110	205.2	2.11E-4
CH_3OH ν=0	338125	78.1	1.70E-4
C_2H_5CN	338142	316.8	3.27E-3
t-HCOOH	338144	180.5	4.09E-4
t-HCOOH	338202	158.3	4.23E-4
C_2H_3CN	338214	312.1	3.23E-3
aGg'$(CH_2OH)_2$	338214	313.4	9.40E-4
aGg'$(CH_2OH)_2$	338221	292.7	8.05E-4
aGg'$(CH_2OH)_2$	338240	313.4	9.28E-4
t-HCOOH	338249	180.5	4.09E-4
C_2H_3CN	338278	300.1	3.22E-3
SO_2	338306	196.8	3.27E-4
$^{34}SO_2$	338320	92.5	2.27E-4
CH_3OCHO ν=0	338338	267.2	5.92E-3
CH_3OH ν=0	338345	70.5	1.67E-4
CH_3OCHO ν=0	338356	267.2	5.39E-4
CH_3OCHO ν=1	338393	443.1	4.61E-3
CH_3OCHO ν=0	338396	257.7	5.50E-4
CH_3OH ν=0	338405	243.8	4.48E-5
CH_3OH ν=0	338409	65.0	1.70E-4
CH_3OCHO ν=0	338414	257.7	5.50E-4
CH_3OH ν=0	338431	253.9	4.51E-5

Table 2.A.1: Detected lines continued.

Species	**Frequency (MHz)**	**E_{up} (K)**	**A_{ij} (s^{-1})**
CH_3OH ν=0	338442	258.7	4.50E-5
C_2H_3CN	338448	312.0	3.24E-3
CH_3OH ν=0	338456	189.0	8.31E-5
CH_2DOH	338463	120.0	5.87E-5
CH_3OH ν=0	338475	201.1	8.30E-5
CH_3OH ν=0	338486	202.9	8.35E-5
CH_3OH ν=0	338504	152.9	1.14E-4
CH_3OH ν=0	338512	145.3	1.15E-4
CH_3OH ν=0	338530	161.0	1.15E-4
CH_3OH ν=0	338541	114.8	1.39E-4
CH_3OH ν=0	338543	114.8	1.39E-4
CH_3OH ν=0	338560	127.7	1.40E-4
CH_3OH ν=0	338583	112.7	1.39E-4
SO_2	338612	198.9	2.87E-4
CH_3OH ν=0	338615	86.1	1.71E-4
CH_3OH ν=0	338640	102.7	1.57E-4
HC_3N ν_7=2	338646	953.8	3.07E-3
t-C_2H_5OH	338672	175.7	2.04E-4
t-C_2H_5OH	338674	175.7	2.04E-4
CH_2DOH	346924	521.6	1.30E-4
C_2H_5CN	346925	161.4	1.64E-4
g-C_2H_5OH	346929	280.5	3.45E-4
CH_3CHO ν=0	346934	268.7	1.22E-3
g-C_2H_5OH	346939	280.5	3.45E-4
C_2H_3CN	346943	325.0	3.46E-3
HC_3N ν_7=1	346949	645.6	3.32E-3
CH_3CHO ν=0	346957	268.6	1.22E-3
t-C_2H_5OH	346963	185.8	2.42E-4
C_2H_5CN	346970	104.6	1.20E-4
C_2H_5CN	346976	129.6	1.49E-4
C_2H_5CN	346979	122.7	1.44E-4
$H_2C^{18}O$	346984	239.6	4.33E-4
$H^{13}CO^+$	346998	41.6	3.29E-3
CH_2DCN	347043	175.0	3.65E-3
CH_3CHO ν=0	347071	239.4	1.28E-3
CH_3CHO ν=0	347090	239.4	1.28E-3
CH_2DCN	347110	309.7	3.42E-3
$H_2C^{18}O$	347133	156.7	7.70E-4
CH_3CHO ν=0	347133	239.3	1.28E-3

Table 2.A.1: Detected lines continued.

Species	**Frequency (MHz)**	**E_{up} (K)**	**A_{ij} (s^{-1})**
$H_2C^{18}O$	347144	156.7	7.70E-4
g-C_2H_5OH	347147	275.5	3.45E-4
g-C_2H_5OH	347158	275.5	3.45E-4
CH_2DCN	347166	261.2	3.52E-3
^{13}CH3OH	347188	254.3	4.36E-4
CH_2DCN	347216	223.5	3.50E-3
CH_3CHO ν=1	347217	420.4	1.33E-3
CH_2DCN	347219	223.5	3.57E-3
CH_2DOH	347222	521.6	1.32E-4
C_2H_3CN	347232	328.7	3.50E-3
CH_3CHO ν=1	347252	419.7	1.33E-3
CH_3CHO ν=0	347288	214.7	1.33E-3
CH_3CHO ν=0	347295	214.7	1.33E-3
SiO	347330	75.0	2.21E-3
CH_3CHO ν=0	347345	214.6	1.33E-3
CH_3CHO ν=0	347349	214.6	1.33E-3
t-C_2H_5OH	347351	99.7	1.75E-4
aGg'$(CH_2OH)_2$	347361	330.4	1.02E-3
CH_3OH ν=0	347370	45.5	1.08E-8
CH_2DOH	347371	478.8	1.30E-4
aGg'$(CH_2OH)_2$	347378	330.4	1.01E-3
aGg'$(CH_2OH)_2$	347387	282.6	9.81E-4
CH_2DCN	347388	196.6	3.62E-3
C_2H_3CN	347434	328.7	3.46E-3
t-C_2H_5OH	347446	185.9	2.67E-4
CH_3OH ν=1	347448	856.3	4.04E-5
CH_3CHO ν=1	347459	473.2	1.22E-3
g-C_2H_5OH	347474	267.1	3.57E-4
CH_3OCHO ν=0	347478	247.3	6.14E-4
aGg'$(CH_2OH)_2$	347487	317.0	9.51E-4
CH_3OCHO ν=0	347494	247.3	6.14E-4
CH_3OH ν=0	347507	57.1	1.78E-8
CH_3CHO ν=0	347519	178.7	1.41E-3
CH_3CHO ν=0	347563	178.1	1.41E-3
CH_3OCHO ν=1	347568	460.2	4.88E-3
$NH_2CH^{18}O$	347589	161.0	3.10E-3
CH_3OCHO ν=0	347590	104.4	4.00E-5
CH_3OCHO ν=0	347599	104.4	3.40E-5
CH_3OCHO ν=0	347605	306.8	5.49E-4

Table 2.A.1: Detected lines continued.

Species	**Frequency (MHz)**	**E_{up} (K)**	**A_{ij} (s^{-1})**
CH_2DOH	347610	478.8	1.31E-4
CH_3OCHO ν=0	347617	306.8	5.59E-4
CH_3OCHO ν=0	347628	306.8	5.49E-4
CH_3CHO ν=1	347645	507.4	2.50E-5
CH_3CHO ν=0	347650	194.5	1.38E-3
CH_3CHO ν=2	347657	544.7	1.38E-3
HC_3N ν_7=2	347663	967.8	3.33E-3
g-C_2H_5OH	347670	262.2	3.57E-4
g-C_2H_5OH	347675	267.1	3.57E-4
C_2H_3CN	347685	707.5	1.19E-4
g-C_2H_5OH	347693	189.7	1.07E-4
CH_3OCHO ν=1	347698	437.8	6.73E-3
NH_2CHO ν=0	347729	435.3	1.06E-4
aGg'$(CH_2OH)_2$	347732	302.2	9.92E-4
aGg'$(CH_2OH)_2$	347738	317.0	9.52E-4
CH_3OH ν=0	347745	71.0	2.64E-8
g-C_2H_5OH	347755	256.2	3.66E-4
CH_3CHO ν=0	347756	194.4	1.36E-3
C_2H_3CN	347759	316.7	3.50E-3
CH_2DOH	347767	438.2	1.29E-4
^{13}CH3OH	347788	302.5	6.74E-5
HC_3N ν_7=2	347791	970.5	3.32E-3
aGg'$(CH_2OH)_2$	347813	115.3	1.12E-4
CH_3CHDCN	347816	354.3	3.56E-3
CH_3OCHO ν=0	347818	274.0	3.40E-4
aGg'$(CH_2OH)_2$	347821	115.0	1.22E-4
CH_3CHO ν=0	347830	194.5	1.36E-3
CH_3CHO ν=0	347838	194.5	1.38E-3
^{13}CH3OH	347848	572.9	7.63E-5
$CH_3^{18}OH$	347865	142.7	1.51E-4
g-C_2H_5OH	347887	262.2	3.58E-4
g-C_2H_5OH	347916	251.4	3.67E-4
HC_3N ν_7=2	347924	970.6	3.33E-3
CH_2DOH	347953	438.2	1.30E-4
aGg'$(CH_2OH)_2$	347963	108.4	1.39E-4
t-C_2H_5OH	347975	222.1	1.01E-4
CH_3OCH_3	347985	581.8	1.18E-4
CH_3OCH_3	347989	581.8	1.87E-4
CH_3OCH_3	347992	581.8	1.87E-4

Table 2.A.1: Detected lines continued.

Species	**Frequency (MHz)**	**E_{up} (K)**	**A_{ij} (s^{-1})**
$NH_2CH^{18}O$	348029	154.7	3.10E-3
$H_2C^{18}O$	348032	97.5	1.02E-3
CH_3OCHO ν=0	348050	266.1	6.10E-4
CH_3OCHO ν=1	348053	491.3	4.67E-5
$CH_3^{18}OH$	348053	283.4	1.04E-3
CH_3OCHO ν=0	348066	266.1	6.10E-4
CH_3OCHO ν=1	348084	469.7	5.58E-4
CH_3CHO ν=1	348088	443.3	1.28E-3
^{13}CH3OH	348100	162.4	1.08E-4
CH_3OH ν=0	348123	87.3	3.27E-8
^{13}CH3CH2CN	348147	352.3	3.51E-3
CH_2DOH	348161	38.2	2.03E-4
CH_3CHO ν=1	348211	383.2	1.41E-3
CH_3CHO ν=1	348229	400.0	1.38E-3
CH_3OCHO ν=1	348247	267.6	1.00E-4
C_2H_5CN	348260	343.8	3.57E-3
NH_2CDO	348283	162.4	3.11E-3
CH_3CHO ν=1	348288	385.2	1.41E-3
aGg'$(CH_2OH)_2$	348326	325.8	4.16E-4
aGg'$(CH_2OH)_2$	348331	311.2	1.04E-3
$HN^{13}C$	348340	41.8	2.03E-3
C_2H_5CN	348344	351.0	3.58E-3
SO_2	348388	292.7	1.91E-4
CH_2DOH	348427	363.3	1.27E-4
$^{33}SO_2$$	348492	110.2	3.19E-4
CH_2DOH	348529	363.3	1.28E-4
H_2CS	348532	105.2	6.30E-4
aGg'$(CH_2OH)_2$	348550	329.1	6.50E-4
C_2H_5CN	348553	351.0	3.59E-3
CH_3CHO ν=1	348570	418.2	1.34E-3
CH_3CHO ν=1	348578	418.2	1.34E-3
CH_2DOH	348592	139.7	6.76E-5
CH_2DOH	348668	219.2	2.04E-5
CH_3OH ν=0	348682	105.8	3.19E-8
CH_2DCN	348691	181.2	3.69E-3
CH_2DOH	348699	329.0	1.26E-4
g-C_2H_5OH	348720	89.6	2.33E-4
$CH_3^{13}CN$	348854	624.3	3.05E-3
CH_3CHO ν=1	348855	398.3	1.38E-3

Table 2.A.1: Detected lines continued.

Species	**Frequency (MHz)**	**E_{up} (K)**	**A_{ij} (s^{-1})**
CH_3OCHO ν=0	348909	294.6	4.65E-3
CH_3CN ν=0	348911	745.4	2.87E-3
CH_3OCHO ν=0	348915	294.6	5.72E-4
CH_2DOH	348939	296.9	1.24E-4
$CH_3^{13}CN$	348954	517.3	3.20E-3
CH_2DOH	348990	296.9	1.25E-4
C_2H_3CN	348991	325.1	3.19E-2
CH_3OCHO ν=0	349015	257.3	4.08E-4
NH2CHO (ν=1)	349020	568.5	3.09E-3
CH_3CN ν=0	349025	624.0	2.10E-3
$CH_3^{13}CN$	349040	424.6	3.34E-3
CH_3OCHO ν=0	349049	294.6	5.72E-4
NH_2CHO ν=0	349053	220.7	9.00E-5
CH_3OCHO ν=0	349066	294.6	5.82E-4
CH_3OH ν=0	349107	260.2	4.41E-4
$CH_3^{13}CN$	349114	346.1	3.45E-3
CH_3CN ν=0	349125	517.0	3.21E-3
CH_2DOH	349149	267.0	1.23E-4
$CH_3^{13}CN$	349174	281.9	3.55E-3
CH_2DOH	349184	267.0	1.23E-4
CH_3CN ν=0	349212	424.7	3.34E-3
$CH_3^{13}CN$	349222	231.9	3.62E-3
$CH_3^{13}CN$	349254	196.2	3.67E-3
$CH_3^{13}CN$	349274	174.8	2.38E-3
$CH_3^{13}CN$	349280	167.6	1.47E-3
CH_3CN ν=0	349286	346.2	2.38E-3
$NH_2^{13}CHO$	349309	152.6	3.1E-3
CH_3CHO ν=1	349320	369.3	1.47E-3
c-HCOOH	349326	157.4	1.66E-3
CH_2DOH	349334	239.1	1.21E-4
CH_3CN ν=0	349346	282.0	2.45E-3
aGg'$(CH_2OH)_2$	349355	309.2	6.03E-4
CH_2DOH	349356	239.1	1.21E-4
C_2H_5CN	349380	495.2	3.29E-3
CH_3CN ν=0	349393	232.0	2.50E-3
CH_2DOH	349411	230.3	7.95E-5
CH_3CN ν=0	349427	196.3	2.54E-3
CH_3CN ν=0	349447	174.9	2.56E-3
CH_3CN ν=0	349453	167.7	2.56E-3

Table 2.A.1: Detected lines continued.

Species	**Frequency (MHz)**	**E_{up} (K)**	**A_{ij} (s^{-1})**
CH_3OH ν=0	349470	118.8	1.92E-8
NH_2CHO ν=0	349482	153.0	3.10E-3
CH_3OCH_3	349487	475.7	6.54E-5
CH_2DOH	349495	213.4	1.18E-4
CH_2DOH	349509	213.4	1.18E-4
aGg'$(CH_2OH)_2$	349541	294.9	8.31E-4
C_2H_5CN	349547	425.4	3.44E-3
C_2H_5CN	349566	618.9	3.03E-3
D_2CO	349630	80.4	1.11E-3
CH_2DOH	349636	189.9	1.15E-4
CH_2DOH	349644	189.9	1.15E-4
C_2H_5CN	349652	655.3	2.95E-3
CH_3OCHO ν=1	349685	459.9	6.26E-4
C_2H_5CN	349730	406.6	3.49E-3
C_2H_5CN	349751	693.8	2.87E-3
CH_3CHO ν=2	349752	565.7	1.40E-3
CH_2DOH	349757	168.5	1.11E-4
CH_2DOH	349762	168.5	1.11E-4
C_2H_5CN	349796	353.9	3.61E-3
CH_3OCH_3	349803	66.5	3.30E-5
CH_3OCH_3	349806	66.5	3.30E-5
CH_3OCH_3	349809	66.5	3.30E-5
CH_3OCH_3	349823	326.0	1.15E-5
CH_3OCH_3	349826	326.0	1.15E-5
CH_3OCH_3	349828	326.0	1.15E-5
CH_3OCH_3	349830	326.0	1.15E-5
CH_3OCHO ν=1	349836	401.3	3.32E-5
CH_2DOH	349862	149.2	1.07E-4
CH_2DOH	349864	149.2	1.07E-4
aGg'$(CH_2OH)_2$	349867	338.1	1.04E-3
CH_3CHDCN	349907	360.9	3.63E-3
CH_2DOH	349952	132.1	1.00E-4
g-C_2H_5OH	349997	256.5	3.73E-4
aGg'$(CH_2OH)_2$	350023	305.1	1.11E-3
CH_2DOH	350027	117.1	9.06E-5
C_2H_5CN	350039	390.1	3.54E-3
C_2H_5CN	350051	390.1	3.54E-3
CH_3CN v_8=1	350059	1136.0	3.01E-3
CH_2DOH	350090	104.2	7.58E-5

Table 2.A.1: Detected lines continued.

Species	**Frequency (MHz)**	**E_{up} (K)**	**A_{ij} (s^{-1})**
^{13}CH3OH	350103	16.8	3.29E-4
CH_3CHO ν=0	350135	179.2	1.44E-3
CH_2DOH	350141	93.5	5.04E-5
aGg'$(CH_2OH)_2$	350142	326.2	7.96E-4
C_2H_5CN	350145	356.1	3.65E-3
CH_3CN v_8=1	350160	1030.0	3.13E-3
CH_3CN v_8=1	350168	687.1	3.46E-3
CH_3CN v_8=1	350190	1142.9	2.87E-3
$CH_3^{18}OH$	350246	43.0	2.96E-4
CH_3CN v_8=1	350247	938.3	3.23E-3
CH_3CN v_8=1	350277	949.5	3.00E-3
CH_3OH ν=1	350288	694.8	2.10E-4
$^{33}SO_2$$	350303	89.1	3.07E-4
CH_3CN v_8=1	350320	860.8	3.55E-3
HNCO	350333	186.2	5.97E-4
CH_3CN v_8=1	350352	870.2	3.14E-3
CH_3CHO ν=0	350363	163.5	1.47E-3
g-C_2H_5OH	350365	251.7	3.75E-4
CH_3CN v_8=1	350380	797.5	3.39E-3
aGg'$(CH_2OH)_2$	350402	327.7	1.91E-4
CH_3CN v_8=1	350415	805.2	3.24E-3
^{13}CH3OH	350422	102.6	7.03E-5
CH_3OCHO ν=0	350442	283.9	4.91E-3
CH_3CHO ν=0	350445	163.4	1.47E-3
CH_3CN v_8=1	350450	713.8	3.47E-3
CH_2DOH	350454	71.6	1.39E-4
CH_3OCHO ν=0	350458	283.9	4.91E-3
CH_3CN v_8=1	350465	754.4	3.33E-3
CH_3CN v_8=1	350507	717.7	3.40E-3
C_2H_5CN	350512	375.9	3.58E-3
t-C_2H_5OH	350534	179.0	1.51E-4
CH_3CN v_8=1	350552	695.4	3.45E-3
CH_2DOH	350632	49.0	2.07E-4

Appendix 2.B Line properties per core (organized by species)

Table 2.B.1: Single line detections

Species	Transition	Frequency	G35.20 A		G35.20 B1		G35.20 B2		G35.20 B3		G35.03 A	
		(MHz)	FWHM (km s^{-1})	T_{peak} (K)	FWHM (km s^{-1})	T_{peak} (K)	FWHM (km s^{-1})	T_{peak} (K)	FWHM (km s^{-1})	T_{peak} (K)	FWHM (km s^{-1})	T_{peak} (K)
2 atom												
SiO	8 - 7	347330	6.18 ± 0.10	10.4 ± 0.1	6.0 ± 0.4	7.9 ± 0.2	1.7 ± 0.5	2.0 ± 0.4	3.1 ± 0.6	2.8 ± 0.3	blended	
SO	10(11)-10(10)	336553	7.1 ± 0.8	4.0 ± 0.3	7.3 ± 0.3	5.1 ± 0.2	3.1 ± 0.6	1.7 ± 0.3	3.28 ± 0.09	6.4 ± 0.1	9.2 ± 0.3	5.7 ± 0.2
$C^{34}S$	7 - 6	337400	4.7 ± 0.4	51.7 ± 8.4	2.7 ± 0.2	24.1 ± 0.7	2.4 ± 0.1	24.5 ± 0.8	2.7 ± 0.1	36.1 ± 0.6	7.6 ± 0.2	23.3 ± 0.5
$C^{17}O$	3 - 2	337060	blended		1.9 ± 0.9	2.5 ± 0.6	2.3 ± 0.3	5.4 ± 0.3	2.83 ± 0.06	5.48 ± 0.08	4.6 ± 0.2	9.7 ± 0.5
3 atom												
HDO	$3_{3,1}$-$4_{2,2}$	335396	⋆6.9 ± 0.3	18.4 ± 0.4	2.5 ± 0.1	8.9 ± 0.2	1.6 ± 0.2	2.6 ± 0.2	2.8 ± 0.1	19.0 ± 0.8	offset by 3km s^{-1} or blended	
$H^{13}CO^+$	4 - 3	346998	1.33 ± 0.06	7.8 ± 0.3	2.2 ± 0.1	11.4 ± 0.4	3.0 ± 0.3	14.9 ± 1.0	2.2 ± 0.2	7.9 ± 0.6	3.8 ± 0.1	9.1 ± 0.3
$HN^{13}C$	4 - 3	348340	5.5 ± 0.2	9.6 ± 0.3	2.0 ± 0.1	4.2 ± 0.2	1.9 ± 0.3	4.3 ± 0.4	3.3 ± 0.2	25.9 ± 0.7	5.4 ± 0.5	4.6 ± 0.1
4 atom												
HNCO	$16_{1,16}$-$15_{1,15}$	350333	6.5 ± 0.3	46.3 ± 1.9	6.1 ± 0.2	14.4 ± 0.3	2.7 ± 0.4	5.3 ± 0.7	3.44 ± 0.09	30.1 ± 0.5	4.55 ± 0.09	11.0 ± 0.2
CCCS	58 - 57	335109	6.7 ± 0.1	3.26 ± 0.4	$< 3\sigma$		$< 3\sigma$		1.8 ± 0.6	0.8 ± 0.1	blended	

⋆ double peaked

Table 2.B.2: Formaldehyde

Transition	Frequency (MHz)	G35.20 A FWHM (km s^{-1})	G35.20 A T_{peak} (K)	G35.20 B1 FWHM (km s^{-1})	G35.20 B1 T_{peak} (K)	G35.20 B2 FWHM (km s^{-1})	G35.20 B2 T_{peak} (K)	G35.20 B3 FWHM (km s^{-1})	G35.20 B3 T_{peak} (K)	G35.03 A FWHM (km s^{-1})	G35.03 A T_{peak} (K)
$H_2C^{18}O$											
$5_{1,5}$- $4_{1,4}$ o	335815	4.9 ± 0.2	3.7 ± 0.1	2.3 ± 0.1	5.7 ± 0.2	1.6 ± 0.2	3.0 ± 0.2	2.23 ± 0.03	16.4 ± 0.1	3.4 ± 0.1	2.65 ± 0.08
$5_{4,2}$- $4_{4,1}$ p	346984	4.4 ± 0.2	8.6 ± 0.2	2.2 ± 0.2	2.1 ± 0.2	1.7 ± 0.2	2.0 ± 0.2	2.4 ± 0.2	5.8 ± 0.1	blended	
$5_{3,3}$- $4_{3,2}$ o	347133	6.4 ± 0.1	6.93 ± 0.09	2.2 ± 2.0	2.1 ± 2.0	2.1 ± 0.4	1.9 ± 0.2	2.46 ± 0.04	9.7 ± 0.1	blended	
$5_{3,2}$- $4_{3,1}$ o	347144	blended		1.5 ± 0.2	3.3 ± 0.2	3.1 ± 0.5	1.1 ± 0.1	1.78 ± 0.06	6.8 ± 0.2	blended	
$5_{2,3}$- $4_{2,2}$ p	348032	5.6 ± 0.1	5.36 ± 0.09	1.7 ± 0.2	2.6 ± 0.1	1.3 ± 0.6	1.4 ± 0.3	2.08 ± 0.05	7.2 ± 0.1	4.1 ± 0.3	2.5 ± 0.1
HDCO											
$5_{1,4}$- $4_{1,3}$	335097	⋆6.6 ± 1.0	8.3 ± 0.4	2.90 ± 0.08	11.6 ± 0.2	1.77 ± 0.10	6.9 ± 0.4	2.6 ± 0.1	32.3 ± 0.6	< 3σ	
D_2CO											
$13_{4,9}$- $14_{2,12}$	338016	1.6 ± 0.2	0.48 ± 0.04	< 3σ		< 3σ		< 3σ		< 3σ	
$6_{2,5}$- $5_{2,4}$	349630	blended		1.2 ± 0.9	0.8 ± 0.1	1.7 ± 0.3	0.54 ± 0.08	2.39 ± 0.09	5.6 ± 0.1	< 3σ	

◇ partially blended with other lines, ⋆ double peaked

Table 2.B.3: Formic Acid

Transition	Frequency (MHz)	G35.20 A FWHM (km s^{-1})	G35.20 A T_{peak} (K)	G35.20 B1 FWHM (km s^{-1})	G35.20 B1 T_{peak} (K)	G35.20 B2 FWHM (km s^{-1})	G35.20 B2 T_{peak} (K)	G35.20 B3 FWHM (km s^{-1})	G35.20 B3 T_{peak} (K)	G35.03 A FWHM (km s^{-1})	G35.03 A T_{peak} (K)
t-HCOOH											
$15_{9,6}$-$14_{9,5}$	337429	5.4 ± 0.4	7.2 ± 0.2	blended		< 3σ		1.7 ± 0.2	1.0 ± 0.1	3.9 ± 0.2	5.6 ± 0.1
$15_{10,6}$-$14_{10,5}$	337436	4.4 ± 0.4	6.1 ± 0.2	blended		< 3σ		1.9 ± 0.4	0.8 ± 0.1	5.5 ± 0.4	4.96 ± 0.09
$15_{8,7}$-$14_{8,6}$	337444	blended		blended		< 3σ		blended		5.3 ± 0.1	7.38 ± 0.09
$15_{7,8}$-$14_{7,7}$	337492	blended		blended		blended		2.1 ± 0.8	7.2 ± 0.7	< 3σ	
$15_{6,10}$-$14_{6,9}$	337590	4.7 ± 0.4	14.1 ± 0.8	blended		< 3σ		2.7 ± 0.1	2.55 ± 0.08	5.9 ± 0.2	8.5 ± 0.2
$15_{5,11}$-$14_{5,10}$	337785	blended		blended		blended		blended		< 3σ	
$15_{4,12}$-$14_{4,11}$	338144	blended		2.99 ± 0.05	1.90 ± 0.05	blended		blended		7.0 ± 0.2	7.9 ± 0.2
$15_{3,13}$-$14_{3,12}$	338202	4.7 ± 0.3	14.5 ± 0.3	2.2 ± 0.8	1.8 ± 0.5	1.4 ± 0.3	0.64 ± 0.10	3.2 ± 0.1	3.4 ± 0.1	6.8 ± 0.2	8.2 ± 0.2
$15_{4,11}$-$14_{4,10}$	338249	5.3 ± 0.2	13.9 ± 0.3	1.8 ± 0.3	2.2 ± 0.7	2.2 ± 0.3	0.61 ± 0.05	◇4.5 ± 0.2	5.9 ± 0.2	6.0 ± 0.2	8.3 ± 0.1
c-HCOOH											
$16_{2,15}$-$15_{2,14}$	349326	blended		2.7 ± 0.1	2.25 ± 0.08	< 3σ		1.5 ± 0.3	2.2 ± 0.3	< 3σ	

◇ partially blended with other lines

Table 2.B.4: Methanol

Transition	Frequency	G35.20 A		G35.20 B1		G35.20 B2		G35.20 B3		G35.03 A	
		FWHM	T_{peak}	FWHM	T_{peak}	FWHM	T_{peak}	FWHM	T_{peak}	FWHM	T_{peak}
	(MHz)	(km s^{-1})	(K)	(km s^{-1})	(K)	(km s^{-1})	(K)	(km s^{-1})	(K)	(km s^{-1})	(K)
CH_3OH ν=0											
$11_{0,11}$- $10_{2,8}$	334970	blended		blended		blended		1.43 ± 0.06	1.22 ± 0.04	out of window	
$2_{2,1}$-$3_{1,2}$- -	335134	5.28 ± 0.09	70.1 ± 0.7	2.89 ± 0.10	37.27 ± 1.14	2.4 ± 0.1	28 ± 1	2.40 ± 0.04	48.7 ± 0.7	5.2 ± 0.2	26.0 ± 0.7
$16_{1,15}$-$16_{-1,16}$	335222	6.0 ± 0.3	1.83 ± 0.06	blended		blended		1.4 ± 0.2	0.9 ± 0.1	2.3 ± 0.1	1.27 ± 0.05
$7_{3,4}$-$8_{0,8}$	335363	blended		blended		blended		⋄1.2 ± 0.2	0.8 ± 0.1	< 3σ	
$7_{1,7}$-$6_{1,6}$++	335582	6.2 ± 0.1	77 ± 2	3.47 ± 0.11	48.98 ± 1.19	3.3 ± 0.2	45 ± 2	2.89 ± 0.06	55 ± 1	6.1 ± 0.1	34.5 ± 0.4
$25_{8,18}$-$26_{7,19}$- -	335702	5.8 ± 0.1	7.3 ± 0.1	1.3 ± 0.4	0.5 ± 0.1	blended		3.1 ± 0.2	1.10 ± 0.06	< 3σ	
$14_{7,8}$-$15_{6,9}$++	336438	5.42 ± 0.08	47.8 ± 0.6	2.52 ± 0.05	19.26 ± 0.51	2.2 ± 0.1	11.1 ± 0.5	2.34 ± 0.01	27.8 ± 0.4	4.23 ± 0.09	17.3 ± 0.4
$12_{1,11}$-$12_{0,12}$-+	336865	6.4 ± 0.2	106 ± 3	4.11 ± 0.07	90.75 ± 0.76	3.1 ± 0.1	59 ± 2	2.87 ± 0.06	72 ± 1	< 3σ	
$3_{3,0}$-$4_{2,2}$	337136	5.04 ± 0.06	52.3 ± 0.5	2.56 ± 0.09	24.08 ± 0.44	2.4 ± 0.1	18.8 ± 0.8	2.37 ± 0.02	34.1 ± 0.4	4.6 ± 1.3	16.6 ± 0.4
$20_{-6,14}$-$21_{-5,16}$	337838	5.51 ± 0.09	21.7 ± 0.4	1.70 ± 0.08	7.55 ± 0.18	2.0 ± 0.1	2.8 ± 0.2	2.30 ± 0.05	11.4 ± 0.2	4.9 ± 0.9	9.0 ± 0.3
$7_{0,7}$-$6_{0,6}$	338125	6.3 ± 0.5	76 ± 2	3.26 ± 0.11	50.87 ± 1.14	3.2 ± 0.2	43 ± 2	2.9 ± 0.1	56 ± 1	6.4 ± 1.8	33.0 ± 0.6
$7_{-1,7}$-$6_{-1,6}$	338345	6.3 ± 0.5	77 ± 2	3.33 ± 0.12	50.71 ± 1.06	2.6 ± 0.1	42 ± 3	2.8 ± 0.1	57 ± 1	6.7 ± 1.6	34.2 ± 0.5
$7_{6,2}$-$6_{6,1}$	338405	4.2 ± 0.2	53 ± 1	2.12 ± 0.22	23.13 ± 1.67	2.9 ± 0.2	26 ± 1	1.74 ± 0.06	28.9 ± 0.8	< 3σ	
$7_{0,7}$-$6_{0,6}$++	338409	4.9 ± 0.4	70 ± 7	3.91 ± 0.15	49.83 ± 1.09	2.9 ± 0.1	39.9 ± 0.9	3.25 ± 0.09	52.7 ± 1.0	8 ± 1	37.4 ± 1.0
$7_{-6,1}$-$6_{-6,0}$	338431	6.0 ± 0.5	62 ± 2	2.69 ± 0.15	28.31 ± 0.33	2.4 ± 0.4	20.1 ± 0.8	2.37 ± 0.06	40.3 ± 0.6	5.5 ± 0.2	21.3 ± 0.6
$7_{6,1}$-$6_{6,0}$++	338442	5.9 ± 0.3	70 ± 1	2.87 ± 0.11	34.19 ± 1.11	2.6 ± 0.5	26 ± 1	2.49 ± 0.08	45.9 ± 0.8	5.8 ± 0.2	23.4 ± 0.6
$7_{-5,2}$-$6_{-5,1}$	338456	5.8 ± 0.2	72.0 ± 0.8	3.15 ± 0.08	37.40 ± 0.75	2.7 ± 0.7	31 ± 1	2.59 ± 0.07	48.1 ± 0.7	< 3σ	
$7_{5,3}$-$6_{5,2}$	338475	5.94 ± 0.08	70.3 ± 0.7	3.04 ± 0.04	36.37 ± 0.33	2.7 ± 0.6	30 ± 1	2.5 ± 0.1	48 ± 1	5.5 ± 0.2	24.2 ± 0.6
$7_{5,3}$-$6_{5,2}$++	338486	6.0 ± 0.4	76 ± 2	3.16 ± 0.10	42.02 ± 1.16	2.8 ± 0.7	35 ± 1	2.64 ± 0.09	51.5 ± 0.9	6.0 ± 0.2	27.8 ± 0.6
$7_{-4,4}$-$6_{-4,3}$	338504	6.7 ± 0.1	74.6 ± 0.9	3.16 ± 0.11	42.27 ± 1.21	3.0 ± 0.7	37 ± 2	2.5 ± 0.2	50 ± 2	5.5 ± 0.2	26.8 ± 0.5
$7_{4,0}$-$6_{4,0}$- -	338512	5.2 ± 0.1	81.6 ± 0.9	3.50 ± 0.11	52.13 ± 1.33	2.7 ± 0.6	46 ± 1	3.0 ± 0.1	56 ± 1	6.7 ± 0.2	35.9 ± 0.5
$7_{2,6}$-$6_{2,5}$- -	338513	blended with 338512		blended with 338512		blended with 338512		blended with 338512		blended with 338512	
$7_{4,3}$-$6_{4,2}$	338530	6.5 ± 0.2	75 ± 1	3.05 ± 0.09	43.24 ± 0.73	2.8 ± 0.8	36 ± 2	2.6 ± 0.1	52 ± 1	5.8 ± 0.1	29.0 ± 0.5
$7_{3,5}$-$6_{3,4}$++	338541	5.0 ± 0.3	87 ± 2	4.34 ± 0.07	69.05 ± 0.72	4.7 ± 0.1	51 ± 1	4.2 ± 0.3	61 ± 3	7.04 ± 0.10	43.5 ± 0.4
$7_{3,4}$-$6_{3,3}$- -	338543	3.9 ± 0.4	41 ± 4	blended with 338541		blended with 338541		4.4 ± 0.2	61 ± 2	blended with 338541	
$7_{-3,5}$-$6_{-3,4}$	338560	5.9 ± 0.4	80 ± 2	3.22 ± 0.12	45.52 ± 0.89	3.0 ± 0.89	40 ± 2	2.7 ± 0.1	54 ± 1	6.2 ± 1.6	30.2 ± 0.5
$7_{3,4}$-$6_{3,3}$	338583	5.9 ± 0.4	81 ± 2	3.25 ± 0.11	46.95 ± 0.88	3 ± 1	41 ± 2	2.8 ± 0.1	55 ± 1	6.2 ± 1.5	31.2 ± 0.5
$7_{1,6}$-$6_{1,5}$	338615	⋄5.1 ± 0.1	81 ± 2	3.25 ± 0.22	38.08 ± 3.08	2.8 ± 0.2	39 ± 2	2.6 ± 0.2	50 ± 7	8.2 ± 1.6	41.4 ± 0.5
$7_{2,5}$-$6_{2,4}$++	338640	6.2 ± 0.3	78 ± 1	3.23 ± 0.12	48.64 ± 0.91	3 ± 1	42 ± 2	2.8 ± 0.1	55 ± 1	7 ± 1	31.4 ± 0.6
$4_{2,2}$-$4_{-1,4}$	347370	blended		1.3 ± 0.3	0.8 ± 0.1	blended		blended		< 3σ	
$5_{2,3}$-$5_{-1,5}$	347507	blended		0.9 ± 0.2	0.7 ± 0.1	blended		2.1 ± 0.3	0.69 ± 0.07	3.4 ± 0.3	1.66 ± 0.06
$6_{2,4}$-$6_{-1,6}$	347745	blended		blended		blended		1.7 ± 0.3	0.49 ± 0.07	2.9 ± 1.3	0.5 ± 0.1
$7_{2,5}$-$7_{-1,7}$	348123	1.3 ± 0.3	1.2 ± 0.2	blended		blended		1.0 ± 0.4	0.6 ± 0.2	1.7 ± 0.2	1.10 ± 0.04
$8_{2,6}$-$8_{-1,8}$	348682	4.1 ± 1.5	1.6 ± 0.1	blended		blended		1.1 ± 0.2	0.7 ± 0.1	< 3σ	
$14_{1,13}$-$14_{0,14}$-+	349107	5.3 ± 0.1	122 ± 1	3.81 ± 0.07	85.18 ± 1.30	2.8 ± 0.1	57 ± 2	2.80 ± 0.07	74 ± 2	7.9 ± 0.1	43.0 ± 0.5
$9_{2,7}$-$9_{-1,9}$	349470	blended		1.8 ± 0.1	1.11 ± 0.06	blended		0.8 ± 0.5	0.7 ± 0.2	1.9 ± 0.2	0.79 ± 0.07
CH_3OH ν=1											
$7_{1,7}$-$6_{1,6}$++	337297	⋄6.2 ± 0.1	65.2 ± 0.5	3.0 ± 0.2	29.2 ± 0.4	2.7 ± 0.5	20 ± 1	2.8 ± 0.1	38 ± 2	1 ± 1.6	15 ± 5
$7_{2,2}$-$6_{2,2}$	337303	⋄3.9 ± 0.3	20.1 ± 0.8	2.43 ± 0.44	9.06 ± 1.01	1.3 ± 0.2	3.8 ± 0.5	2.22 ± 0.06	13.0 ± 0.3	4.9 ± 1.0	11.0 ± 2.7
$7_{6,1}$-$6_{6,0}$++	337464	5.7 ± 0.1	34.3 ± 0.5	2.1 ± 0.2	12.5 ± 0.4	2.1 ± 0.2	6.4 ± 0.3	2.36 ± 0.07	17.3 ± 0.4	5.8 ± 1.0	12.8 ± 0.3
$10_{10,1}$- $9_{9,1}$ -	337473	5.9 ± 0.3	16.1 ± 0.5	1.64 ± 0.09	3.9 ± 0.2	2.3 ± 0.2	1.41 ± 0.09	3.2 ± 0.2	4.8 ± 0.2	5.3 ± 0.1	7.7 ± 0.1

Table 2.B.4: Methanol continued.

Transition	Frequency	G35.20 A		G35.20 B1		G35.20 B2		G35.20 B3		G35.03 A	
		FWHM	T_{peak}	FWHM	T_{peak}	FWHM	T_{peak}	FWHM	T_{peak}	FWHM	T_{peak}
	(MHz)	(km s^{-1})	(K)	(km s^{-1})	(K)	(km s^{-1})	(K)	(km s^{-1})	(K)	(km s^{-1})	(K)
$7_{-6,2}$-$6_{-6,1}$	337491	5.9 ± 0.1	30.2 ± 0.6	2.5 ± 0.2	9.5 ± 0.4	2.2 ± 0.1	5.0 ± 0.3	2.65 ± 0.04	11.7 ± 0.1	6.1 ± 0.8	11.5 ± 0.3
$7_{3,5}$-$6_{3,4}$	337519	5.3 ± 0.2	48.8 ± 0.7	2.4 ± 0.2	19.0 ± 0.4	2.3 ± 0.2	11.9 ± 0.5	2.32 ± 0.04	28.3 ± 0.3	4.7 ± 1.2	16.6 ± 0.4
$7_{5,3}$-$6_{5,2}$++	337546	5.7 ± 0.2	48.6 ± 0.7	2.5 ± 0.1	19.2 ± 0.3	2.2 ± 0.3	12.2 ± 0.7	2.47 ± 0.07	28.2 ± 0.6	5.4 ± 1.6	15.9 ± 0.5
$7_{4,4}$-$6_{4,3}$	337582	5.9 ± 0.2	53.4 ± 0.8	⋄3.3 ± 0.2	25 ± 3	⋄2.2 ± 0.2	12 ± 1	⋄3.6 ± 0.1	33 ± 1	5.8 ± 0.5	17.7 ± 1.6
$7_{-2,5}$-$6_{-2,4}$	337605	5.1 ± 0.2	53.8 ± 0.9	2.29 ± 0.08	24.4 ± 0.7	2.5 ± 0.2	16.8 ± 0.4	2.33 ± 0.04	30.9 ± 0.5	3.4 ± 0.2	18.8 ± 0.7
$7_{-3,4}$-$6_{-3,3}$	337611	5.0 ± 0.2	57.8 ± 1.0	2.92 ± 0.08	25.2 ± 0.5	2.2 ± 0.8	17 ± 2	2.44 ± 0.04	37.4 ± 0.5	5.5 ± 0.2	21.9 ± 0.4
$7_{2,5}$-$6_{2,4}$++	337626	5.37 ± 0.10	64.5 ± 0.9	2.7 ± 0.1	28.6 ± 0.8	2.5 ± 0.5	21 ± 1	2.41 ± 0.08	40.7 ± 0.8	5.0 ± 0.1	21.4 ± 0.4
$7_{2,6}$-$6_{2,5}$- -	337636	4.69 ± 0.10	56.7 ± 0.9	2.6 ± 0.1	29.5 ± 0.9	2.7 ± 0.3	21.0 ± 0.6	2.3 ± 0.2	39 ± 2	5.7 ± 0.2	23.6 ± 0.4
$7_{1,7}$-$6_{1,6}$	337642	8.6 ± 0.2	73.9 ± 0.6	2.0 ± 0.5	38 ± 21	2 ± 1	23 ± 30	1.8 ± 0.3	31 ± 29	3.1 ± 0.9	19.0 ± 32.5
$7_{0,7}$-$6_{0,6}$	337644	blended with 337642		⋄2 ± 1	36 ± 22	⋄2 ± 2	23 ± 26	⋄2 ± 2	37 ± 34	⋄4 ± 3	22 ± 20
$7_{-4,3}$-$6_{-4,2}$	337646	blended with 337642		⋄2 ± 1	25 ± 14	⋄2 ± 2	6 ± 7	⋄2 ± 2	25 ± 30	⋄5 ± 3	16 ± 10
$7_{-5,3}$-$6_{-5,2}$	337648	blended with 337642		⋄2 ± 1	10 ± 9	blended		2 ± 1	11 ± 16	$< 3\sigma$	
$7_{3,5}$-$6_{3,4}$++	337655	4.88 ± 0.09	55.2 ± 0.7	2.7 ± 0.1	24.9 ± 0.6	2.4 ± 0.3	17.3 ± 0.6	2.44 ± 0.04	35.4 ± 0.4	4.7 ± 0.3	20.6 ± 0.6
$7_{2,6}$-$6_{2,5}$	337671	5.4 ± 0.2	52.4 ± 0.7	2.5 ± 0.1	21.0 ± 0.8	2.3 ± 0.3	13.9 ± 0.6	2.33 ± 0.03	31.2 ± 0.3	4.9 ± 1.3	17.4 ± 0.4
$7_{4,3}$-$6_{4,2}$++	337685	5.5 ± 0.2	55.5 ± 0.7	2.6 ± 0.1	23.1 ± 0.3	2.3 ± 0.4	14.7 ± 0.7	2.39 ± 0.03	33.1 ± 0.3	5.1 ± 1.3	19.3 ± 0.4
$7_{-1,6}$-$6_{-1,5}$	337708	5.6 ± 0.2	50.6 ± 0.7	2.5 ± 0.1	20.2 ± 0.8	2.3 ± 0.3	12.6 ± 0.5	2.5 ± 0.1	29 ± 1	5.2 ± 1.4	17.2 ± 0.5
$7_{0,7}$-$6_{0,6}$++	337749	5.6 ± 0.1	52.7 ± 0.6	2.7 ± 0.3	20.9 ± 0.6	2.4 ± 0.4	12.4 ± 0.8	2.50 ± 0.03	29.4 ± 0.3	5.2 ± 1.4	18.0 ± 0.5
$7_{1,6}$-$6_{1,5}$- -	337969	5.5 ± 0.1	60.8 ± 0.6	2.75 ± 0.07	27.6 ± 0.6	2.4 ± 0.4	19.5 ± 0.8	2.45 ± 0.04	38.6 ± 0.4	5.1 ± 1.5	20.2 ± 0.5
$19_{3,17}$-$19_{2,18}$	347448	5.5 ± 0.1	27.6 ± 0.6	1.9 ± 0.1	9.2 ± 0.5	2.0 ± 0.2	4.1 ± 0.4	2.36 ± 0.06	9.8 ± 0.2	$< 3\sigma$	
$15_{3,13}$-$16_{4,13}$	350288	5.5 ± 0.2	48.5 ± 0.8	2.2 ± 0.1	16.0 ± 0.7	2.0 ± 0.2	7.9 ± 0.7	2.25 ± 0.04	24.3 ± 0.3	5.4 ± 0.1	18.0 ± 0.4
CH_3OH ν=2											
$7_{1,2}$-$6_{1,2}$++	336606	6.0 ± 0.1	19.2 ± 0.4	1.6 ± 0.2	5.4 ± 0.3	1.7 ± 0.3	2.6 ± 0.2	2.28 ± 0.07	7.8 ± 0.1	5.2 ± 0.2	7.7 ± 0.2
$7_{6,-2}$- $6_{6,-2}$	336970	5.7 ± 0.2	8.0 ± 0.2	blended		blended		2.8 ± 0.1	1.85 ± 0.07	5.7 ± 0.2	2.19 ± 0.07
$7_{3,2}$-$6_{3,2}$ - -	337022	5.4 ± 0.5	4.1 ± 0.2	0.8 ± 0.2	0.8 ± 0.1	1.0 ± 0.4	0.6 ± 0.2	1.3 ± 0.2	1.2 ± 0.2	3.5 ± 0.2	2.08 ± 0.08
$7_{2,2}$-$6_{2,2}$ ++	337030	5.6 ± 0.2	10.2 ± 0.1	1.6 ± 0.1	2.51 ± 0.08	1.6 ± 0.2	1.2 ± 0.1	2.23 ± 0.09	3.2 ± 0.1	5.4 ± 0.1	4.62 ± 0.06
$7_{4,2}$-$6_{4,2}$	337066	blended		2 ± 1	0.7 ± 0.3	0.9 ± 0.4	0.6 ± 0.2	2.8 ± 0.2	1.56 ± 0.08	blended	
$7_{5,2}$-$6_{5,2}$	337079	blended		1.2 ± 0.2	0.67 ± 0.08	0.86 ± 0.09	0.54 ± 0.03	1.7 ± 0.2	0.8 ± 0.1	4.3 ± 1.1	2.2 ± 0.1
$7_{5,2}$-$6_{5,2}$ ++	337099	⋆6.6 ± 0.2	7.5 ± 0.2	1.2 ± 0.2	1.9 ± 0.1	1.9 ± 0.3	0.8 ± 0.1	2.0 ± 0.1	2.7 ± 0.2	3.4 ± 0.4	2.60 ± 0.05
$7_{1,2}$-$6_{1,2}$	337114	6.3 ± 0.2	9.1 ± 0.2	1.29 ± 0.05	2.15 ± 0.05	1.7 ± 0.1	1.30 ± 0.05	2.0 ± 0.2	3.0 ± 0.2	3.3 ± 0.2	4.32 ± 0.09
$7_{6,2}$-$6_{6,2}$ - -	337118	blended with 337114		1.8 ± 0.7	0.6 ± 0.2	1.7 ± 0.6	0.5 ± 0.1	2.5 ± 0.3	0.70 ± 0.07	2.1 ± 0.4	2.3 ± 0.7
$7_{6,2}$-$6_{6,2}$	337159	⋆5.5 ± 0.2	4.8 ± 0.2	1.1 ± 0.2	1.2 ± 0.1	1.5 ± 0.6	0.7 ± 0.2	2.1 ± 0.1	1.8 ± 0.1	3.6 ± 0.3	2.37 ± 0.10
$7_{4,2}$-$6_{4,2}$ - -	337175	⋆6.2 ± 0.2	8.7 ± 0.2	1.38 ± 0.07	2.41 ± 0.07	1.8 ± 0.4	0.9 ± 0.1	2.3 ± 0.2	3.0 ± 0.2	4.4 ± 0.3	4.10 ± 0.10
$7_{0,2}$-$6_{0,2}$	337186	5.8 ± 0.2	13.4 ± 0.3	1.49 ± 0.04	3.96 ± 0.07	2.2 ± 0.2	1.5 ± 0.1	2.7 ± 0.2	5.1 ± 0.2	4.0 ± 0.6	6.6 ± 1.8
$7_{5,2}$-$6_{5,2}$ - -	337198	5.6 ± 0.1	15.8 ± 0.3	3.2 ± 0.2	7.2 ± 0.4	3.0 ± 0.5	2.0 ± 0.3	3.3 ± 0.1	8.8 ± 0.3	5.7 ± 0.4	6.5 ± 0.2
$7_{3,-2}$-$6_{3,-2}$	337252	5.7 ± 0.1	26.0 ± 0.5	1.83 ± 0.08	9.5 ± 0.2	2.0 ± 0.2	4.4 ± 0.2	2.35 ± 0.08	12.2 ± 0.4	4.7 ± 0.7	10.0 ± 0.2
$7_{4,2}$-$6_{4,2}$ ++	337274	blended		1.73 ± 0.09	9.9 ± 0.2	2.08 ± 0.09	5.0 ± 0.2	2.25 ± 0.07	13.8 ± 0.4	4.3 ± 0.2	11.6 ± 0.2
$7_{-2,2}$-$6_{-2,2}$	337279	blended		1.4 ± 0.2	5.3 ± 0.5	1.6 ± 0.1	3.5 ± 0.2	2.3 ± 0.1	7.8 ± 0.4	2.8 ± 0.3	7.2 ± 0.5
$7_{0,2}$-$6_{0,2}$	337284	6.5 ± 0.2	39.7 ± 0.8	2.3 ± 0.3	14.3 ± 0.7	2.1 ± 0.2	8.4 ± 0.4	2.47 ± 0.05	20.3 ± 0.4	5.9 ± 0.2	14.8 ± 0.2
$7_{-1,2}$-$6_{-1,2}$	337312	5.5 ± 0.1	33.7 ± 0.6	2.0 ± 0.1	12.6 ± 0.3	2.1 ± 0.2	6.9 ± 0.3	2.27 ± 0.04	17.4 ± 0.3	5.8 ± 2.0	11.4 ± 0.6
$7_{1,-2}$-$6_{1,-2}$	337878	5.87 ± 0.09	17.8 ± 0.4	1.72 ± 0.08	5.7 ± 0.2	1.77 ± 0.06	2.3 ± 0.1	2.26 ± 0.07	7.2 ± 0.2	6.2 ± 0.8	7.9 ± 0.2
$CH_3^{18}OH$ ν=0											
$13_{1,12}$ - $13_{0,13}$	335775	⋆5.4 ± 0.2	7.8 ± 0.3	1.70 ± 0.09	3.8 ± 0.2	1.30 ± 0.11	1.6 ± 0.1	2.27 ± 0.09	4.3 ± 0.1	$< 3\sigma$	

Table 2.B.4: Methanol continued.

Transition	Frequency	G35.20 A		G35.20 B1		G35.20 B2		G35.20 B3		G35.03 A	
		FWHM	T_{peak}	FWHM	T_{peak}	FWHM	T_{peak}	FWHM	T_{peak}	FWHM	T_{peak}
	(MHz)	(km s^{-1})	(K)	(km s^{-1})	(K)	(km s^{-1})	(K)	(km s^{-1})	(K)	(km s^{-1})	(K)
$8_{1,7}$ - $7_{2,5}$	336100	⋄⋆5.3 ± 0.9	3.9 ± 0.5	⋄1.3 ± 0.3	0.83 ± 0.10	< 3σ	⋄1.8 ± 0.1	1.9 ± 0.1	< 3σ		
$4_{0,4}$ - $3_{1,3}$	336743	⋄8.9 ± 1.0	4.8 ± 0.2	3.4 ± 0.2	1.6 ± 0.2	< 3σ		2.7 ± 0.2	1.46 ± 0.07	< 3σ	
$8_{3,6}$ - $9_{2,8}$	347865	⋆6.2 ± 0.3	6.4 ± 0.2	1.21 ± 0.19	0.9 ± 0.1	1.78 ± 0.24	0.9 ± 0.1	2.9 ± 0.2	1.41 ± 0.08	< 3σ	
$15_{1,14}$ - $15_{0,15}$	348053	blended		1.46 ± 0.15	2.6 ± 0.2	1.45 ± 0.06	1.33 ± 0.05	2.0 ± 0.2	3.1 ± 0.2	< 3σ	
$4_{1,3}$ - $3_{0,3}$	350246	blended		2.15 ± 0.26	2.3 ± 0.2	1.89 ± 0.29	1.0 ± 0.1	blended		< 3σ	
^{13}CH3OH ν=0											
$12_{1,11}$-$12_{0,12}$-+	335560	5.04 ± 0.10	48.3 ± 0.8	2.4 ± 0.1	19.8 ± 0.5	2.2 ± 0.1	13.0 ± 0.6	2.26 ± 0.04	29.4 ± 0.5	4.6 ± 0.1	16.1 ± 0.3
$14_{1,13}$-$14_{0,14}$-+	347188	5.3 ± 0.2	47.9 ± 1.2	2.05 ± 0.08	18.9 ± 0.6	2.1 ± 0.1	11.2 ± 0.6	2.31 ± 0.03	30.6 ± 0.4	4.6 ± 0.1	14.1 ± 0.2
$13_{4,9}$-$14_{3,11}$	347788	5.0 ± 0.2	9.1 ± 0.2	1.5 ± 0.2	2.2 ± 0.2	1.8 ± 0.2	1.2 ± 0.1	2.18 ± 0.10	3.4 ± 0.1	2.5 ± 0.3	2.4 ± 0.2
$21_{3,19}$-$20_{4,16}$++	347848	blended		blended		blended		2.1 ± 0.2	1.16 ± 0.07	2.2 ± 0.8	1.7 ± 0.3
$11_{0,11}$-$10_{1,9}$	348100	⋄5.1 ± 0.4	20.1 ± 0.3	1.8 ± 0.1	9.8 ± 0.6	1.9 ± 0.1	5.6 ± 0.3	2.15 ± 0.05	14.7 ± 0.3	4.0 ± 0.1	7.1 ± 0.2
$19_{2,17}$-$18_{1,18}$ ++	348942	blended		blended		blended		blended		< 3σ	
$21_{3,18}$-$20_{4,17}$- -	349996	blended		blended		blended		blended		< 3σ	
$1_{1,1}$-$0_{0,0}$++	350103	⋆4.9 ± 0.2	26.8 ± 0.9	2.03 ± 0.08	12.7 ± 0.4	1.9 ± 0.2	9.1 ± 0.6	2.10 ± 0.03	19.6 ± 0.3	3.9 ± 0.1	8.3 ± 0.2
$8_{1,7}$-$7_{2,5}$	350422	blended		1.51 ± 0.10	6.7 ± 0.5	2.12 ± 0.03	5.23 ± 0.07	3.5 ± 0.2	15.8 ± 0.6	blended	
CH_2DOH											
$18_{2,17}$ - $17_{3,14}$	335796	blended		1.9 ± 0.5	0.64 ± 0.06	1.3 ± 0.7	0.5 ± 0.1	2.1 ± 0.2	1.9 ± 0.1	< 3σ	
$8_{1,7}$ - $7_{0,7}$	335997	3.1 ± 0.8	3.0 ± 1.9	1.8 ± 0.1	2.23 ± 0.07	1.1 ± 0.2	0.8 ± 0.1	2.10 ± 0.09	2.7 ± 0.1	< 3σ	
$19_{2,18}$ - $19_{1,19}$	336325	blended		1.1 ± 0.1	0.64 ± 0.06	blended		3.1 ± 0.3	0.97 ± 0.08	< 3σ	
$9_{0,9}$ - $8_{1,8}$	337349	blended		⋄2.5 ± 0.2	6.6 ± 0.3	1.5 ± 0.3	2.0 ± 0.3	⋄2.2 ± 0.1	9.4 ± 0.3	< 3σ	
$12_{2,11}$ - $11_{3,9}$	337977	blended		1.0 ± 0.2	1.1 ± 0.2	1.56 ± 0.07	0.49 ± 0.02	2.0 ± 0.1	1.32 ± 0.06	< 3σ	
$9_{1,8}$ - $8_{2,6}$	338463	blended		2.0 ± 1.5	1.7 ± 1.0	2.1 ± 3.3	1.7 ± 1.3	2.0 ± 0.8	2.2 ± 0.4	< 3σ	
$20_{4,17}$ - $20_{3,17}$	346924	⋄1.3 ± 0.2	4.5 ± 0.7	blended		blended		3.8 ± 0.1	1.52 ± 0.03	< 3σ	
$20_{4,16}$ - $20_{3,18}$	347222	⋄2.3 ± 0.4	4.2 ± 1.4	< 3σ		< 3σ		2.0 ± 0.5	1.4 ± 0.1	< 3σ	
$19_{4,16}$ - $19_{3,16}$	347371	⋄3.1 ± 1.5	2.3 ± 0.7	2.0 ± 0.2	0.82 ± 0.08	blended		2.1 ± 0.4	0.6 ± 0.1	< 3σ	
$19_{4,15}$ - $19_{3,17}$	347610	blended		2.15 ± 2.06	1.0 ± 0.1	1.0 ± 0.4	0.5 ± 0.2	blended		< 3σ	
$18_{4,15}$ - $18_{3,15}$	347767	blended		1.1 ± 0.3	0.6 ± 0.2	0.9 ± 0.1	0.59 ± 0.06	1.8 ± 0.2	0.85 ± 0.07	< 3σ	
$18_{4,14}$ - $18_{3,16}$	347953	5.43 ± 0.09	4.48 ± 0.05	1.9 ± 0.3	0.7 ± 0.1	blended		2.1 ± 0.3	0.7 ± 0.1	< 3σ	
$4_{1,3}$ - $4_{0,4}$	348161	blended		1.9 ± 0.1	8.4 ± 0.4	1.6 ± 0.3	4.2 ± 1.4	2.36 ± 0.04	16.1 ± 0.3	5.3 ± 0.2	0.93 ± 0.06
$16_{4,13}$ - $16_{3,13}$	348427	2.0 ± 0.3	3.2 ± 0.3	1.5 ± 0.1	2.1 ± 0.1	blended		1.8 ± 0.3	1.8 ± 0.3	< 3σ	
$16_{4,12}$ - $16_{3,14}$	348529	blended		blended		2.0 ± 0.6	5.1 ± 1.1	blended		< 3σ	
$10_{1,10}$ - $9_{2,8}$	348592	blended		1.8 ± 0.2	1.00 ± 0.09	1.1 ± 0.3	0.8 ± 0.2	2.2 ± 0.4	1.0 ± 0.1	< 3σ	
$13_{1,12}$ - $12_{2,11}$	348668	partially blended		1.1 ± 0.4	0.8 ± 0.1	1.4 ± 0.2	0.91 ± 0.04	1.0 ± 0.2	0.8 ± 0.2	< 3σ	
$15_{4,12}$ - $15_{3,12}$	348699	blended		1.52 ± 0.09	1.72 ± 0.09	1.6 ± 0.3	0.9 ± 0.1	1.7 ± 0.2	2.3 ± 0.2	< 3σ	
$14_{4,11}$ - $14_{3,11}$	348939	blended		1.32 ± 0.07	2.3 ± 0.1	blended		2.2 ± 0.1	2.4 ± 0.1	< 3σ	
$14_{4,10}$ - $14_{3,12}$	348990	blended		1.3 ± 0.2	2.3 ± 0.2	1.3 ± 0.2	0.9 ± 0.1	blended		< 3σ	
$13_{4,10}$ - $13_{3,10}$	349149	⋄⋆6.1 ± 0.3	4.3 ± 0.2	1.3 ± 0.1	2.3 ± 0.2	1.0 ± 0.2	1.2 ± 0.2	2.10 ± 0.09	3.1 ± 0.1	< 3σ	
$13_{4,9}$ - $13_{3,11}$	349184	⋄⋆6.1 ± 0.4	4.4 ± 0.1	1.43 ± 0.06	2.42 ± 0.09	1.0 ± 0.4	1.0 ± 0.4	1.9 ± 0.1	3.4 ± 0.2	< 3σ	
$12_{4,9}$ - $12_{3,9}$	349334	2.6 ± 0.2	6.6 ± 0.3	1.8 ± 0.2	2.7 ± 0.3	2.7 ± 0.1	6.8 ± 0.2	blended		< 3σ	
$12_{4,8}$ - $12_{3,10}$	349356	blended		1.84 ± 0.07	4.1 ± 0.1	1.3 ± 0.5	1.1 ± 0.3	2.19 ± 0.06	3.73 ± 0.09	< 3σ	
$13_{2,12}$ - $13_{1,12}$	349411	blended		1.8 ± 0.3	3.8 ± 0.3	1.3 ± 0.3	1.7 ± 0.2	1.91 ± 0.07	4.2 ± 0.1	< 3σ	
$11_{4,8}$ - $11_{3,8}$	349495	⋆6.3 ± 0.3	7.9 ± 0.3	1.62 ± 0.09	3.4 ± 0.2	1.2 ± 0.2	1.6 ± 0.1	2.7 ± 0.1	4.9 ± 0.2	< 3σ	

Table 2.B.4: Methanol continued.

Transition	Frequency	G35.20 A		G35.20 B1		G35.20 B2		G35.20 B3		G35.03 A	
		FWHM	T_{peak}	FWHM	T_{peak}	FWHM	T_{peak}	FWHM	T_{peak}	FWHM	T_{peak}
	(MHz)	(km s^{-1})	(K)	(km s^{-1})	(K)	(km s^{-1})	(K)	(km s^{-1})	(K)	(km s^{-1})	(K)
$11_{4,7}$ - $11_{3,9}$	349509	⋆5.8 ± 0.4	5.5 ± 0.3	1.70 ± 0.09	3.7 ± 0.2	1.7 ± 0.6	1.2 ± 0.2	1.97 ± 0.08	4.4 ± 0.2	$< 3\sigma$	
$10_{4,7}$ - $10_{3,7}$	349636	⋆5.3 ± 0.2	9.7 ± 0.3	1.7 ± 0.1	4.5 ± 0.3	1.2 ± 0.2	1.7 ± 0.1	2.13 ± 0.04	5.51 ± 0.08	$< 3\sigma$	
$10_{4,6}$ - $10_{3,8}$	349644	⋆6.6 ± 0.2	6.7 ± 0.3	1.43 ± 0.07	4.0 ± 0.2	1.2 ± 0.2	2.0 ± 0.3	1.89 ± 0.06	5.4 ± 0.2	$< 3\sigma$	
$9_{4,6}$ - $9_{3,6}$	349757	◇2.6 ± 0.3	10.4 ± 0.8	1.7 ± 0.2	3.6 ± 0.4	1.6 ± 0.3	1.7 ± 0.2	2.12 ± 0.07	5.8 ± 0.1	$< 3\sigma$	
$9_{4,5}$ - $9_{3,7}$	349762	◇3.9 ± 0.6	6.8 ± 0.3	1.7 ± 0.1	4.1 ± 0.2	0.9 ± 0.3	1.6 ± 0.5	1.98 ± 0.06	5.5 ± 0.1	$< 3\sigma$	
$8_{4,5}$ - $8_{3,5}$	349862	blended 349864		1.4 ± 0.2	3.9 ± 0.4	1.5 ± 0.1	2.3 ± 0.1	3.6 ± 0.2	7.3 ± 0.3	$< 3\sigma$	
$8_{4,4}$ - $8_{3,6}$	349864	blended with 349862		1.7 ± 0.2	4.7 ± 0.2	0.9 ± 0.3	1.2 ± 0.2	blended with 349862		$< 3\sigma$	
$7_{4,4}$ - $7_{3,4}$	349952	⋆6.2 ± 0.2	14.2 ± 0.4	2.07 ± 0.03	7.6 ± 0.1	1.8 ± 0.1	3.2 ± 0.2	2.31 ± 0.04	10.1 ± 0.2	$< 3\sigma$	
$6_{4,3}$ - $6_{3,3}$	350027	⋆5.4 ± 0.4	13.8 ± 0.8	1.67 ± 0.04	7.2 ± 0.2	1.7 ± 0.2	3.0 ± 0.2	2.11 ± 0.04	10.3 ± 0.2	$< 3\sigma$	
$5_{4,2}$ - $5_{3,2}$	350090	⋆6.3 ± 0.6	10.8 ± 0.6	1.81 ± 0.09	6.2 ± 0.3	1.4 ± 0.2	2.8 ± 0.3	2.07 ± 0.02	8.07 ± 0.07	$< 3\sigma$	
$4_{4,1}$ - $4_{3,1}$	350141	blended		1.71 ± 0.08	3.6 ± 0.1	2.1 ± 0.4	1.7 ± 0.2	3.7 ± 0.1	5.7 ± 0.1	$< 3\sigma$	
$6_{2,5}$ - $5_{1,5}$	350454	blended		1.5 ± 0.2	3.4 ± 0.2	1.3 ± 0.1	1.13 ± 0.08	1.9 ± 0.1	3.8 ± 0.2	$< 3\sigma$	
$5_{1,4}$ - $5_{0,5}$	350632	⋆5.5 ± 0.4	13.3 ± 0.7	1.92 ± 0.09	8.4 ± 0.3	1.7 ± 0.2	4.7 ± 0.4	2.07 ± 0.04	12.1 ± 0.2	$< 3\sigma$	

◇ partially blended with other lines, ⋆ double peaked.

Table 2.B.5: Acetaldehyde

Transition	Frequency (MHz)	G35.20 A FWHM (km s^{-1})	G35.20 A T_{peak} (K)	G35.20 B1 FWHM (km s^{-1})	G35.20 B1 T_{peak} (K)	G35.20 B2 FWHM (km s^{-1})	G35.20 B2 T_{peak} (K)	G35.20 B3 FWHM (km s^{-1})	G35.20 B3 T_{peak} (K)	G35.03 A FWHM (km s^{-1})	G35.03 A T_{peak} (K)
CH_3CHO ν=0											
$18_{1,4}$-$17_{1,4}$	334980	⋆4.8 ± 0.3	2.07 ± 0.07	0.8 ± 0.1	0.55 ± 0.09	0.9 ± 0.2	0.5 ± 0.1	1.4 ± 0.4	1.0 ± 0.1	< 3σ	
$18_{0,18}$-$17_{0,17}$E	335318	5.1 ± 0.1	8.9 ± 0.2	2.0 ± 0.2	3.3 ± 0.2	2.3 ± 0.1	2.0 ± 0.1	1.7 ± 0.1	3.7 ± 0.2	4.2 ± 0.2	2.42 ± 0.10
$18_{0,18}$-$17_{0,17}$A	335358	5.38 ± 0.09	12.8 ± 0.2	2.2 ± 0.5	3.8 ± 0.3	1.7 ± 0.2	1.7 ± 0.2	2.5 ± 0.1	5.6 ± 0.1	< 3σ	
$18_{7,11}$-$17_{7,10}$E	346934	blended		blended		1.4 ± 0.3	1.55 ± 0.10	2.5 ± 0.1	2.8 ± 0.2	3.1 ± 1.4	5.8 ± 0.9
$18_{7,12}$-$17_{7,11}$A	346957	⋄3.3 ± 0.4	8.4 ± 0.8	1.54 ± 0.08	1.46 ± 0.06	2.3 ± 0.2	1.47 ± 0.10	2.7 ± 0.1	8.3 ± 0.3	< 3σ	
$18_{6,12}$-$17_{6,11}$A	347071	5.6 ± 0.2	9.2 ± 0.2	1.8 ± 0.1	3.2 ± 0.2	1.7 ± 0.4	1.7 ± 0.3	2.6 ± 0.1	5.1 ± 0.1	4.0 ± 0.2	2.6 ± 0.1
$18_{6,12}$-$17_{6,11}$E	347090	6.2 ± 0.5	6.2 ± 0.1	1.7 ± 0.2	1.2 ± 0.1	1.3 ± 0.4	1.2 ± 0.3	2.9 ± 0.1	2.63 ± 0.08	4.9 ± 0.3	1.94 ± 0.10
$18_{6,13}$-$17_{6,12}$E	347133	blended		1.5 ± 0.9	2.3 ± 4.2	2.4 ± 0.3	1.8 ± 0.1	2.46 ± 0.05	9.7 ± 0.1	< 3σ	
$18_{5,14}$-$17_{5,13}$A	347288	⋆4.6 ± 0.3	5.3 ± 0.3	1.6 ± 0.2	2.6 ± 0.5	1.7 ± 0.2	1.23 ± 0.10	2.26 ± 0.08	3.6 ± 0.1	3.1 ± 0.3	1.84 ± 0.04
$18_{5,13}$-$17_{5,12}$A	347295	⋆7.2 ± 0.8	6.1 ± 0.1	2.16 ± 0.07	2.72 ± 0.07	1.6 ± 0.1	1.27 ± 0.09	2.3 ± 0.1	3.5 ± 0.1	< 3σ	
$18_{5,13}$-$17_{5,12}$E	347345	blended		1.3 ± 0.4	2.1 ± 0.6	1.7 ± 0.2	1.4 ± 0.1	2.6 ± 0.3	3.53 ± 0.07	3.4 ± 0.3	2.8 ± 0.1
$18_{5,14}$-$17_{5,13}$E	347349	blended		blended		blended		2.87 ± 0.05	5.86 ± 0.09	4.0 ± 0.2	4.57 ± 0.09
$18_{3,16}$-$17_{3,15}$A	347519	5.3 ± 0.2	8.4 ± 0.2	2.1 ± 0.2	3.4 ± 0.2	2.2 ± 0.3	1.3 ± 0.1	2.2 ± 0.1	5.1 ± 0.1	4.0 ± 0.2	2.21 ± 0.06
$18_{3,16}$-$17_{3,15}$E	347563	⋆3.6 ± 0.4	7.5 ± 0.5	1.8 ± 0.2	3.2 ± 0.3	⋄1.4 ± 0.3	2.0 ± 0.3	2.16 ± 0.08	5.6 ± 0.1	< 3σ	
$18_{4,15}$-$17_{4,14}$A	347650	6.2 ± 0.4	10.1 ± 0.3	1.9 ± 0.2	3.2 ± 0.3	2.0 ± 0.3	1.6 ± 0.2	2.4 ± 0.2	5.0 ± 0.2	3.7 ± 0.5	3.3 ± 0.1
$18_{4,15}$-$17_{4,14}$E	347756	⋆5.8 ± 0.1	18.5 ± 0.3	2.7 ± 0.2	4.6 ± 0.2	blended		2.3 ± 0.2	6.2 ± 0.5	< 3σ	
$18_{4,14}$-$17_{4,13}$E	347830	6.2 ± 0.6	6.4 ± 0.2	1.93 ± 0.10	2.3 ± 0.1	⋄1.9 ± 0.3	1.5 ± 0.2	2.2 ± 0.1	4.2 ± 0.2	3.0 ± 0.6	1.59 ± 0.08
$18_{4,14}$-$17_{4,13}$A	347838	blended		1.3 ± 0.3	2.2 ± 0.3	1.6 ± 0.3	1.7 ± 0.3	1.6 ± 0.1	5.5 ± 0.2	< 3σ	
$18_{3,15}$-$17_{3,14}$A	350135	⋄6.8 ± 0.2	17.5 ± 0.2	2.4 ± 0.1	5.3 ± 0.2	1.9 ± 0.5	2.5 ± 2.0	3.0 ± 0.1	8.0 ± 0.1	5.4 ± 0.2	5.1 ± 0.1
$18_{1,17}$-$17_{1,16}$E	350363	blended		1.8 ± 0.3	4.8 ± 0.6	blended		1.5 ± 0.2	4.6 ± 0.6	< 3σ	
$18_{1,17}$-$17_{1,16}$A	350445	blended		2.1 ± 0.2	5.8 ± 0.8	1.3 ± 0.2	2.1 ± 0.3	blended		< 3σ	
CH_3CHO ν=1											
$18_{0,18}$-$17_{0,17}$ A	335382	partially blended		2.5 ± 0.2	0.60 ± 0.08	< 3σ		1.9 ± 0.2	1.1 ± 0.1	< 3σ	
$18_{0,18}$-$17_{0,17}$ E	336416	3.4 ± 0.5	1.46 ± 0.09	1.2 ± 0.3	0.8 ± 0.2	< 3σ		< 3σ		< 3σ	
$18_{5,13}$-$17_{5,12}$E	347217	blended		blended		< 3σ		2.4 ± 0.3	5.8 ± 1.0	< 3σ	
$18_{5,14}$-$17_{5,13}$E	347252	3.0 ± 0.6	1.77 ± 0.09	< 3σ		< 3σ		1.7 ± 0.3	1.14 ± 0.08	< 3σ	
$18_{7,11}$-$17_{7,10}$A	347459	< 3σ		< 3σ		< 3σ		2.1 ± 0.2	0.83 ± 0.07	< 3σ	
$18_{8,11}$-$19_{7,12}$A	347645	2.0 ± 1.0	1.1 ± 0.5	< 3σ		< 3σ		2.1 ± 0.4	0.8 ± 0.1	< 3σ	
$18_{9,10}$-$17_{9,9}$	347819	< 3σ		< 3σ		< 3σ		< 3σ		< 3σ	
$18_{6,13}$-$17_{6,12}$ A	348088	blended		blended		< 3σ		2.5 ± 0.1	1.43 ± 0.06	4.1 ± 0.7	1.8 ± 0.1
$18_{3,16}$-$17_{3,15}$A	348211	5.8 ± 0.1	4.86 ± 0.09	< 3σ		1.1 ± 0.3	0.9 ± 0.2	2.3 ± 0.3	2.0 ± 0.1	5.5 ± 0.4	1.26 ± 0.06
$18_{4,15}$-$17_{4,14}$E	348229	blended		1.4 ± 0.2	1.0 ± 0.1	1.7 ± 0.2	1.01 ± 0.08	1.4 ± 0.4	0.9 ± 0.1	< 3σ	
$18_{3,15}$-$17_{3,14}$E	348288	blended		1.9 ± 0.2	0.93 ± 0.08	1.8 ± 0.2	0.92 ± 0.06	0.8 ± 0.2	0.49 ± 0.07	< 3σ	
$18_{5,14}$-$17_{5,13}$A	348570	3.8 ± 1.4	2.7 ± 0.6	2.3 ± 0.2	0.93 ± 0.08	1.4 ± 0.3	0.59 ± 0.03	2.6 ± 0.4	0.9 ± 0.2	4.4 ± 0.3	0.97 ± 0.05
$18_{5,13}$-$17_{5,12}$A	348578	⋄3.7 ± 4.6	1.2 ± 2.4	⋄1.6 ± 0.3	0.60 ± 0.06	< 3σ		⋄1.25 ± 1.28	0.4 ± 0.2	< 3σ	
$18_{4,15}$-$17_{4,14}$A	348855	blended		< 3σ		< 3σ		2.8 ± 0.4	0.8 ± 0.2	< 3σ	
$18_{1,17}$-$17_{1,16}$A	349320	5.3 ± 0.2	4.03 ± 0.10	1.6 ± 0.2	1.0 ± 0.1	< 3σ		1.9 ± 0.2	1.4 ± 0.1	3.9 ± 0.2	1.72 ± 0.04
	349650	< 3σ		< 3σ		< 3σ		< 3σ		3.0 ± 0.4	0.81 ± 0.06
CH_3CHO ν=2											
$17_{9,9}$-$16_{9,8}$ A	335224	6.2 ± 0.7	1.87 ± 0.08	< 3σ		< 3σ		< 3σ		< 3σ	
$18_{1,18}$-$17_{1,17}$E	336025	blended		< 3σ		blended		1.2 ± 7.1	0.9 ± 0.1	< 3σ	

Table 2.B.5: Acetaldehyde continued.

Transition	Frequency	G35.20 A		G35.20 B1		G35.20 B2		G35.20 B3		G35.03 A	
	(MHz)	FWHM (km s^{-1})	T_{peak} (K)	FWHM (km s^{-1})	T_{peak} (K)	FWHM (km s^{-1})	T_{peak} (K)	FWHM (km s^{-1})	T_{peak} (K)	FWHM (km s^{-1})	T_{peak} (K)
$18_{1,18}$-$17_{1,17}$ A	337082	7.3 ± 0.3	5.6 ± 0.1	$< 3\sigma$		$< 3\sigma$		3.4 ± 0.6	0.85 ± 0.05	4.1 ± 0.6	2.4 ± 0.2
$18_{2,17}$- $17_{2,16}$ A	347657	⋄2.4 ± 1.0	2.4 ± 0.5	$< 3\sigma$		$< 3\sigma$		$< 3\sigma$		$< 3\sigma$	
$18_{3,15}$-$17_{3,14}$ A	349752	⋄2.4 ± 0.2	8.6 ± 0.3	0.7 ± 0.7	0.6 ± 0.5	$< 3\sigma$		2.4 ± 0.7	0.9 ± 0.1	$< 3\sigma$	

⋄ partially blended with other lines, ⋆ double peaked.

Table 2.B.6: Methyl formate

Transition	Frequency	G35.20 A		G35.20 B1		G35.20 B2		G35.20 B3		G35.03 A	
		FWHM	T_{peak}	FWHM	T_{peak}	FWHM	T_{peak}	FWHM	T_{peak}	FWHM	T_{peak}
	(MHz)	(km s^{-1})	(K)	(km s^{-1})	(K)	(km s^{-1})	(K)	(km s^{-1})	(K)	(km s^{-1})	(K)
CH_3OCHO ν=0											
$15_{6,10}$-$14_{5,10}$E	335145	blended		◇2.0 ± 0.2	0.62 ± 0.02	< 3σ		< 3σ		blended	
$28_{4,24}$-$27_{5,23}$E	335158	blended		◇2.2 ± 0.5	0.7 ± 0.1	< 3σ		blended		blended	
$28_{4,24}$-$27_{5,23}$A	335183	6.0 ± 0.1	3.26 ± 0.05	2.3 ± 0.5	0.77 ± 0.09	< 3σ		< 3σ		4.4 ± 0.2	2.42 ± 0.09
$13_{2,11}$-$12_{1,12}$A	335336	blended		< 3σ		< 3σ		< 3σ		< 3σ	
$15_{6,9}$-$14_{5,10}$A	335403	blended		1.90 ± 0.11	0.85 ± 0.04	1.1 ± 0.3	0.5 ± 0.1	blended		< 3σ	
$15_{6,9}$-$14_{5,10}$E	335454	3.1 ± 1.1	1.3 ± 0.6	< 3σ		< 3σ		< 3σ		blended	
$26_{5,22}$-$25_{4,21}$A	335828	5.6 ± 0.8	2.6 ± 0.2	1.9 ± 0.2	0.87 ± 0.06	< 3σ		1.8 ± 0.2	0.82 ± 0.08	2.5 ± 0.1	1.27 ± 0.06
$26_{5,22}$-$25_{4,21}$E	335839	blended		3.0 ± 0.2	0.79 ± 0.06	< 3σ		1.6 ± 1.9	0.6 ± 0.6	blended	
$27_{9,19}$-$26_{9,17}$E	335900	blended		1.9 ± 0.7	0.5 ± 0.1	< 3σ		< 3σ		< 3σ	
$27_{9,19}$-$26_{9,18}$A	336028	◇7.3 ± 0.1	24.4 ± 0.3	◇1.58 ± 0.06	3.88 ± 0.07	◇2.5 ± 0.1	2.8 ± 0.1	◇2.9 ± 0.2	4.6 ± 0.1	◇4.3 ± 0.3	6.7 ± 0.1
$27_{9,19}$-$26_{9,18}$E	336032	blended with 336028		◇1.63 ± 0.06	3.99 ± 0.07	◇1.1 ± 0.2	1.2 ± 0.2	◇2.5 ± 0.2	4.1 ± 0.1	◇3.9 ± 0.5	6.3 ± 0.6
$27_{9,18}$-$26_{9,17}$E	336086	blended		blended		3.66 ± 0.09	7.8 ± 0.1	blended		< 3σ	
$27_{9,18}$-$26_{9,17}$A	336111	5.4 ± 0.1	15.0 ± 0.3	1.8 ± 0.2	3.9 ± 0.3	1.8 ± 0.2	1.8 ± 0.1	2.58 ± 0.09	4.1 ± 0.1	5.0 ± 0.1	4.64 ± 0.10
$27_{9,18}$-$26_{9,18}$E	336219	blended		< 3σ		< 3σ		2.7 ± 0.3	0.52 ± 0.05	< 3σ	
$27_{6,22}$-$26_{6,21}$E	336351	◇6.8 ± 0.1	26.9 ± 0.5	◇1.7 ± 0.1	3.9 ± 0.2	◇2.29 ± 0.07	2.80 ± 0.06	◇1.9 ± 0.1	5.7 ± 0.3	◇3.6 ± 0.3	4.1 ± 0.2
$26_{5,21}$-$25_{5,20}$E	336355	blended with 336351		◇1.9 ± 0.1	5.6 ± 0.2	◇1.66 ± 0.06	2.91 ± 0.07	◇2.9 ± 0.2	6.3 ± 0.2	◇3.8 ± 0.2	6.8 ± 0.2
$27_{6,22}$-$26_{6,21}$A	336368	◇⋆5.0 ± 0.6	14.9 ± 1.3	1.4 ± 0.2	4.6 ± 0.5	2.1 ± 0.2	2.4 ± 0.2	1.99 ± 0.06	4.9 ± 0.1	3.8 ± 0.3	5.1 ± 0.2
$26_{5,21}$-$25_{5,20}$A	336374	◇⋆5.7 ± 0.6	18.0 ± 0.9	1.81 ± 0.09	4.9 ± 0.2	1.7 ± 0.2	3.6 ± 0.2	2.2 ± 0.2	6.4 ± 0.4	4.5 ± 0.4	5.3 ± 0.2
$26_{6,20}$-$25_{6,19}$E	336889	⋆5.0 ± 0.2	16.2 ± 0.5	1.4 ± 0.1	4.9 ± 0.3	1.8 ± 0.2	2.8 ± 0.2	2.16 ± 0.06	5.9 ± 0.1	4.7 ± 0.3	4.8 ± 0.2
$26_{6,20}$-$25_{6,19}$A	336918	5.8 ± 0.2	17.6 ± 0.5	1.72 ± 0.07	4.8 ± 0.2	2.0 ± 0.1	3.0 ± 0.1	2.34 ± 0.04	5.60 ± 0.08	5.6 ± 0.3	5.4 ± 0.2
$27_{8,20}$-$26_{8,19}$E	337490	5.9 ± 0.1	30.2 ± 0.6	2.5 ± 0.2	9.5 ± 0.5	2.22 ± 0.07	5.0 ± 0.1	2.1 ± 0.8	7 ± 0.6	< 3σ	
$27_{8,20}$-$26_{8,19}$A	337504	⋆5.1 ± 0.2	14.6 ± 0.4	1.57 ± 0.09	4.1 ± 0.2	1.9 ± 0.4	2.2 ± 0.4	2.26 ± 0.04	4.63 ± 0.08	4.6 ± 0.2	3.9 ± 0.1
$27_{8,19}$-$26_{8,18}$E	338338	5.6 ± 0.3	22.2 ± 0.7	1.4 ± 0.2	4.4 ± 0.4	blended		1.74 ± 0.02	4.92 ± 0.06	< 3σ	
$27_{8,19}$-$26_{8,18}$A	338356	⋆6.0 ± 0.3	14.6 ± 0.5	1.5 ± 0.1	4.2 ± 0.3	1.7 ± 0.3	2.3 ± 0.3	2.32 ± 0.05	4.67 ± 0.09	5.9 ± 0.3	4.5 ± 0.1
$27_{7,21}$-$26_{7,20}$E	338396	◇7.6 ± 0.5	17.8 ± 0.5	1.4 ± 0.1	4.2 ± 0.3	1.8 ± 0.1	2.5 ± 0.2	2.00 ± 0.10	4.1 ± 0.1	< 3σ	
$27_{7,21}$-$26_{7,20}$A	338414	7.3 ± 1.2	23.4 ± 3.2	blended		1.5 ± 0.2	1.8 ± 0.2	1.9 ± 1.2	5.2 ± 1.5	< 3σ	
$27_{5,22}$-$26_{5,21}$E	347478	⋆7.2 ± 0.5	19.6 ± 1.5	1.7 ± 0.1	5.6 ± 0.3	1.71 ± 0.07	3.9 ± 0.1	2.17 ± 0.05	6.7 ± 0.1	5.2 ± 0.3	6.6 ± 0.1
$27_{5,22}$-$26_{5,21}$A	347494	⋆5.6 ± 1.3	19.1 ± 1.5	1.59 ± 0.05	5.9 ± 0.2	2.10 ± 0.09	3.4 ± 0.1	2.14 ± 0.04	7.4 ± 0.1	5.1 ± 0.3	5.03 ± 0.10
$16_{6,10}$-$15_{5,11}$A	347590	⋆7.1 ± 0.8	3.7 ± 0.2	3.0 ± 0.2	1.46 ± 0.08	1.1 ± 0.4	0.8 ± 0.2	1.4 ± 0.2	1.2 ± 0.1	< 3σ	
$16_{6,10}$-$15_{5,11}$E	347599	⋆2.8 ± 2.0	2.7 ± 4.3	2.3 ± 0.2	1.26 ± 0.09	1.5 ± 0.4	0.7 ± 0.1	< 3σ		< 3σ	
$28_{10,18}$-$27_{10,17}$E	347605	⋆6.3 ± 0.2	11.2 ± 0.3	1.4 ± 0.2	3.2 ± 0.3	1.6 ± 0.1	2.4 ± 0.2	2.10 ± 0.06	3.72 ± 0.09	5.3 ± 0.4	3.1 ± 0.1
$28_{10,19}$-$27_{10,18}$A	347617	⋆5.8 ± 0.3	11.3 ± 0.4	1.24 ± 0.08	3.7 ± 0.2	1.8 ± 0.1	2.0 ± 0.1	2.02 ± 0.07	3.52 ± 0.10	3.5 ± 0.1	3.13 ± 0.10
$28_{10,19}$-$27_{10,18}$E	347628	⋆5.4 ± 0.2	20.5 ± 0.7	1.7 ± 0.1	5.5 ± 0.4	1.7 ± 0.3	3.6 ± 0.5	2.26 ± 0.04	7.4 ± 0.1	4.5 ± 0.3	4.9 ± 0.2
$29_{4,25}$-$28_{5,24}$E	347818	blended		1.12 ± 0.04	1.04 ± 0.03	1.4 ± 0.2	0.55 ± 0.09	< 3σ		< 3σ	
$28_{6,23}$-$27_{6,22}$E	348050	5.0 ± 1.0	12.2 ± 2.0	1.49 ± 0.06	4.3 ± 0.1	1.8 ± 0.1	3.0 ± 0.2	2.26 ± 0.07	5.6 ± 0.1	6.0 ± 0.2	4.4 ± 0.1
$28_{6,23}$-$27_{6,22}$A	348066	5.6 ± 0.2	17.7 ± 0.5	1.56 ± 0.04	4.9 ± 0.1	1.7 ± 0.1	2.8 ± 0.1	2.0 ± 0.1	5.5 ± 0.2	4.6 ± 0.3	4.4 ± 0.2
$28_{9,20}$-$27_{9,19}$E	348909	blended with 348915		2.1 ± 0.2	3.8 ± 0.3	2.2 ± 0.2	2.7 ± 0.2	2.2 ± 0.1	5.1 ± 0.4	5.9 ± 0.2	6.5 ± 0.1
$28_{9,20}$-$27_{9,19}$A	348915	◇⋆8.0 ± 0.1	27.4 ± 0.4	◇2.5 ± 0.2	4.0 ± 0.3	◇1.2 ± 0.2	1.8 ± 0.2	◇2.2 ± 0.1	3.8 ± 0.2	◇5.9 ± 0.2	6.8 ± 0.2
$28_{5,24}$-$27_{4,23}$A	349015	blended		0.8 ± 0.3	0.9 ± 0.2	0.7 ± 0.2	0.6 ± 0.1	< 3σ		< 3σ	
$28_{5,24}$-$27_{4,23}$E	349019	blended		< 3σ		blended		blended		< 3σ	
$28_{9,19} - 27_{9,18}$E	349049	⋆6.9 ± 0.3	12.6 ± 0.4	1.5 ± 0.1	3.9 ± 0.3	1.6 ± 0.3	2.0 ± 0.3	2.24 ± 0.07	4.00 ± 0.09	4.0 ± 0.4	3.5 ± 0.2

Table 2.B.6: Methyl formate continued.

Transition	Frequency	G35.20 A		G35.20 B1		G35.20 B2		G35.20 B3		G35.03 A	
		FWHM	T_{peak}	FWHM	T_{peak}	FWHM	T_{peak}	FWHM	T_{peak}	FWHM	T_{peak}
	(MHz)	(km s^{-1})	(K)	(km s^{-1})	(K)	(km s^{-1})	(K)	(km s^{-1})	(K)	(km s^{-1})	(K)
$28_{9,19}$-$27_{9,18}$A	349066	⋆6.3 ± 0.3	13.1 ± 0.5	1.50 ± 0.07	4.2 ± 0.2	1.4 ± 0.2	2.1 ± 0.2	2.23 ± 0.07	4.26 ± 0.12	4.8 ± 0.2	3.6 ± 0.1
$26_{7,19}$-$26_{5,22}$E	350306	blended		blended		< 3σ		< 3σ		< 3σ	
$28_{8,21}$-$27_{8,20}$E	350442	blended		⋄1.61 ± 0.07	4.5 ± 0.1	⋄3.1 ± 0.2	2.74 ± 0.08	blended		< 3σ	
$28_{8,21}$-$27_{8,20}$A	350458	blended		2.02 ± 0.09	4.3 ± 0.2	1.4 ± 0.2	1.9 ± 0.2	2.09 ± 0.09	4.89 ± 0.17	4.7 ± 0.4	3.6 ± 0.2
CH_3OCHO ν=1											
$27_{7,21}$-$26_{7,20}$A	335016	5.6 ± 0.2	4.15 ± 0.10	1.3 ± 0.1	1.5 ± 0.1	< 3σ		1.6 ± 0.2	0.72 ± 0.07	2.1 ± 0.3	0.99 ± 0.10
$15_{6,10}$-$14_{5,10}$E	335208	3.9 ± 0.3	1.17 ± 0.09	< 3σ		< 3σ		< 3σ		< 3σ	
$27_{8,20}$-$26_{8,19}$E	335392	blended		in abs feature		2.6 ± 0.3	3.0 ± 0.2	blended		4.0 ± 0.5	1.24 ± 0.06
$27_{7,21}$-$26_{7,20}$E	335961	5.4 ± 0.2	4.0 ± 0.2	1.8 ± 0.3	0.8 ± 0.1	< 3σ		1.8 ± 0.2	1.04 ± 0.10	2.3 ± 0.2	1.2 ± 0.1
$28_{5,24}$-$27_{5,23}$A	338393	blended with 338396		blended with 338396		blended with 338396		1.3 ± 0.3	1.3 ± 0.2	< 3σ	
$28_{7,22}$-$27_{7,21}$A	347568	1.1 ± 0.2	2.4 ± 0.4	1.0 ± 0.2	1.5 ± 0.2	0.8 ± 0.9	0.7 ± 0.2	2.2 ± 0.3	1.0 ± 0.1	< 3σ	
$27_{6,21}$-$26_{6,20}$E	347698	blended		1.5 ± 0.2	1.5 ± 0.2	< 3σ		1.59 ± 0.07	1.59 ± 0.06	3.0 ± 0.4	2.24 ± 0.09
$25_{13,12}$-$25_{12,13}$E	348053	⋄4.5 ± 1.0	9.6 ± 2.0	< 3σ		< 3σ		⋄2.2 ± 0.1	5.7 ± 0.2	< 3σ	
$28_{8,21}$-$27_{8,20}$E	348084	6.8 ± 0.2	9.2 ± 0.2	1.86 ± 0.08	1.87 ± 0.07	2.50 ± 0.27	0.67 ± 0.05	2.8 ± 0.1	1.76 ± 0.08	5.5 ± 0.3	2.22 ± 0.06
$9_{9,1}$-$8_{8,1}$E	348247	5.5 ± 1.4	1.3 ± 0.1	< 3σ		< 3σ		< 3σ		< 3σ	
$29_{5,25}$-$28_{5,24}$E	349685	5.5 ± 0.2	5.7 ± 0.1	1.27 ± 0.10	1.21 ± 0.08	0.5 ± 1.3	0.6 ± 1.3	2.1 ± 0.3	1.3 ± 0.1	3.5 ± 0.2	1.26 ± 0.06
$18_{13,5}$-$18_{12,6}$E	349836	2.2 ± 0.3	1.1 ± 0.1	< 3σ		< 3σ		< 3σ		< 3σ	

⋄ partially blended with other lines, ⋆ double peaked.

Table 2.B.7: Dimethyl ether

Transition	Frequency	G35.20 A		G35.20 B1		G35.20 B2		G35.20 B3		G35.03 A	
		FWHM	T_{peak}	FWHM	T_{peak}	FWHM	T_{peak}	FWHM	T_{peak}	FWHM	T_{peak}
	(MHz)	(km s^{-1})	(K)	(km s^{-1})	(K)	(km s^{-1})	(K)	(km s^{-1})	(K)	(km s^{-1})	(K)
CH_3OCH_3 ν=0											
$21_{2,19}$-$20_{3,18}$AA	337421	⋆5.4 ± 0.2	13.2 ± 0.4	2.05 ± 0.05	10.8 ± 0.2	1.7 ± 0.2	3.2 ± 0.3	2.53 ± 0.04	22.5 ± 0.3	4.7 ± 0.2	6.1 ± 0.2
$7_{4,4}$- $6_{3,3}$ EA	337712	blended		⋄1.5 ± 1.2	2.2 ± 1.7	< 3σ		⋄2.40 ± 0.04	5.35 ± 0.07	< 3σ	
$7_{4,4}$- $6_{3,3}$ EE	337722	⋆6.8 ± 3.4	10.5 ± 1.9	1.89 ± 0.06	7.9 ± 0.2	1.6 ± 0.2	3.3 ± 0.3	2.25 ± 0.05	19.8 ± 0.4	4.1 ± 0.1	4.57 ± 0.08
$7_{4,3}$- $6_{3,3}$ EA	337731	⋆6.7 ± 1.7	16.4 ± 6.8	2.45 ± 0.05	11.3 ± 0.2	2.1 ± 0.2	3.3 ± 0.3	3.00 ± 0.08	24.8 ± 0.6	5.5 ± 0.2	6.5 ± 0.1
$7_{4,4}$- $6_{3,4}$ EA	337770	⋆4.4 ± 1.4	2.5 ± 0.5	1.2 ± 0.2	2.5 ± 0.3	1.3 ± 0.6	0.6 ± 0.2	1.8 ± 0.1	7.5 ± 0.5	< 3σ	
$7_{4,3}$- $6_{3,4}$ EE	337779	⋆5.1 ± 0.3	13.7 ± 0.4	2.5 ± 0.1	9.7 ± 0.3	2.2 ± 0.3	3.0 ± 0.3	2.73 ± 0.08	22.5 ± 0.6	5.0 ± 0.1	6.05 ± 0.08
$7_{4,3}$- $6_{3,4}$ EE	337787	6.0 ± 0.1	29.4 ± 0.4	2.32 ± 0.04	15.1 ± 0.1	2.2 ± 0.2	4.9 ± 0.4	2.45 ± 0.09	27.0 ± 1.0	6.5 ± 0.1	14.1 ± 0.2
$7_{4,4}$- $6_{3,4}$ EE	337790	blended with 337787		2.0 ± 0.1	4.2 ± 0.1	in abs feature		2.8 ± 0.4	7.0 ± 0.8	< 3σ	
$35_{3,33}$- $35_{2,34}$	347985	2.5 ± 1.0	2.7 ± 0.9	< 3σ		< 3σ		1.53 ± 0.06	1.46 ± 0.03	< 3σ	
$35_{3,32}$-$35_{2,33}$EE	347989	2.5 ± 3.1	1.6 ± 0.8	< 3σ		< 3σ		1.56 ± 0.06	2.01 ± 0.04	< 3σ	
$35_{3,33}$-$35_{2,34}$AA	347992	2.5 ± 1.2	1.7 ± 0.6	< 3σ		< 3σ		1.3 ± 0.1	1.04 ± 0.05	< 3σ	
$32_{2,31}$- $32_{1,32}$ EE	349487	blended		< 3σ		< 3σ		2.2 ± 0.2	2.1 ± 0.2	< 3σ	
$11_{2,9}$-$10_{1,10}$AE	349803	blended with 349806		1.4 ± 0.1	2.1 ± 0.1	1.3 ± 0.3	0.9 ± 0.2	1.70 ± 0.07	8.8 ± 0.3	< 3σ	
$11_{2,9}$-$10_{1,10}$EE	349806	⋄⋆7.8 ± 0.2	7.6 ± 0.2	⋄1.9 ± 0.1	3.9 ± 0.1	⋄0.9 ± 0.2	0.7 ± 0.1	⋄2.4 ± 0.1	12.7 ± 0.2	< 3σ	
$11_{2,9}$-$10_{1,10}$AA	349809	blended with 349806		1.46 ± 0.09	3.29 ± 0.14	in abs feature		2.1 ± 0.1	8.5 ± 0.2	< 3σ	

⋄ partially blended with other lines, ⋆ double peaked

Table 2.B.8: Ethanol

Transition	Frequency (MHz)	G35.20 A FWHM (km s^{-1})	G35.20 A T_{peak} (K)	G35.20 B1 FWHM (km s^{-1})	G35.20 B1 T_{peak} (K)	G35.20 B2 FWHM (km s^{-1})	G35.20 B2 T_{peak} (K)	G35.20 B3 FWHM (km s^{-1})	G35.20 B3 T_{peak} (K)	G35.03 A FWHM (km s^{-1})	G35.03 A T_{peak} (K)
t-C_2H_5OH											
$24_{1,23}$ - $23_{2,21}$	335192	◇4 ± 2	1.2 ± 0.5	< 3σ		< 3σ		< 3σ		2.5 ± 0.2	1.00 ± 0.09
$23_{7,16}$-$23_{6,17}$	335441	⋆5.1 ± 0.2	6.4 ± 0.2	1.6 ± 0.2	1.98 ± 0.08	1.9 ± 0.5	0.6 ± 0.2	2.3 ± 0.1	1.78 ± 0.08	2.8 ± 0.2	1.8 ± 0.1
$23_{7,17}$-$23_{6,18}$	335631	⋆5.5 ± 0.2	7.0 ± 0.2	1.9 ± 0.2	2.2 ± 0.1	1.3 ± 0.7	1.1 ± 0.2	2.2 ± 0.2	1.8 ± 0.1	3.6 ± 0.2	2.16 ± 0.10
$13_{3,11}$-$12_{2,10}$	335950	⋆5.0 ± 0.2	10.3 ± 0.4	2.1 ± 0.2	3.9 ± 0.2	1.9 ± 0.2	1.8 ± 0.2	1.9 ± 0.3	4.2 ± 0.2	3.1 ± 0.2	2.79 ± 0.09
$22_{7,15}$-$22_{6,16}$	336158	5.6 ± 0.6	4.1 ± 0.2	1.6 ± 0.2	2.6 ± 0.2	1.7 ± 0.4	1.3 ± 0.1	1.5 ± 0.4	1.8 ± 1.0	2.7 ± 0.3	2.7 ± 0.2
$22_{7,16}$-$22_{6,17}$	336270	◇6.3 ± 0.1	10.9 ± 0.2	2.6 ± 0.3	3.3 ± 0.3	1.6 ± 0.9	1.5 ± 0.3	3.0 ± 0.6	6.9 ± 0.4	4.9 ± 0.1	3.66 ± 0.06
$19_{2,18}$-$18_{1,17}$	336626	5.6 ± 0.1	18.6 ± 0.4	< 3σ		< 3σ		< 3σ		4.0 ± 0.2	5.6 ± 0.2
$21_{7,14}$-$21_{6,15}$	336767	⋆5.3 ± 0.2	7.9 ± 0.2	1.9 ± 0.1	2.6 ± 0.1	1.3 ± 0.7	0.9 ± 0.2	2.1 ± 0.1	2.32 ± 0.07	3.9 ± 0.2	2.9 ± 0.1
$21_{7,15}$-$21_{6,16}$	336832	⋆6.1 ± 0.2	8.9 ± 0.2	edge of window		edge of window		edge of window		< 3σ	
$20_{7,14}$-$20_{6,15}$	337323	6.4 ± 0.5	9.7 ± 0.5	1.33 ± 0.01	2.86 ± 0.01	1.3 ± 0.2	1.7 ± 0.3	2.6 ± 0.2	2.8 ± 0.1	5.4 ± 0.7	5.09 ± 0.08
$19_{7,12}$-$19_{6,13}$	337727	blended		1.4 ± 0.1	2.2 ± 0.2	1.2 ± 0.4	1.3 ± 0.5	blended		2.1 ± 0.2	2.3 ± 0.2
$18_{7,11}$-$18_{6,12}$	338099	⋆6.8 ± 0.4	13.2 ± 0.3	1.5 ± 0.2	3.3 ± 0.2	1.6 ± 0.3	1.7 ± 0.4	2.5 ± 0.2	3.7 ± 0.1	6.0 ± 0.3	4.1 ± 0.1
$18_{7,12}$-$18_{6,13}$	338110	⋆7.0 ± 0.4	15.0 ± 0.3	1.9 ± 0.2	3.5 ± 0.1	1.8 ± 0.2	1.3 ± 0.2	3.0 ± 0.4	3.3 ± 0.3	5.4 ± 0.4	4.51 ± 0.09
$17_{7,10}$-$17_{6,11}$	338411	blended		blended		blended		blended		< 3σ	
$17_{7,11}$-$17_{6,12}$	338416	blended		< 3σ		< 3σ		< 3σ		< 3σ	
$16_{7,9}$-$16_{6,10}$	338672	blended with 338674		1.7 ± 0.1	3.6 ± 0.2	2.2 ± 0.1	1.77 ± 0.09	2.2 ± 0.4	3.3 ± 0.2	5.3 ± 0.1	4.40 ± 0.10
$16_{7,10}$-$16_{6,11}$	338674	⋆6.0 ± 0.1	17.4 ± 0.3	1.8 ± 0.4	4.1 ± 0.9	1.0 ± 0.3	1.2 ± 0.2	2.2 ± 0.3	3.4 ± 0.3	< 3σ	
$21_{0,21}$-$20_{1,20}$	346963	6.2 ± 0.2	26.2 ± 0.4	2.4 ± 0.1	8.8 ± 0.4	1.8 ± 0.4	3.5 ± 0.3	2.6 ± 0.2	8.4 ± 0.2	5.6 ± 0.1	8.8 ± 0.1
$14_{3,12}$-$13_{2,11}$	347351	⋆5.6 ± 0.1	17.1 ± 0.4	3.1 ± 0.1	6.5 ± 0.2	1.9 ± 0.5	1.8 ± 0.4	2.9 ± 0.1	5.9 ± 0.1	3.8 ± 0.2	4.5 ± 0.1
$21_{1,21}$-$20_{0,20}$	347446	blended		1.9 ± 0.1	9.3 ± 0.4	2.0 ± 0.5	4.1 ± 0.4	2.3 ± 0.2	9.9 ± 0.3	4.5 ± 0.1	8.0 ± 0.2
$22_{2,20}$-$21_{3,19}$	347975	⋆6.9 ± 0.2	11.0 ± 0.1	1.9 ± 0.1	3.2 ± 0.2	1.5 ± 0.3	1.5 ± 0.2	2.6 ± 0.2	3.0 ± 0.2	< 3σ	
$20_{2,19}$-$19_{1,18}$	350534	⋆4.8 ± 0.2	16.1 ± 0.5	1.8 ± 0.2	6.1 ± 0.3	1.7 ± 0.4	3.0 ± 0.4	2.08 ± 0.09	5.3 ± 0.2	3.1 ± 0.2	4.1 ± 0.2
g-C_2H_5OH											
$19_{3,16}$-$18_{3,15}$,vt=0-0	336030	blended		◇1.34 ± 0.04	4.0 ± 0.2	blended		blended		< 3σ	
$19_{3,16}$-$18_{3,15}$,vt=1-1	336572	6.1 ± 0.2	10.7 ± 0.3	1.8 ± 0.1	3.4 ± 0.1	1.1 ± 0.4	1.7 ± 0.4	2.4 ± 0.2	3.3 ± 0.1	4.1 ± 0.2	3.4 ± 0.1
$19_{2,17}$-$18_{2,16}$,vt=1-1	336795	⋆5.3 ± 0.1	13.7 ± 0.3	2.1 ± 0.2	4.0 ± 0.2	1.7 ± 0.9	1.9 ± 0.3	2.3 ± 0.2	4.4 ± 0.2	4.2 ± 0.1	4.6 ± 0.1
$19_{2,17}$-$18_{2,16}$,vt=0-0	337801	⋆5.9 ± 0.2	7.5 ± 0.2	1.72 ± 0.04	2.45 ± 0.05	1.0 ± 0.2	1.0 ± 0.2	2.33 ± 0.08	2.28 ± 0.07	3.7 ± 0.1	2.61 ± 0.03
$20_{6,15}$-$19_{6,14}$,vt=1-1	346929	⋆6.6 ± 0.7	11.0 ± 0.4	2.1 ± 0.1	3.6 ± 0.3	1.5 ± 0.3	1.4 ± 0.3	2.13 ± 0.09	3.1 ± 0.1	< 3σ	
$20_{6,14}$-$19_{6,13}$,vt=1-1	346939	◇6.8 ± 1.0	13.0 ± 0.7	1.9 ± 0.1	2.5 ± 0.1	1.2 ± 0.2	1.7 ± 0.2	2.1 ± 1.1	3.1 ± 0.9	4.5 ± 0.7	9.6 ± 0.2
$20_{6,15}$-$19_{6,14}$,vt=0-0	347147	⋆5.2 ± 0.2	10.9 ± 0.3	1.53 ± 0.08	3.2 ± 0.1	0.8 ± 0.4	0.7 ± 0.3	2.5 ± 0.2	3.6 ± 0.1	3.64 ± 0.07	2.63 ± 0.04
$20_{6,14}$-$19_{6,13}$,vt=0-0	347158	⋆5.4 ± 0.2	11.2 ± 0.2	1.7 ± 0.2	3.4 ± 0.1	1.18 ± 0.07	1.71 ± 0.08	2.34 ± 0.08	3.0 ± 0.1	3.52 ± 0.09	2.94 ± 0.06
$20_{5,16}$-$19_{5,15}$,vt=1-1	347474	< 3σ		1.1 ± 0.6	2.4 ± 0.4	2.3 ± 0.3	1.2 ± 0.2	1.8 ± 0.2	2.4 ± 0.3	4.6 ± 0.5	2.7 ± 0.3
$20_{5,16}$-$19_{5,15}$,vt=0-0	347670	◇⋆5.5 ± 1.0	13.7 ± 0.3	1.9 ± 0.2	3.5 ± 0.2	1.8 ± 0.2	1.7 ± 0.1	2.30 ± 0.08	3.72 ± 0.09	4.8 ± 0.2	4.6 ± 0.1
$20_{5,15}$-$19_{5,14}$,vt=1-1	347675	◇⋆5.5 ± 1.0	9.5 ± 0.4	1.7 ± 0.1	3.5 ± 0.2	1.2 ± 0.3	1.8 ± 0.3	2.0 ± 0.2	2.8 ± 0.2	3.9 ± 0.1	2.91 ± 0.05
$16_{4,12}$-$15_{3,12}$,vt=0-1	347693	⋆5.5 ± 1.2	7.7 ± 0.2	1.6 ± 0.1	2.0 ± 0.1	1.0 ± 0.3	1.2 ± 0.3	2.2 ± 0.1	1.7 ± 0.1	4.9 ± 0.4	2.13 ± 0.07
$20_{4,17}$-$19_{4,16}$,vt=1-1	347755	< 3σ		±	±	2.7 ± 0.2	2.2 ± 0.2	3.0 ± 0.2	6.4 ± 0.2	5.5 ± 0.2	4.30 ± 0.10
$20_{5,15}$-$19_{5,14}$,vt=0-0	347887	⋆5.2 ± 0.2	12.1 ± 0.4	2.1 ± 0.1	3.8 ± 0.1	1.7 ± 0.3	1.9 ± 0.3	2.0 ± 0.1	3.4 ± 0.2	3.7 ± 0.1	3.00 ± 0.10
$20_{4,17}$-$19_{4,16}$,vt=0-0	347916	5.4 ± 0.4	22.5 ± 2.7	1.6 ± 0.1	4.2 ± 0.2	1.7 ± 0.2	1.2 ± 0.1	2.3 ± 0.2	4.0 ± 0.2	< 3σ	
$4_{4,0}$-$3_{3,0}$,vt=1-0	348720	5.5 ± 0.2	13.6 ± 0.3	2.0 ± 0.2	4.3 ± 0.2	1.4 ± 0.2	2.3 ± 0.2	2.3 ± 0.1	4.4 ± 0.2	3.6 ± 0.1	3.25 ± 0.10
$4_{4,1}$-$3_{3,1}$,vt=1-0	348721	blended with 348720		blended with 348720		blended with 348720		blended with 348720		< 3σ	
$20_{4,16}$-$19_{4,15}$,vt=1-1	349997	5.3 ± 0.1	12.2 ± 0.2	< 3σ		< 3σ		2.33 ± 0.09	3.3 ± 0.1	4.1 ± 0.1	3.46 ± 0.09
$20_{4,16}$-$19_{4,15}$,vt=0-0	350365	blended		◇1.9 ± 0.1	5.4 ± 0.4	2.6 ± 0.8	2.9 ± 0.4	blended		4.7 ± 0.1	5.4 ± 0.1

◇ partially blended with other lines, ⋆ double peaked

Table 2.B.9: Ethylene glycol

Transition	Frequency (MHz)	G35.20 A FWHM (km s^{-1})	G35.20 A T_{peak} (K)	G35.20 B1 FWHM (km s^{-1})	G35.20 B1 T_{peak} (K)	G35.20 B2 FWHM (km s^{-1})	G35.20 B2 T_{peak} (K)	G35.20 B3 FWHM (km s^{-1})	G35.20 B3 T_{peak} (K)	G35.03 A FWHM (km s^{-1})	G35.03 A T_{peak} (K)
aGg' (CH_2OH)$_2$											
$32_{6,27}$ ν= 1 - $31_{6,26}$ ν= 0	335030	5.7 ± 0.2	4.6 ± 0.1	< 3σ		< 3σ		< 3σ		3.9 ± 0.1	2.72 ± 0.09
$33_{9,25}$ ν= 0 - $32_{9,24}$ ν= 1	335180	6.1 ± 0.2	3.23 ± 0.07	< 3σ		< 3σ		< 3σ		3.6 ± 0.2	2.15 ± 0.10
$32_{11,21}$ ν= 1 - $31_{11,20}$ ν= 0	335357	blended		< 3σ		< 3σ		< 3σ		3.78 ± 0.06	6.48 ± 0.09
$33_{9,24}$ ν= 0 - $32_{9,23}$ ν= 1	335397	blended		< 3σ		< 3σ		< 3σ		4.7 ± 0.3	2.38 ± 0.09
$33_{5,29}$ ν= 1 - $32_{4,28}$ ν= 1	335657	2.7 ± 0.1	0.82 ± 0.03	< 3σ		< 3σ		< 3σ		2.6 ± 0.4	1.1 ± 0.1
$34_{5,30}$ ν= 0 - $33_{5,29}$ ν= 1	335739	6.1 ± 0.1	7.2 ± 0.1	< 3σ		< 3σ		< 3σ		4.2 ± 0.1	3.57 ± 0.10
$33_{8,26}$ ν= 0 - $32_{8,25}$ ν= 1	335906	6.7 ± 0.3	3.11 ± 0.09	< 3σ		< 3σ		< 3σ		3.80 ± 0.10	2.46 ± 0.05
$32_{10,23}$ ν= 1 - $31_{10,22}$ ν= 0	336012	4.5 ± 0.2	3.04 ± 0.08	< 3σ		< 3σ		< 3σ		3.7 ± 0.4	1.9 ± 0.2
$34_{4,30}$ ν= 0 - $33_{4,29}$ ν= 1	336223	5.5 ± 0.2	3.5 ± 0.1	< 3σ		< 3σ		< 3σ		4.0 ± 0.2	2.40 ± 0.09
$34_{3,32}$ ν= 1 - $33_{3,31}$ ν= 0	336323	7.3 ± 0.3	6.6 ± 0.2	< 3σ		< 3σ		< 3σ		5.1 ± 0.1	4.18 ± 0.06
$33_{7,27}$ ν= 0 - $32_{7,26}$ ν= 1	336334	4.3 ± 0.2	3.15 ± 0.09	< 3σ		< 3σ		< 3σ		3.0 ± 0.1	2.16 ± 0.08
$37_{1,37}$ ν= 0 - $36_{1,36}$ ν= 1	336756	4.0 ± 0.3	6.9 ± 0.5	< 3σ		< 3σ		< 3σ		3.6 ± 0.1	4.5 ± 0.1
$31_{6,25}$ ν= 1 - $30_{6,24}$ ν= 0	336828	blended		< 3σ		< 3σ		< 3σ		5.3 ± 0.3	3.4 ± 0.1
$32_{9,24}$ ν= 1 - $31_{9,23}$ ν= 0	336939	4.1 ± 0.2	3.6 ± 0.1	< 3σ		< 3σ		< 3σ		4.7 ± 0.2	2.75 ± 0.06
$33_{8,25}$ ν=0- $32_{8,24}$ ν=1	337082	blended		< 3σ		< 3σ		< 3σ		3.8 ± 0.2	3.0 ± 0.1
$32_{9,23}$ ν=1-$31_{9,22}$ ν=0	337094	blended		< 3σ		< 3σ		< 3σ		< 3σ	
$32_{7,26}$ ν=1-$31_{7,25}$ ν=0	337571	blended		< 3σ		< 3σ		< 3σ		< 3σ	
$33_{5,28}$ ν= 0 - $32_{5,27}$ ν= 1	337816	4.7 ± 0.7	4.5 ± 2.0	< 3σ		< 3σ		< 3σ		< 3σ	
$35_{4,32}$ ν=0-$34_{4,31}$ ν=1	338214	blended		< 3σ		< 3σ		< 3σ		4.2 ± 0.6	2.7 ± 0.3
$32_{8,25}$ ν= 1 - $31_{8,24}$ ν= 0	338221	3.86 ± 0.10	3.45 ± 0.05	< 3σ		< 3σ		< 3σ		2.8 ± 0.4	2.1 ± 0.2

Table 2.B.9: Ethylene glycol continued.

Transition	Frequency	G35.20 A		G35.20 B1		G35.20 B2		G35.20 B3		G35.03 A	
		FWHM	T_{peak}	FWHM	T_{peak}	FWHM	T_{peak}	FWHM	T_{peak}	FWHM	T_{peak}
	(MHz)	(km s^{-1})	(K)	(km s^{-1})	(K)	(km s^{-1})	(K)	(km s^{-1})	(K)	(km s^{-1})	(K)
$35_{3,32}$ ν= 0 - $34_{3,31}$ ν= 1	338240	3.9 ± 0.8	6.1 ± 0.2	< 3σ		< 3σ		< 3σ		4.7 ± 0.4	3.2 ± 0.1
$36_{4,33}$ ν= 0 - $35_{4,32}$ ν= 1	347361	4.6 ± 0.3	4.6 ± 0.2	< 3σ		< 3σ		< 3σ		2.94 ± 0.07	2.74 ± 0.05
$36_{3,33}$ ν= 0 - $35_{3,32}$ ν= 1	347378	4.9 ± 0.2	4.5 ± 0.1	< 3σ		< 3σ		< 3σ		3.5 ± 0.2	2.29 ± 0.07
$32_{6,26}$ ν=1-$31_{6,25}$ ν=0	347387	blended		< 3σ		< 3σ		< 3σ		3.49 ± 0.08	3.00 ± 0.06
$33_{9,25}$ ν=1-$32_{9,24}$ ν=0	347487	blended		< 3σ		< 3σ		< 3σ		3.0 ± 0.3	3.2 ± 0.2
$33_{7,27}$ ν= 1 - $32_{7,26}$ ν= 0	347732	⋄4.28 ± 0.09	6.1 ± 0.1	< 3σ		< 3σ		< 3σ		4.1 ± 0.3	4.2 ± 0.6
$33_{9,24}$ ν= 1 - $32_{9,23}$ ν= 0	347738	4.27 ± 0.09	5.83 ± 0.07	< 3σ		< 3σ		< 3σ		3.7 ± 0.2	2.88 ± 0.07
$17_{9,8}$ ν= 1 - $16_{8,9}$ ν= 1	347813	blended		< 3σ		< 3σ		< 3σ		2.9 ± 0.3	0.82 ± 0.05
$17_{9,8}$ ν= 0 - $16_{8,9}$ ν= 0	347821	blended		< 3σ		< 3σ		< 3σ		2.3 ± 0.1	1.14 ± 0.06
$15_{10,5}$ ν= 0 - $14_{9,6}$ ν= 0	347963	4.6 ± 0.4	4.1 ± 0.2	< 3σ		< 3σ		< 3σ		3.8 ± 0.4	1.84 ± 0.08
$34_{8,27}$ ν= 0 - $33_{8,25}$ ν= 0	348326	⋄4.3 ± 0.5	3.9 ± 0.2	< 3σ		< 3σ		< 3σ		< 3σ	
$36_{1,35}$ ν= 1 - $35_{1,34}$ ν= 0	348331	⋄4.3 ± 0.5	9.0 ± 0.2	< 3σ		< 3σ		< 3σ		< 3σ	
$35_{6,30}$ ν= 0 - $34_{6,29}$ ν= 1	348550	5.7 ± 0.2	9.8 ± 0.3	< 3σ		< 3σ		< 3σ		4.9 ± 0.2	2.56 ± 0.07
$33_{8,26}$ ν= 1 - $32_{8,25}$ ν= 0	349355	blended		< 3σ		< 3σ		< 3σ		5.0 ± 0.4	1.73 ± 0.04
$34_{5,30}$ ν=1-$33_{5,29}$ ν=0	349445	blended		< 3σ		< 3σ		< 3σ		< 3σ	
$33_{5,28}$ ν=1-$32_{5,27}$ ν=0	349541	blended		< 3σ		< 3σ		< 3σ		6.4 ± 2.3	2.18 ± 0.08
$37_{3,35}$ ν=0-$36_{3,34}$ ν=1	349867	blended		< 3σ		< 3σ		< 3σ		2.94 ± 0.10	4.2 ± 0.1
$34_{4,30}$ ν=1-$33_{4,29}$ ν=0	350023	blended		< 3σ		< 3σ		< 3σ		3.35 ± 0.10	2.35 ± 0.06
$34_{8,26}$ ν=0-$33_{8,25}$ ν=1	350142	blended		< 3σ		< 3σ		< 3σ		5.2 ± 0.7	2.44 ± 0.09
$37_{1,36}$ ν= 0 - $36_{2,35}$ ν= 0	350402	blended		< 3σ		< 3σ		< 3σ		2.4 ± 0.0754	1.43 ± 0.02

⋄ partially blended with other lines.

Table 2.B.10: Formamide

Transition	Frequency	G35.20 A		G35.20 B1		G35.20 B2		G35.20 B3		G35.03 A	
		FWHM	T_{peak}	FWHM	T_{peak}	FWHM	T_{peak}	FWHM	T_{peak}	FWHM	T_{peak}
	(MHz)	(km s^{-1})	(K)	(km s^{-1})	(K)	(km s^{-1})	(K)	(km s^{-1})	(K)	(km s^{-1})	(K)
NH_2CHO ν=0											
$16_{2,15}$-$15_{2,14}$	336136	5.8 ± 0.2	30.8 ± 0.8	5.0 ± 0.1	8.0 ± 0.1	2.8 ± 0.4	2.3 ± 0.1	3.17 ± 0.09	8.2 ± 0.1	4.63 ± 0.09	15.4 ± 0.3
$16_{1,16}$-$15_{0,15}$	336161	8.5 ± 0.2	9.4 ± 0.2	3.2 ± 0.6	1.54 ± 0.07	< 3σ		2.7 ± 0.2	5.6 ± 0.3	4.3 ± 0.2	4.24 ± 0.10
$28_{2,26}$-$28_{1,27}$	347729	blended		< 3σ		< 3σ		4.1 ± 0.5	0.85 ± 0.05	< 3σ	
	349053	blended		< 3σ		< 3σ		2.0 ± 0.2	1.66 ± 0.09	< 3σ	
$16_{2,14}$-$15_{2,13}$	349482	5.4 ± 0.2	33.4 ± 1.0	5.4 ± 0.1	8.3 ± 0.2	2.2 ± 0.2	1.9 ± 0.1	3.4 ± 0.1	7.2 ± 0.2	5.0 ± 0.1	12.9 ± 0.3
NH_2CHO v12=1											
	349020	blended		< 3σ		2.3 ± 0.3	0.92 ± 0.09	< 3σ		< 3σ	
NH_2CDO											
$16_{4,13}$- $15_{4,12}$	335234	10.7 ± 0.5	2.81 ± 0.07	< 3σ		< 3σ		< 3σ		< 3σ	
$18_{1,18}$- $17_{1,17}$	348283	blended		< 3σ		< 3σ		1.4 ± 0.4	0.6 ± 0.1	< 3σ	
$18_{0,18}$- $17_{0,17}$	348730	blended		< 3σ		< 3σ		< 3σ		< 3σ	
$NH_2^{13}CHO$											
	335403	⋄3.6 ± 0.6	3.9 ± 0.4	1.9 ± 0.1	0.84 ± 0.05	1.1 ± 0.2	0.54 ± 0.09	2.2 ± 0.3	1.4 ± 0.2	< 3σ	
	349309	5.7 ± 0.2	3.6 ± 0.1	1.21 ± 0.09	0.78 ± 0.04	0.9 ± 0.2	0.7 ± 0.2	2.2 ± 0.2	1.3 ± 0.1	< 3σ	
$NH_2CH^{18}O$											
$18_{0,18}$-$17_{0,17}$	347589	⋄6 ± 2	3 ± 2	1.2 ± 0.4	0.6 ± 0.1	1.85 ± 0.2	0.8 ± 0.2	1.4 ± 0.4	1.2 ± 0.2	< 3σ	
$17_{1,16}$-$16_{1,15}$	348029	blended		< 3σ		2.6 ± 0.5	0.66 ± 0.07	< 3σ		< 3σ	

⋄ partially blended with other lines

Table 2.B.11: Methyl cyanide

Transition	Frequency (MHz)	G35.20 A FWHM (km s^{-1})	G35.20 A T_{peak} (K)	G35.20 B1 FWHM (km s^{-1})	G35.20 B1 T_{peak} (K)	G35.20 B2 FWHM (km s^{-1})	G35.20 B2 T_{peak} (K)	G35.20 B3 FWHM (km s^{-1})	G35.20 B3 T_{peak} (K)	G35.03 A FWHM (km s^{-1})	G35.03 A T_{peak} (K)
CH_3CN ν=0											
19_9 - 18_9	348911	⋆8.0 ± 0.2	27.3 ± 0.4	blended		blended		2.0 ± 0.2	8 ± 1	< 3σ	
19_8 - 18_8	349025	⋆7.8 ± 0.2	19.1 ± 0.5	1.5 ± 0.2	3.0 ± 0.2	1.6 ± 0.3	1.2 ± 0.2	2.22 ± 0.06	12.2 ± 0.4	7.6 ± 0.1	8.2 ± 0.1
19_7 - 18_7	349125	⋆6.3 ± 0.2	26.6 ± 0.8	2.1 ± 0.1	6.3 ± 0.3	1.6 ± 0.2	2.6 ± 0.3	2.58 ± 0.08	22.0 ± 0.5	5.97 ± 0.09	10.9 ± 0.2
19_6 - 18_6	349212	⋆6.6 ± 0.3	47.0 ± 1.0	3.2 ± 0.3	18 ± 1	1.8 ± 0.2	8.4 ± 1.0	2.82 ± 0.06	39.9 ± 0.8	4.4 ± 0.2	13.6 ± 0.5
19_5 - 18_5	349286	⋆7.0 ± 0.3	48.9 ± 1.8	3.2 ± 0.2	18.4 ± 1.0	1.9 ± 0.2	8.9 ± 0.6	2.70 ± 0.03	41.7 ± 0.3	5.6 ± 0.5	19.4 ± 0.3
19_4 - 18_4	349346	⋆6.3 ± 0.2	54.8 ± 1.6	3.2 ± 0.2	24 ± 1	2.3 ± 0.2	14.7 ± 1.2	2.89 ± 0.03	47.7 ± 0.5	7.1 ± 0.2	21.9 ± 0.6
19_3 - 18_3	349393	6.2 ± 0.2	62.3 ± 1.8	3.3 ± 0.1	26.6 ± 1.0	3.35 ± 0.08	25.9 ± 0.5	3.14 ± 0.06	38.8 ± 0.5	6.2 ± 0.3	25.4 ± 0.9
19_2 - 18_2	349427	6.5 ± 0.2	65.0 ± 1.4	3.5 ± 0.2	32 ± 2	2.8 ± 0.2	23.4 ± 1.3	3.01 ± 0.05	53.1 ± 0.8	7.6 ± 0.2	26.6 ± 0.5
19_1 - 18_1	349447	⋄6.7 ± 0.2	68.0 ± 0.8	⋄3.3 ± 0.2	38 ± 2	⋄2.7 ± 0.2	26.7 ± 1.6	⋄2.94 ± 0.03	50.3 ± 0.4	⋄6.9 ± 0.5	30.2 ± 0.5
19_0 - 18_0	349453	⋄5.0 ± 0.3	64.5 ± 1.5	⋄3.3 ± 0.2	40 ± 2	⋄2.7 ± 0.2	24.9 ± 1.5	⋄3.10 ± 0.04	54.5 ± 0.6	⋄5.1 ± 0.3	27.6 ± 1.1
CH_3CN v_8=1, F=19-18											
$19_{10,2}$ - $18_{10,2}$	349975	blended		< 3σ		< 3σ		< 3σ		< 3σ	
$19_{7,1}$ - $18_{7,1}$	350059	⋄3.1 ± 0.8	1.6 ± 1.7	< 3σ		< 3σ		1.4 ± 0.7	0.6 ± 0.1	3.2 ± 0.3	0.91 ± 0.08
$19_{6,1}$ - $18_{6,1}$	350160	7.5 ± 1.7	3.9 ± 0.4	< 3σ		< 3σ		1.5 ± 0.2	1.6 ± 0.1	< 3σ	
$19_{1,2}$ - $18_{-1,2}$	350168	6.5 ± 0.2	15.7 ± 0.5	3.1 ± 0.3	2.6 ± 0.2	1.3 ± 0.3	0.9 ± 0.2	2.6 ± 0.1	11.2 ± 0.4	< 3σ	
$19_{8,2}$ - $18_{8,2}$	350190	7.0 ± 0.3	3.07 ± 0.06	< 3σ		< 3σ		⋄1.4 ± 0.9	0.8 ± 0.9	4.6 ± 0.2	1.27 ± 0.03
$19_{5,1}$ - $18_{5,1}$	350247	8.2 ± 0.2	10.1 ± 0.3	blended		< 3σ		3.33 ± 0.08	4.44 ± 0.09	< 3σ	
$19_{7,2}$ - $18_{7,2}$	350277	⋄7.0 ± 1.2	7.2 ± 0.7	blended		< 3σ		2.38 ± 0.06	3.16 ± 0.07	< 3σ	
$19_{4,1}$ - $18_{4,1}$	350320	blended		blended		< 3σ		2.12 ± 0.09	3.5 ± 0.1	< 3σ	
$19_{6,1}$ - $18_{6,1}$	350352	5.1 ± 1.0	6.7 ± 0.3	< 3σ		< 3σ		2.5 ± 0.1	2.8 ± 0.1	5.4 ± 0.3	2.93 ± 0.09
$19_{3,1}$ - $18_{3,1}$	350380	7.3 ± 0.1	10.1 ± 0.2	blended		< 3σ		2.3 ± 0.1	5.7 ± 0.1	6.0 ± 0.2	4.19 ± 0.10
$19_{5,2}$ - $18_{5,2}$	350415	blended		1.9 ± 0.3	0.9 ± 0.1	1.1 ± 0.1	0.72 ± 0.07	2.33 ± 0.07	5.0 ± 0.1	< 3σ	
$19_{2,1}$ - $18_{2,1}$	350423	blended		blended		blended		blended		< 3σ	
$19_{0,2}$ - $18_{0,2}$	350445	blended		blended		blended		blended		< 3σ	
$19_{1,1}$ - $18_{1,1}$	350450	blended		blended		< 3σ		2.5 ± 0.2	9.8 ± 0.4	< 3σ	
$19_{4,2}$ - $18_{4,2}$	350465	4.9 ± 0.3	16.0 ± 1.2	3.7 ± 0.3	2.9 ± 0.1	2.3 ± 0.5	0.9 ± 0.2	2.46 ± 0.05	11.9 ± 0.2	5.9 ± 0.2	7.7 ± 0.1
$19_{3,2}$ - $18_{3,2}$	350507	8.2 ± 0.2	15.6 ± 0.3	⋄3.7 ± 0.4	1.79 ± 0.10	1.8 ± 0.2	1.6 ± 0.2	2.59 ± 0.07	9.3 ± 0.2	6.6 ± 0.1	6.19 ± 0.05
$19_{2,2}$ - $18_{2,2}$	350552	6.9 ± 0.2	17.4 ± 0.3	⋄3.5 ± 0.2	2.61 ± 0.07	blended		2.8 ± 0.1	10.5 ± 0.4	6.4 ± 0.1	6.96 ± 0.08
$CH_3^{13}CN$											
19_8 - 18_8	348854	blended		< 3σ		< 3σ		1 ± 2	0.7 ± 0.2	< 3σ	
19_7 - 18_7	348954	blended		< 3σ		< 3σ		2.2 ± 0.4	0.64 ± 0.08	< 3σ	
19_6 - 18_6	349040	blended		< 3σ		< 3σ		2.1 ± 0.2	3.2 ± 0.3	< 3σ	
19_5 - 18_5	349114	blended		blended		< 3σ		2.5 ± 0.1	2.9 ± 0.1	< 3σ	
19_4 - 18_4	349174	⋄⋆6.2 ± 0.3	8.0 ± 0.1	2.3 ± 0.4	1.6 ± 0.2	< 3σ		2.95 ± 0.03	5.67 ± 0.05	< 3σ	
19_3 - 18_3	349222	blended		2.5 ± 0.3	4.1 ± 0.4	1.3 ± 0.4	1.3 ± 0.2	2.48 ± 0.05	12.5 ± 0.2	4.9 ± 1.1	5.0 ± 0.5
19_2 - 18_2	349254	⋆5.7 ± 0.2	9.0 ± 0.3	1.7 ± 0.4	1.5 ± 0.3	1.4 ± 0.3	1.1 ± 0.2	2.46 ± 0.09	10.4 ± 0.2	5.2 ± 0.2	3.3 ± 0.1
19_1 - 18_1	349274	blended		1.6 ± 0.2	1.8 ± 0.2	1.4 ± 0.5	0.9 ± 0.3	2.6 ± 0.1	11.7 ± 0.4	5.5 ± 0.5	4.4 ± 0.3
19_0 - 18_0	349280	blended		blended		blended		3.1 ± 0.3	10.4 ± 0.3	5.5 ± 0.5	6.7 ± 0.3
CH_2DCN											
$20_{7,13}$ - $19_{7,12}$	346968	blended		< 3σ		< 3σ		blended		< 3σ	
$20_{0,20}$ - $19_{0,19}$	347043	5.8 ± 0.3	7.1 ± 0.3	1.5 ± 0.3	1.0 ± 0.2	1 ± 1	0.54 ± 0.09	3.01 ± 0.08	10.0 ± 0.2	< 3σ	

Table 2.B.11: Methyl cyanide continued.

Transition	Frequency	G35.20 A		G35.20 B1		G35.20 B2		G35.20 B3		G35.03 A	
	(MHz)	FWHM (km s^{-1})	T_{peak} (K)	FWHM (km s^{-1})	T_{peak} (K)	FWHM (km s^{-1})	T_{peak} (K)	FWHM (km s^{-1})	T_{peak} (K)	FWHM (km s^{-1})	T_{peak} (K)
$20_{5,15}$ - $19_{5,14}$	347110	7.5 ± 0.2	3.8 ± 0.1	0.9 ± 0.2	0.52 ± 0.09	$< 3\sigma$		2.4 ± 0.1	5.6 ± 0.2	$< 3\sigma$	
$20_{4,16}$ - $19_{4,15}$	347166	blended		1.4 ± 0.5	0.5 ± 0.3	$< 3\sigma$		2.7 ± 0.1	7.4 ± 0.3	$< 3\sigma$	
$20_{3,18}$ - $19_{3,17}$	347216	blended		1.6 ± 0.2	0.61 ± 0.04	$< 3\sigma$		4.2 ± 0.1	7.8 ± 0.2	$< 3\sigma$	
$20_{3,17}$ - $19_{3,16}$	347219	blended		1.09 ± 0.06	1.26 ± 0.04	$< 3\sigma$		blended with 347216		$< 3\sigma$	
$20_{2,18}$ - $19_{2,17}$	347388	5.7 ± 0.1	8.7 ± 0.2	1.2 ± 0.1	0.75 ± 0.06	$< 3\sigma$		2.59 ± 0.08	7.6 ± 0.2	3.49 ± 0.09	3.00 ± 0.06
$20_{1,19}$ - $19_{1,18}$	348691	◇2.84 ± 0.07	3.9 ± 0.1	1.6 ± 0.3	1.1 ± 0.2	$< 3\sigma$		2.36 ± 0.09	7.7 ± 0.3	$< 3\sigma$	

◇ partially blended with other lines, ⋆ double peaked.

Table 2.B.12: Vinyl cyanide

Transition	Frequency (MHz)	G35.20 A FWHM (km s^{-1})	G35.20 A T_{peak} (K)	G35.20 B1 FWHM (km s^{-1})	G35.20 B1 T_{peak} (K)	G35.20 B2 FWHM (km s^{-1})	G35.20 B2 T_{peak} (K)	G35.20 B3 FWHM (km s^{-1})	G35.20 B3 T_{peak} (K)	G35.03 A FWHM (km s^{-1})	G35.03 A T_{peak} (K)
C_2H_3CN											
$36_{2,35}$-$35_{2,34}$	337040	◇4.0 ± 0.3	3.4 ± 0.2	blended		< 3σ		2.38 ± 0.09	1.96 ± 0.06	8.1 ± 3.1	1.25 ± 0.10
$35_{3,32}$-$34_{3,31}$	337051	blended		blended		< 3σ		2.0 ± 0.9	0.9 ± 0.3	2.5 ± 0.2	2.8 ± 0.1
$37_{1,37}$-$36_{1,36}$	338214	◇7.2 ± 0.3	5.4 ± 0.1	< 3σ		< 3σ		2.8 ± 0.1	2.49 ± 0.09	< 3σ	
$35_{2,33}$-$34_{2,32}$	338278	4.31 ± 0.09	3.90 ± 0.03	< 3σ		< 3σ		2.32 ± 0.08	2.09 ± 0.06	5.7 ± 0.8	1.12 ± 0.06
$37_{0,37}$-$36_{0,36}$	338448	blended		< 3σ		< 3σ		◇1.3 ± 0.9	2.4 ± 1.2	< 3σ	
$36_{3,33}$-$35_{3,32}$	346943	blended		< 3σ		< 3σ		◇2.0 ± 0.5	2.7 ± 0.5	< 3σ	
$38_{1,38}$-$37_{1,37}$	347232	5.3 ± 0.2	4.03 ± 0.07	< 3σ		< 3σ		2.7 ± 0.1	2.23 ± 0.08	< 3σ	
$38_{0,38}$-$37_{0,37}$	347434	6.1 ± 1.1	6.3 ± 0.5	< 3σ		< 3σ		2.8 ± 0.2	2.6 ± 0.1	5.5 ± 0.4	2.00 ± 0.07
$53_{5,48}$-$53_{4,49}$	347685	blended		< 3σ		< 3σ		◇1.35 ± 0.08	0.61 ± 0.02	< 3σ	
$36_{2,34}$-$35_{2,33}$	347759	blended		blended		< 3σ		3.2 ± 0.4	1.8 ± 0.1	< 3σ	
$38_{1,38}$-$37_{0,37}$	348637	blended		< 3σ		< 3σ		blended		< 3σ	
$37_{1,36}$-$36_{1,35}$	348991	4.8 ± 0.1	6.2 ± 0.1	< 3σ		< 3σ		◇2.31 ± 0.05	4.71 ± 0.09	< 3σ	
$49_{4,46}$-$49_{3,47}$	350364	< 3σ		blended		blended		blended		< 3σ	

◇ partially blended with other lines

Table 2.B.13: Ethyl cyanide

Transition	Frequency	G35.20 A		G35.20 B1		G35.20 B2		G35.20 B3		G35.03 A	
	(MHz)	FWHM (km s^{-1})	T_{peak} (K)	FWHM (km s^{-1})	T_{peak} (K)	FWHM (km s^{-1})	T_{peak} (K)	FWHM (km s^{-1})	T_{peak} (K)	FWHM (km s^{-1})	T_{peak} (K)
C_2H_5CN ν=0											
$55_{8,48}$-$55_{7,49}$	335274	$< 3\sigma$		$< 3\sigma$		$< 3\sigma$		1.65 ± 0.22	0.72 ± 0.08	$< 3\sigma$	
$9_{6,4}$- $8_{5,3}$	335321	blended		blended		$< 3\sigma$		blended		$< 3\sigma$	
$52_{8,44}$-$52_{7,45}$	335895	2.89 ± 0.29	1.14 ± 0.04	$< 3\sigma$		$< 3\sigma$		$< 3\sigma$		$< 3\sigma$	
$20_{4,17}$-$19_{3,16}$	336614	blended		$< 3\sigma$		$< 3\sigma$		1.59 ± 0.18	0.50 ± 0.05	$< 3\sigma$	
$38_{3,36}$-$37_{3,35}$	337347	blended		blended		blended		2.76 ± 0.07	4.05 ± 0.09	$< 3\sigma$	
$37_{4,33}$-$36_{4,32}$	337445	5.3 ± 0.1	14.5 ± 0.2	2.7 ± 0.1	1.71 ± 0.06	$< 3\sigma$		2.77 ± 0.07	4.05 ± 0.09	$< 3\sigma$	
$37_{3,34}$-$36_{3,33}$	338142	blended		blended		1.9 ± 0.2	1.08 ± 0.0854	2.87 ± 0.06	5.49 ± 0.10	$< 3\sigma$	
$20_{8,12}$-$20_{7,13}$	346925	blended		$< 3\sigma$		$< 3\sigma$		3.66 ± 0.11	1.54 ± 0.03	$< 3\sigma$	
$12_{8,4}$-$12_{7,5}$	346970	blended		1.11 ± 0.09	0.83 ± 0.06	$< 3\sigma$		blended		$< 3\sigma$	
$16_{8,9}$-$16_{7,10}$	346976	blended		$< 3\sigma$		$< 3\sigma$		2.84 ± 0.11	3.10 ± 0.08	$< 3\sigma$	
$15_{8,7}$-$15_{7,8}$	346979	blended		$< 3\sigma$		1.5 ± 0.2	1.2 ± 0.1	2.69 ± 0.15	2.20 ± 0.09	$< 3\sigma$	
$38_{3,35}$-$37_{3,34}$	346983	blended		blended		blended		blended		$< 3\sigma$	
$39_{2,37}$-$38_{2,36}$	348260	5.7 ± 0.1	9.0 ± 0.1	$< 3\sigma$		$< 3\sigma$		2.96 ± 0.16	3.96 ± 0.17	4.6 ± 0.8	1.39 ± 0.07
$40_{2,39}$-$39_{2,38}$	348344	blended		blended		$< 3\sigma$		blended		4.8 ± 1.6	2.1 ± 0.1
$40_{1,39}$-$39_{1,38}$	348553	5.4 ± 0.2	10.0 ± 0.2	1.1 ± 0.1	0.76 ± 0.06	$< 3\sigma$		2.08 ± 0.17	4.24 ± 0.28	5.1 ± 0.2	2.55 ± 0.08
$39_{12,28}$-$38_{12,27}$	349380	5.8 ± 1.0	5.8 ± 0.6	1.1 ± 0.2	1.02 ± 0.07	$< 3\sigma$		2.21 ± 0.26	1.97 ± 0.18	$< 3\sigma$	
$39_{9,31}$-$38_{9,30}$	349547	5.5 ± 0.5	7.5 ± 2.0	$< 3\sigma$		$< 3\sigma$		2.47 ± 0.13	3.42 ± 0.15	$< 3\sigma$	
$39_{16,23}$-$38_{16,22}$	349566	4.65 ± 0.06	3.79 ± 0.05	$< 3\sigma$		$< 3\sigma$		$< 3\sigma$		$< 3\sigma$	
$39_{17,22}$-$38_{17,21}$	349652	4.7 ± 0.7	2.9 ± 0.2	$< 3\sigma$		$< 3\sigma$		$< 3\sigma$		$< 3\sigma$	
$39_{8,32}$-$38_{8,31}$	349730	5.3 ± 0.1	7.4 ± 0.2	1.2 ± 0.2	1.0 ± 0.1	$< 3\sigma$		2.37 ± 0.08	3.67 ± 0.10	$< 3\sigma$	
$39_{18,21}$ - $38_{18,20}$	349751	4.1 ± 0.6	3.6 ± 0.1	$< 3\sigma$		$< 3\sigma$		$< 3\sigma$		$< 3\sigma$	
$39_{4,36}$-$38_{4,35}$	349796	4.86 ± 0.04	6.73 ± 0.08	$< 3\sigma$		$< 3\sigma$		2.26 ± 0.10	3.09 ± 0.11	4.9 ± 0.7	0.97 ± 0.04
$39_{20,19}$ - $38_{20,18}$	349981	blended		$< 3\sigma$		$< 3\sigma$		$< 3\sigma$		$< 3\sigma$	
$39_{7,33}$-$38_{7,32}$	350039	4.9 ± 0.1	5.1 ± 0.1	1.0 ± 0.5	0.5 ± 0.2	blended		2.04 ± 0.10	2.87 ± 0.11	3.6 ± 1.0	0.95 ± 0.10
$39_{7,32}$-$38_{7,31}$	350051	5.5 ± 0.3	5.6 ± 0.1	$< 3\sigma$		$< 3\sigma$		2.21 ± 0.12	2.36 ± 0.11	3.0 ± 0.4	1.36 ± 0.07
$41_{1,41}$-$40_{1,40}$	350140	blended		blended		$< 3\sigma$		blended		$< 3\sigma$	
$41_{0,41}$-$40_{0,40}$	350145	blended		$\diamond$1.4 ± 0.2	1.2 ± 0.1	$< 3\sigma$		$\diamond$2.02 ± 0.24	2.54 ± 0.13	$\diamond$3.9 ± 0.1	2.53 ± 0.04
$39_{6,34}$-$38_{6,33}$	350512	blended		1.0 ± 0.2	0.9 ± 0.1	1.3 ± 0.2	0.71 ± 0.08	2.17 ± 0.21	2.59 ± 0.19	$< 3\sigma$	
CH_3CHDCN											
$40_{0,40}$ - $39_{1,39}$	335229	$\diamond$1.8 ± 0.2	1.6 ± 0.1	$< 3\sigma$		$< 3\sigma$		$< 3\sigma$		$< 3\sigma$	
$40_{1,40}$ - $39_{1,39}$	335237	$\diamond$2.0 ± 0.7	2.4 ± 2.0	$< 3\sigma$		$< 3\sigma$		$< 3\sigma$		$< 3\sigma$	
$40_{0,40}$ - $39_{1,39}$	335239	$\diamond$2.3 ± 0.7	2.4 ± 0.2	$< 3\sigma$		$< 3\sigma$		$< 3\sigma$		$< 3\sigma$	
$40_{1,40}$ - $39_{0,39}$	335246	2.4 ± 0.3	0.93 ± 0.06	$< 3\sigma$		$< 3\sigma$		$< 3\sigma$		$< 3\sigma$	
$38_{14,25}$ - $37_{14,24}$	335427	$\diamond$1.83 ± 0.07	1.44 ± 0.02	$< 3\sigma$		$< 3\sigma$		$< 3\sigma$		$< 3\sigma$	
$38_{13,26}$ - $37_{13,25}$	335430	$\diamond$2.05 ± 0.07	2.00 ± 0.01	$< 3\sigma$		$< 3\sigma$		$< 3\sigma$		$< 3\sigma$	
$38_{4,35}$ - $37_{4,34}$	335511	$\diamond$2.7 ± 0.5	1.27 ± 0.06	$< 3\sigma$		$< 3\sigma$		$< 3\sigma$		$< 3\sigma$	
$38_{11,27}$ - $37_{11,26}$	335513	$\diamond$1.9 ± 0.3	1.0 ± 0.1	$< 3\sigma$		$< 3\sigma$		$< 3\sigma$		$< 3\sigma$	
$43_{9,34}$ - $43_{8,35}$	335989	2.1 ± 0.5	0.9 ± 0.2	$< 3\sigma$		$< 3\sigma$		$< 3\sigma$		$< 3\sigma$	
$38_{7,32}$ - $37_{7,31}$	336425	$\diamond$5.5 ± 0.1	3.30 ± 0.04	$< 3\sigma$		$< 3\sigma$		$< 3\sigma$		$< 3\sigma$	
$36_{7,29}$ - $35_{7,28}$	336453	3.8 ± 0.2	2.54 ± 0.07	$< 3\sigma$		$< 3\sigma$		$< 3\sigma$		$< 3\sigma$	
$38_{6,33}$ - $37_{6,32}$	336971	blended		$< 3\sigma$		$< 3\sigma$		$< 3\sigma$		$< 3\sigma$	

Table 2.B.13: Ethyl cyanide continued.

Transition	Frequency	G35.20 A		G35.20 B1		G35.20 B2		G35.20 B3		G35.03 A	
	(MHz)	FWHM (km s^{-1})	T_{peak} (K)	FWHM (km s^{-1})	T_{peak} (K)	FWHM (km s^{-1})	T_{peak} (K)	FWHM (km s^{-1})	T_{peak} (K)	FWHM (km s^{-1})	T_{peak} (K)
$38_{6,32}$ - $37_{6,31}$	337336	blended		$< 3\sigma$		$< 3\sigma$		$< 3\sigma$		$< 3\sigma$	
$40_{3,38}$ - $39_{3,37}$	347816	1.83 ± 0.04	2.28 ± 0.02	$< 3\sigma$		$< 3\sigma$		$< 3\sigma$		$< 3\sigma$	
$41_{2,40}$ - $40_{2,39}$	349907	5.4 ± 0.1	1.85 ± 0.05	$< 3\sigma$		$< 3\sigma$		$< 3\sigma$		$< 3\sigma$	
$CH_3^{13}CH_2CN$											
$38_{8,31}$ - $38_{7,32}$	335362	$< 3\sigma$		$< 3\sigma$		$< 3\sigma$		1.2 ± 0.2	0.77 ± 0.09	$< 3\sigma$	
$38_{3,36}$ - $37_{3,35}$	335369	4.2 ± 2.4	1.5 ± 0.1	$< 3\sigma$		$< 3\sigma$		$< 3\sigma$		$< 3\sigma$	
$39_{1,38}$ - $38_{1,37}$	337951	6.5 ± 0.3	2.32 ± 0.07	$< 3\sigma$		$< 3\sigma$		$< 3\sigma$		$< 3\sigma$	
$^{13}CH_3CH_2CN$											
$40_{2,38}$ - $39_{2,37}$	348147	3 ± 1	2.45 ± 0.08	$< 3\sigma$		$< 3\sigma$		$< 3\sigma$		$< 3\sigma$	

◇ partially blended with other lines.

Table 2.B.14: Cyanoacetylene

Transition	Frequency	G35.20 A		G35.20 B1		G35.20 B2		G35.20 B3		G35.03 A	
		FWHM	T_{peak}	FWHM	T_{peak}	FWHM	T_{peak}	FWHM	T_{peak}	FWHM	T_{peak}
	(MHz)	(km s^{-1})	(K)	(km s^{-1})	(K)	(km s^{-1})	(K)	(km s^{-1})	(K)	(km s^{-1})	(K)
HC_3N ν=0											
37 - 36	336520	7.4 ± 0.1	27.6 ± 0.4	4.53 ± 0.10	17.0 ± 0.3	◇1.6 ± 0.1	6.5 ± 0.4	3.32 ± 0.04	47.2 ± 0.5	blended	
HC_3N v6=1											
37 $_1$ - 36 $_{-1}$	337070	blended		< 3σ		< 3σ		2.4 ± 0.1	2.64 ± 0.08	< 3σ	
37 $_{-1}$ - 36 $_1$	337335	5.3 ± 0.8	3.1 ± 0.3	< 3σ		< 3σ		2.2 ± 0.1	2.1 ± 0.1	< 3σ	
HC_3N v7=1											
37 $_1$ - 36 $_{-1}$	337344	blended		◇1.8 ± 0.5	1.7 ± 0.4	◇1.4 ± 0.1	1.20 ± 0.07	◇2.84 ± 0.05	19.2 ± 0.2	blended	
37 $_{-1}$ - 36 $_1$	337825	◇5.3 ± 0.5	9.3 ± 1.4	◇3.9 ± 0.4	3.08 ± 0.09	< 3σ		◇2.83 ± 0.08	18.8 ± 0.4	blended	
38 $_1$ - 37 $_{-1}$	346949	6.2 ± 1.4	13.6 ± 1.3	3.8 ± 0.2	2.5 ± 0.1	0.9 ± 0.3	0.7 ± 0.2	2.8 ± 0.1	22.6 ± 0.8	6.3 ± 1.1	10.8 ± 0.3
HC_3N v7=2											
37 $_2$ - 36 $_{-2}$	338646	blended		< 3σ		< 3σ		2.53 ± 0.05	3.57 ± 0.06	< 3σ	
38 $_0$ - 37 $_0$	347663	5.2 ± 1.2	5.3 ± 0.4	< 3σ		< 3σ		2.62 ± 0.09	3.4 ± 0.1	< 3σ	
38 $_{-2}$ - 37 $_2$	347791	blended		< 3σ		< 3σ		◇1.94 ± 0.09	3.5 ± 0.1	< 3σ	
38 $_2$ - 37 $_{-2}$	347924	blended		< 3σ		< 3σ		2.36 ± 0.08	3.4 ± 0.1	< 3σ	
$HC^{13}CCN$ ν=0											
37 - 36	335092	⋆5.0 ± 0.4	13.4 ± 0.9	blended		◇3.4 ± 0.4	3.43 ± 0.10	blended		< 3σ	
$HCC^{13}CN$ ν=0											
37 - 36	335124	blended		< 3σ		< 3σ		2.3 ± 0.3	6.9 ± 0.7	< 3σ	
$H^{13}CCCN$ v7=1											
37 $_{-1}$ - 36 $_1$	335760	4.1 ± 0.2	1.29 ± 0.05	< 3σ		< 3σ		1.8 ± 0.2	0.60 ± 0.04	3.1 ± 0.3	1.36 ± 0.10
37 $_1$ - 36 $_{-1}$	336227	5.6 ± 0.2	3.4 ± 0.1	< 3σ		< 3σ		1.4 ± 0.2	0.77 ± 0.07	4.3 ± 0.3	2.36 ± 0.09
$HC^{13}CCN$ v7=1											
37 $_1$ - 36 $_{-1}$	335883	4.3 ± 0.5	1.22 ± 0.09	< 3σ		< 3σ		2.7 ± 0.2	0.97 ± 0.07	< 3σ	
$HCC^{13}CN$ v7=1											
37 $_1$ - 36 $_{-1}$	335930	5.3 ± 0.2	7.0 ± 0.2	1.9529 ± 0.3336	1.16 ± 0.1159	< 3σ		2.81 ± 0.08	2.17 ± 0.05	3.3 ± 0.1	4.5 ± 0.2
37 $_{-1}$ - 36 $_1$	336410	blended		< 3σ		< 3σ		2.0 ± 0.2	0.65 ± 0.05	< 3σ	
$HCC^{13}CN$ v6=1											
37 $_{-1}$ - 36 $_1$	335921	1.8 ± 0.6	1.2 ± 0.4	< 3σ		< 3σ		< 3σ		< 3σ	

◇ partially blended with other lines, ⋆ double peaked.

Table 2.B.15: Thioformaldehyde

Transition	Frequency	G35.20 A		G35.20 B1		G35.20 B2		G35.20 B3		G35.03 A	
		FWHM	T_{peak}	FWHM	T_{peak}	FWHM	T_{peak}	FWHM	T_{peak}	FWHM	T_{peak}
	(MHz)	(km s^{-1})	(K)	(km s^{-1})	(K)	(km s^{-1})	(K)	(km s^{-1})	(K)	(km s^{-1})	(K)
H_2CS ν=0											
$10_{1,10}$ - $9_{1,9}$ o	338083	5.9 ± 0.1	51.7 ± 0.9	2.7 ± 0.1	27.3 ± 1.0	2.4 ± 0.1	28 ± 1	2.54 ± 0.06	44.3 ± 0.9	6.6 ± 0.1	21.0 ± 0.3
$10_{1,9}$-$9_{1,8}$ o	348532	5.8 ± 0.1	59.2 ± 1.3	2.6 ± 0.1	31 ± 1	2.3 ± 0.1	31 ± 1	2.5806 ± 0.0374	52.1 ± 0.7	6.33 ± 0.09	21.3 ± 0.3
$H_2C^{33}S$											
$10_{1,10}$-$9_{1,9}$	335160	7.5 ± 0.2	3.91 ± 0.09	1.6 ± 0.5	0.4 ± 0.1	1.5 ± 0.6	0.4 ± 0.2	2.5 ± 0.2	1.47 ± 0.08	< 3σ	
$H_2C^{34}S$											
$10_{0,10}$-$9_{0,9}$	337125	blended		1.2 ± 0.7	0.7 ± 0.4	1.5 ± 0.2	1.0 ± 0.1	1.9 ± 0.1	2.5 ± 0.1	< 3σ	
$10_{4,6}$ - $9_{4,5}$	337460	blended		in abs feature		1.5 ± 0.4	0.55 ± 0.09	blended		< 3σ	
$10_{2,9}$ - $9_{2,8}$	337475	⋄6.3 ± 0.3	16.0 ± 0.3	⋄1.66 ± 0.08	3.8 ± 0.2	⋄1.7 ± 0.1	3.8 ± 0.2	⋄3.1 ± 0.2	4.9 ± 0.2	< 3σ	
$10_{3,8}$ - $9_{3,7}$	337555	blended		2.0 ± 0.2	0.78 ± 0.05	1.7 ± 0.5	0.6 ± 0.2	2.03 ± 0.04	2.35 ± 0.03	< 3σ	
$10_{3,7}$ - $9_{3,6}$	337559	blended		2.16 ± 0.09	1.55 ± 0.04	1.3 ± 0.1	0.54 ± 0.04	2.37 ± 0.06	2.26 ± 0.03	< 3σ	
$10_{2,8}$ - $9_{2,7}$	337933	blended		1.2 ± 0.5	0.8 ± 0.2	1.8 ± 0.5	0.7 ± 0.1	2.3 ± 0.1	2.4 ± 0.1	< 3σ	

⋄ partially blended with other lines

Table 2.B.16: Sulfur dioxide

Transition	Frequency	G35.20 A		G35.20 B1		G35.20 B2		G35.20 B3		G35.03 A	
		FWHM	T_{peak}	FWHM	T_{peak}	FWHM	T_{peak}	FWHM	T_{peak}	FWHM	T_{peak}
	(MHz)	(km s^{-1})	(K)	(km s^{-1})	(K)	(km s^{-1})	(K)	(km s^{-1})	(K)	(km s^{-1})	(K)
SO_2 ν=0											
$23_{3,21}$-$23_{2,22}$	336089	7.7 ± 0.2	24.1 ± 0.5	7.8 ± 0.1	19.2 ± 0.3	3.4 ± 0.2	8.0 ± 0.4	4.1 ± 0.1	24.4 ± 0.7	10.0 ± 0.3	21.0 ± 0.5
$16_{7,9}$-$17_{6,12}$	336670	8.8 ± 0.3	6.8 ± 0.2	7.3 ± 0.2	6.0 ± 0.1	2.4 ± 0.1	3.2 ± 0.2	3.4 ± 0.1	11.0 ± 0.3	8.4 ± 0.2	10.1 ± 0.1
$18_{4,14}$-$18_{3,15}$	338306	8.0 ± 0.2	22.8 ± 0.5	7.6 ± 0.2	25.4 ± 0.6	4.0 ± 0.3	7.5 ± 0.5	3.84 ± 0.07	31.2 ± 0.5	9.8 ± 0.1	25.2 ± 0.2
$20_{1,19}$-$19_{2,18}$	338612	5.6 ± 0.5	28.5 ± 1.6	7.5 ± 0.4	27.7 ± 1.9	4.1 ± 0.6	15.3 ± 0.9	3.8 ± 1.0	32 ± 2	10.0 ± 0.3	39.4 ± 0.9
$24_{2,22}$-$23_{3,21}$	348388	7.7 ± 0.1	18.3 ± 0.3	7.9 ± 0.2	18.9 ± 0.4	3.2 ± 0.3	5.5 ± 0.4	3.41 ± 0.09	30.2 ± 0.7	9.6 ± 0.2	20.3 ± 0.3
$^{33}SO_2$											
$12_{4,8}$-$12_{3,9}$	348492	blended		blended		blended		3.1 ± 0.3	2.0 ± 0.1	$< 3\sigma$	
$10_{4,6}$-$10_{3,7}$	350303	5.5 ± 0.2	12.0 ± 0.4	3.0 ± 0.1	2.46 ± 0.09	2.5 ± 0.4	1.2 ± 0.2	2.7 ± 0.1	4.00 ± 0.10	5.9 ± 0.2	3.12 ± 0.05
$^{34}SO_2$											
$13_{2,12}$-$12_{1,11}$	338320	6.4 ± 0.2	3.69 ± 0.05	6.7 ± 0.1	4.08 ± 0.06	1.9 ± 0.4	1.7 ± 0.3	3.2 ± 0.1	8.2 ± 0.2	7.8 ± 0.3	5.97 ± 0.08

Appendix 2.C XCLASS fit errors

In this section we give the error values on each of our XCLASS fit results. They are rarely symmetrical, so they are reported in the format, value, lower error (-), and upper error (+), except for column density, which is listed as value, lower limit (value-error), and upper limit (value+error). The errors were calculated using the interval nested sampling (INS) error estimator algorithm in XCLASS.

Table 2.C.1: Error values for G35.20 A. The columns indicated by a minus sign (-) indicate the error to the left of the result and those indicated by a plus sign (+) indicate the error to the right.

XCLASS Catalog Entry	Source size	-	+	T_{ex}	-	+	N_{col}	lower limit	upper limit
CH3OH;v=0	0.6	0.2	0.3	164	18	36	3.52E+18	6.88E+17	7.00E+18
CH3OH;v12=1	0.5	0.1	0.2	218	24	32	4.79E+18	9.77E+17	3.00E+19
CH3OH;v12=2	0.39	0.09	0.11	227	18	73	3.78E+18	7.93E+17	1.00E+19
C-13-H3OH;v=0;	1.0	0.3	0.2	121	70	39	1.62E+17	4.27E+16	3.00E+17
CH3O-18-H;v=0;	1.1	0.2	0.1	121	62	49	4.42E+16	1.35E+16	7.00E+16
CH3CN;v=0;	0.45	0.10	0.15	208	23	32	3.91E+16	1.16E+16	3.00E+17
CH3CN;v8=1;	0.6	0.1	0.2	359	54	41	3.22E+16	1.10E+16	6.00E+16
CH2DCN;v=0;	0.5	0.2	0.3	82	12	63	4.14E+15	1.16E+15	8.00E+15
CH3C-13-N;v=0;	1.0	0.4	0.0	263	73	37	5.00E+14	1.19E+14	8.00E+14
CH3OCHO;v=0;	0.98	0.20	0.02	103	17	77	8.10E+16	1.03E+16	1.00E+17
CH3OCH3;v=0;	0.34	0.09	0.62	229	43	71	3.67E+17	4.13E+16	8.00E+17
CH3CHO;v=0;	0.4	0.3	0.2	234	8	66	1.69E+16	6.78E+14	8.00E+16
CH3CHO;v15=1;	1.102	0.576	0.002	278	38	22	5.45E+15	1.09E+14	1.00E+16
CH3CHO;v15=2;	0.7	0.6	0.5	295	92	5	4.33E+15	3.88E+13	1.00E+16
HC(O)NH2;v=0;	0.7	0.2	0.8	98	9	62	7.58E+15	2.34E+15	3.00E+16
C2H5OH;v=0;	0.8	0.2	0.4	281	35	19	7.13E+16	2.23E+16	8.00E+17
H2CS;v=0;	1.3	0.2	0.3	165	14	65	1.41E+16	4.10E+15	3.00E+16
SO2;v=0;	1.36	0.10	0.30	260	52	40	1.74E+16	4.43E+15	1.50E+17

Table 2.C.1: XCLASS errors for G35.20 A continued.

XCLASS Catalog Entry	Source size	-	+	T_{ex}	-	+	N_{col}	lower limit	upper limit
C2H5CN;v=0;	0.9	0.3	0.3	125	15	35	1.53E+16	2.56E+15	3.00E+16
CH3CHDCN	0.6	0.1	0.3	97	4	63	2.90E+15	4.64E+14	5.00E+15
C2H3CN;v=0;	0.6	0.5	0.3	77	6	53	1.28E+16	3.46E+15	3.50E+16
HCCCN;v=0;	1.2	0.3	0.003	176	41	61	1.69E+15	7.47E+14	2.00E+16
HCCCN;v6=1;	0.6	0.1	0.3	200	22	68	3.08E+15	1.04E+15	8.00E+15
HCCCN;v7=1;	0.37	0.08	0.23	251	35	49	5.31E+15	1.22E+15	9.00E+15
HCCCN;v7=2;	0.20	0.03	0.40	350	51	105	2.22E+15	3.93E+14	7.00E+15
aGg'-(CH2OH)2;v=0;	0.6	0.2	0.6	172	27	28	3.47E+16	9.06E+15	6.00E+17
HCOOH	0.6	0.5	0.2	103	37	97	1.37E+16	3.42E+15	3.00E+17
H2CO-18;v=0;	0.6	0.2	0.4	188	53	66	8.51E+14	3.56E+14	5.00E+15

Table 2.C.2: Error values for G35.20 B1. Star ($\star$) indicates a catalog entry that was not modeled. The columns indicated by a minus sign (-) indicate the error to the left of the result and those indicated by a plus sign (+) indicate the error to the right.

XCLASS Catalog Entry	Source size	-	+	T_{ex}	-	+	N_{col}	lower limit	upper limit
CH3OH;v=0	0.3	0.2	0.2	234	35	63	6.99E+17	2.16E+17	5.00E+18
CH3OH;v12=1	0.36	0.06	0.12	153	3	25	1.07E+18	3.34E+17	5.00E+19
CH3OH;v12=2	0.18	0.01	0.22	154	1	46	2.23E+18	6.90E+17	6.80E+18
C-13-H3OH;v=0;	0.3	0.2	0.2	113	41	36	3.87E+16	1.57E+16	1.50E+17
CH3O-18-H;v=0;	0.3	0.1	0.2	82	19	35	1.45E+16	8.20E+15	1.20E+17
CH3CN;v=0;	0.32	0.09	0.16	129	78	20	7.24E+15	5.45E+15	1.32E+16
CH3CN;v8=1;	0.29	0.04	0.11	283	43	17	3.50E+15	2.94E+15	7.00E+16
CH2DCN;v=0;	0.1	0.0	0.3	180	59	101	3.00E+13	1.77E+13	2.05E+15
CH3C-13-N;v=0;	0.7	0.2	0.3	262	34	38	2.01E+14	5.59E+13	8.00E+14
CH3OCHO;v=0;	0.5	0.1	0.2	285	79	15	4.49E+16	5.63E+15	1.00E+17

Table 2.C.2: XCLASS errors for G35.20 B1 continued.

XCLASS Catalog Entry	Source size	-	+	T_{ex}	-	+	N_{col}	lower limit	upper limit
CH3OCH3;v=0;	0.22	0.02	0.28	156	8	34	3.76E+17	1.05E+17	6.00E+17
CH3CHO;v=0;	0.25	0.06	0.50	100	0	30	1.11E+16	1.12E+15	3.39E+16
CH3CHO;v15=1;	0.25	0.15	0.08	150	26	25	8.94E+14	1.99E+13	1.16E+16
CH3CHO;v15=2;	⋆								
HC(O)NH2;v=0;	0.3	0.2	0.2	50	0	100	5.67E+15	2.15E+15	7.00E+16
C2H5OH;v=0;	0.7	0.2	0.3	78	24	63	6.03E+15	4.39E+15	1.00E+17
H2CS;v=0;	2.0	0.2	0.5	230	35	61	3.29E+15	1.48E+15	7.00E+16
SO2;v=0;	1.44	0.09	0.95	279	36	21	3.28E+16	8.15E+15	6.00E+17
C2H5CN;v=0;	⋆								
C2H3CN;v=0;	⋆								
HCCCN;v=0;	0.9	0.2	0.3	119	43	70	9.29E+14	5.50E+14	8.00E+15
HCCCN;v6=1;	⋆								
HCCCN;v7=1;	0.8	0.2	0.2	219	49	45	5.84E+14	3.39E+14	6.00E+14
HCCCN;v7=2;	⋆								
H2CO-18;v=0;	0.3	0.1	0.3	41	1	61	5.66E+14	3.46E+14	7.00E+15
HCOOH	0.3	0.2	0.2	156	30	99	1.11E+15	2.79E+14	7.00E+16

Table 2.C.3: Error values for G35.20 B2. Star (⋆) indicates a catalog entry that was not modeled. The columns indicated by a minus sign (-) indicate the error to the left of the result and those indicated by a plus sign (+) indicate the error to the right.

XCLASS Catalog Entry	Source size	-	+	T_{ex}	-	+	N_{col}	lower limit	upper limit
CH3OH;v=0	0.36	0.05	0.84	136	5	164	5.25E+17	1.75E+17	5.00E+19
CH3OH;v12=1	0.32	0.05	0.38	145	0	155	6.18E+17	2.24E+17	5.00E+19
CH3OH;v12=2	0.15	0.03	0.24	152	0	148	1.06E+18	2.77E+17	5.00E+19
C-13-H3OH;v=0;	1.1	0.2	0.1	97	34	36	7.99E+15	4.94E+15	1.00E+18

Table 2.C.3: XCLASS errors for G35.20 B2 continued.

XCLASS Catalog Entry	Source size	-	+	T_{ex}	-	+	N_{col}	lower limit	upper limit
CH3O-18-H;v=0;	0.9	0.3	0.2	75	26	40	1.36E+15	1.34E+15	2.00E+17
CH3CN;v=0;	0.62	0.08	0.08	132	7	10	1.30E+15	1.20E+15	1.74E+15
CH3CN;v8=1;	⋆								
CH2DCN;v=0;	⋆								
CH3C-13-N;v=0;	0.44	0.19	0.07	55	5	66	1.40E+14	7.24E+13	1.00E+16
CH3OCHO;v=0;	0.5	0.1	0.2	64	14	59	2.02E+16	3.10E+15	1.00E+17
CH3OCH3;v=0;	0.4	0.1	0.3	67	17	62	1.30E+16	3.94E+15	1.00E+18
CH3CHO;v=0;	0.26	0.08	0.35	88	38	40	2.28E+15	1.89E+14	1.00E+17
CH3CHO;v15=1;	⋆								
CH3CHO;v15=2;	⋆								
HC(O)NH2;v=0;	0.6	0.2	0.3	45	30	55	2.32E+14	2.01E+14	4.79E+16
C2H5OH;v=0;	0.12	0.02	0.31	297	247	0	1.01E+15	1.01E+15	4.17E+16
H2CS;v=0;	1.0	0.0	1.0	50	0	183	1.18E+15	5.01E+14	1.00E+17
SO2;v=0;	2.42	0.69	0.08	114	66	48	6.58E+15	2.25E+15	1.00E+18
C2H5CN;v=0;	⋆								
C2H3CN;v=0;	⋆								
HCCCN;v=0;	0.8	0.3	0.3	122	44	99	1.96E+14	1.58E+14	1.00E+16
HCCCN;v6=1;	⋆								
HCCCN;v7=1;	⋆								
HCCCN;v7=2;	⋆								
H2CO-18;v=0;	0.32	0.02	0.98	29	2	183	1.51E+15	6.71E+14	1.00E+16

Table 2.C.4: Error values for G35.20 B3. The columns indicated by a minus sign (-) indicate the error to the left of the result and those indicated by a plus sign (+) indicate the error to the right.

XCLASS Catalog Entry	Source size	-	+	T_{ex}	-	+	N_{col}	lower limit	upper limit
CH3OH;v=0	0.35	0.04	0.02	155	6	36	6.23E+17	5.55E+17	8.13E+17
CH3OH;v12=1	0.36	0.02	0.07	189	14	14	9.81E+17	7.62E+17	1.12E+18
CH3OH;v12=2	0.20	0.02	0.02	172	5	20	1.80E+18	1.32E+18	2.33E+18
C-13-H3OH;v=0;	1.20	0.06	0.03	89	10	9	1.63E+16	1.20E+16	1.93E+16
CH3O-18-H;v=0;	1.20	0.01	0.00	111	43	18	5.75E+15	4.17E+15	1.21E+16
CH3CN;v=0;	0.35	0.06	0.04	208	30	30	6.46E+15	5.21E+15	1.06E+16
CH3CN;v8=1;	0.8	0.2	0.2	213	47	27	1.30E+15	5.69E+14	1.00E+18
CH2DCN;v=0;	0.8	0.2	0.2	90	5	203	1.12E+15	2.40E+14	1.00E+16
CH3C-13-N;v=0;	0.7	0.1	0.3	118	14	156	5.44E+14	1.97E+14	1.00E+16
CH3OCHO;v=0;	0.59	0.28	0.01	67	5	2	2.74E+16	2.36E+16	4.30E+16
CH3OCH3;v=0;	0.49	0.10	0.23	97	4	13	1.66E+17	6.31E+16	4.37E+17
CH3CHO;v=0;	1.16	0.05	0.05	170	49	33	2.14E+15	1.90E+15	2.68E+15
CH3CHO;v15=1;	0.56	0.05	0.21	224	114	74	1.44E+15	8.65E+14	2.19E+15
CH3CHO;v15=2;	0.12	0.02	0.03	102	1	2	8.07E+14	2.46E+13	1.40E+16
HC(O)NH2;v=0;	0.3	0.1	0.5	53	8	19	1.62E+15	9.12E+14	1.66E+16
C2H5OH;v=0;	0.43	0.03	0.06	178	35	87	1.29E+16	1.02E+16	1.51E+16
H2CS;v=0;	0.9	0.1	1.1	87	23	123	6.05E+15	1.99E+15	1.00E+17
SO2;v=0;	1.3	0.2	1.2	288	73	12	3.92E+16	8.92E+15	1.00E+18
C2H5CN;v=0;	0.8	0.2	0.2	90	0	16	1.29E+15	8.51E+14	2.00E+15
C2H3CN;v=0;	0.8	0.3	0.1	207	77	49	7.29E+14	4.08E+14	1.00E+16
HCCCN;v=0;	1.2	0.6	0.0	251	11	13	1.76E+15	1.64E+15	1.93E+15
HCCCN;v6=1;	0.4	0.3	0.3	256	34	34	2.43E+15	1.53E+15	3.54E+15
HCCCN;v7=1;	0.98	0.17	0.02	288	27	32	2.12E+15	1.85E+15	2.25E+15
HCCCN;v7=2;	0.35	0.06	0.35	473	10	4	1.31E+15	9.70E+14	1.65E+15

Table 2.C.4: XCLASS errors for G35.20 B3 continued.

XCLASS Catalog Entry	Source size	-	+	T_{ex}	-	+	N_{col}	lower limit	upper limit
HCOOH	0.4	0.3	0.5	173	38	22	3.82E+15	1.70E+15	1.00E+16
H2CO-18;v=0;	1.09	0.06	0.06	125	18	18	4.18E+14	3.78E+14	4.74E+14

Table 2.C.5: Error values for G35.03 A. Star ($\star$) indicates a catalog entry that was not modeled. The columns indicated by a minus sign (-) indicate the error to the left of the result and those indicated by a plus sign (+) indicate the error to the right.

XCLASS Catalog Entry	Source size	-	+	T_{ex}	-	+	N_{col}	lower limit	upper limit
CH3OH;v=0	0.40	0.09	0.71	142	18	68	1.80E+18	3.99E+17	1.00E+19
CH3OH;v12=1	0.30	0.06	0.62	239	40	61	2.64E+18	6.01E+17	1.00E+19
CH3OH;v12=2	0.20	0.05	0.52	192	19	108	5.06E+18	9.95E+17	1.00E+19
C-13-H3OH;v=0;	0.6	0.1	0.6	120	24	51	5.00E+16	1.58E+16	1.00E+18
CH3O-18-H;v=0;	1.2	0.3	0.3	130	21	41	9.99E+15	3.48E+15	1.00E+16
CH3CN;v=0;	0.30	0.06	0.40	186	21	114	3.04E+16	1.04E+16	1.00E+19
CH3CN;v8=1;	0.30	0.05	0.20	216	19	54	3.57E+16	1.35E+16	1.29E+19
CH2DCN;v=0;	$\star$								
CH3C-13-N;v=0;	0.35	0.08	0.55	70	1	80	1.44E+15	3.48E+14	1.00E+18
CH3OCHO;v=0;	0.2	0.1	0.2	100	21	66	2.29E+15	2.13E+15	1.00E+18
CH3OCH3;v=0;	0.7	0.2	0.1	150	39	56	8.27E+16	2.45E+16	2.68E+17
CH3CHO;v=0;	0.5	0.3	0.3	120	21	77	1.29E+15	8.11E+14	1.00E+18
CH3CHO;v15=1;	0.5	0.3	0.3	220	53	91	1.29E+15	9.55E+14	1.00E+17
CH3CHO;v15=2;	$\star$								
HC(O)NH2;v=0;	0.8	0.2	0.4	43	1	78	4.68E+15	1.74E+15	1.86E+16
C2H5OH;v=0;	0.4	0.1	0.7	150	29	150	4.88E+16	1.56E+16	4.88E+17
H2CS;v=0;	1.7	0.4	0.3	96	3	105	3.65E+15	1.40E+15	2.51E+16
SO2;v=0;	1.2	0.2	0.8	281	72	19	7.47E+16	1.55E+16	5.01E+17

Table 2.C.5: XCLASS errors for G35.03 A continued.

XCLASS Catalog Entry	Source size	-	+	T_{ex}	-	+	N_{col}	lower limit	upper limit
C2H5CN;v=0;	0.5	0.1	0.3	78	7	70	4.98E+15	1.20E+15	2.07E+16
HCCCN;v=0;	0.6	0.2	0.2	140	27	61	2.28E+15	9.95E+14	1.00E+16
HCCCN;v7=1;	0.8	0.2	0.2	194	21	32	5.87E+15	1.87E+15	1.84E+16
HCOOH	0.7	0.3	0.2	100	48	82	5.00E+15	1.70E+15	1.00E+16
aGg'-(CH2OH)2;v=0;	0.70	0.10	0.50	100	3	50	2.81E+16	4.99E+15	1.00E+17
H2CO-18;v=0;	0.50	0.03	0.20	52	0	128	2.10E+14	1.56E+14	1.00E+15

Appendix 2.D XCLASS analysis details

2.D.1 S-bearing

We detected two S-bearing species with more than one transition in our sources.

- Sulfur dioxide (SO_2) - As a species with extended emission, the source size ranges from 1.2″ at G35.03 to 2.4″ at B2. The column densities for this species are relatively consistent at 0.6-4.3 x 10^{16} cm^{-2} across G35.20 and 7.5 x 10^{16} cm^{-2} at G35.03. The T_{ex} values are from 114 K in B2 to 288 K in B3. The fits were based on 24 different transitions within the spectral window, five of which were measured in the survey (others were not present or within the noise).

- Thioformaldehyde (H_2CS) - This species was observed to have fairly extended emission so the source size ranged from 0.9″ for B3 to 2.5″ for B1. The T_{ex} range is on the cooler side at 50 K for B2, less than 100 K for B1, B3, and G35.03, and 165 K at A. A had the highest column density at 1.4 x 10^{16} cm^{-2}, where the others ranged from 1.2 - 6.1 x 10^{15} cm^{-2}.

2.D.2 O-bearing organics

- Formaldehyde (H_2CO) - Only the isotopologues $H_2C^{18}O$, HDCO, and D_2CO were in the spectral range of these observations. See subsection D.6.

- Formic acid (HCOOH) - This species was detected at all peaks, but it was not modeled for B2 because the emission lines were only just above 3σ.

- Methanol (CH_3OH) - The ν=0 state of CH_3OH was modeled to a maximum source size of 1″, so the source size fits were 0.4-0.6″. The temperature range was from 132-268 K. The column densities for this species ranged from 0.3-4.8 x 10^{18} cm^{-2}. The vibrationally excited states and isotopologues were modeled separately as their spatial extents are different from the main state and are likely part of different gas; see § C.5 and C.6.

- Acetaldehyde (CH_3CHO) - The ν=0 state was modeled separately from the vibrationally excited states (see subsection D.5). This species was observed to have a fairly compact emitting region, so the source size was limited to 1.5″. The best-fit source sizes were 0.3-1.2″ with relatively high excitation temperatures between 193 K and 300 K. The column densities ranged from 1.5-17 x 10^{15} cm^{-2}.

- Methyl formate (CH_3OCHO) - Only the ν=0 state was fit as the ν=1 transitions were not in the XCLASS database. The emission from this species was fairly compact so the model was allowed a maximum source size of 1.2″. The final source sizes were 0.2-1.0″ and column densities ranged from 1.9-29 x 10^{16} cm^{-2}. Generally the T_{ex} values were high (182-295 K for B1, B2, and B3), but the excitation temperatures of A and G35.03 were 103 K and 151 K, respectively.

- Dimethyl ether (CH_3OCH_3) - There was a lot of variation between the sources for this species. The source size was very compact for A, B1, and B2 (0.3, 0.4, and 0.5″, respectively), but more extended for B3 and G35.03 at 0.8″. The temperature differences were also large. The T_{ex} for B3 was 90 K, 170, and 180 K for B2 and B1, 229 K at A, and 260 K at G35.03. The column densities were lower for B2 (1.6 x 10^{16} cm^{-2}) and higher for the other peaks (8.8 x 10^{16}-9.7 x 10^{17} cm^{-2}).

- Ethanol (C_2H_5OH) - The trans- and gauche- transitions for ethanol were modeled from a single JPL database entry. The temperatures varied widely with best-fit values of 88 K for B1 and 120 K for B2, and much higher values of 260, 281, and 300 K for B3, A and G35.03, respectively. The column densities ranged between 0.6 and 7.1 x 10^{16} cm^{-2} range with the lowest at B1 and B2 and the highest at A. The source sizes were 0.4-0.8″.

- Ethylene glycol ($(CH_2OH)_2$) - This species was only modeled for G35.20 core A and for G35.03 as it was not detected in any part of core B. In G35.20 core A and G35.03, the best-fit source sizes are 0.6″ and 0.2″, respectively, and the T_{ex} was 172 K for G35.20

and 75 K in G35.03. The column densities were 3.5 x 10^{16} cm^{-2} in G35.20 core A and 7.8 x 10^{16} cm^{-2} in G35.03.

2.D.3 N-bearing organics

- Cyanoacetylene (HC_3N) - The ν=0 state was modeled for all regions and the isotopologue $HC^{13}CCN$ ν=0 was coupled with HC_3N ν=0 to improve the uncertainty (from fitting one transition to fitting two). The fit for $HCC^{13}CN$ ν=0 was also coupled for B3, as this is the only location where this species was detected. When fits of species are coupled together they share the same temperature and source size, but the isotope ratio (and therefore the column density) vary. See § C.5 for excited states. The column densities for this species ranged from 2.1 x 10^{14} cm^{-2} at B2 to 2.2 x 10^{15} cm^{-2} at G35.03. The source sizes were fairly consistent, ranging between 0.9 and 1.2″ and the T_{ex} range was 132-208 K.

- Methyl cyanide (CH_3CN) - The ν=0 state was modeled for all regions, but the isotopologues were not coupled with the main species because their spatial extents were dramatically different. The modeled source sizes for this species were quite compact, i.e., 0.3-0.6″ ; the temperature range was 124-235 K. The range of column densities was 1.8-7.2 x 10^{16} cm^{-2}. See subsections D.5 and D.6 for excited states and isotopologues.

- Vinyl cyanide (C_2H_3CN) - The results for vinyl cyanide are very different for the two regions where it was detected. G35.20 A has a source size of 0.6″, an excitation temperature of 77 K, and a column density of 1.3 x 10^{16} cm^{-2}. On the other end of this source, B3 has a size of 0.8″, a T_{ex} of 207 K, and a column density of 7.3 x 10^{14} cm^{-2}.

- Ethyl cyanide (C_2H_5CN) - This species was only modeled for G35.20 core A, region B3, and G35.03 core A. The temperatures for this species were all low compared to many of the other species. At B3, the T_{ex} was 50 K, at A it was 71 K, and at G35.03 it was 78 K. Column densities were 5.0-45 x 10^{15} cm^{-2} with the highest value at B3 and the source sizes were somewhat similar at 0.3″ for B3, 0.5″ for G35.03, and 0.6″ for A.

2.D.4 H-, N-, and O-bearing organics

- Isocyanic acid (HNCO) - The fit was based on a single strong transition so some assumptions were made. The source size was fixed based on the 3σ level emission and the column density was modeled at temperatures of 50 K and 100 K. These temperatures are reasonable for a more extended emitting region, as the bulk of the emission is not likely to come from very near the heating source. The resulting column densities are between 2.2 x 10^{15} cm^{-2} and 2.0 x 10^{16} cm^{-2} at 50 K and range from 9.4 x 10^{14} cm^{-2} to 7.5 x 10^{16} cm^{-2} at 100 K.

- Formamide (NH_2CHO) - The ν=0 transitions were fit with the $NH_2{}^{13}CHO$ transitions coupled with the same parameters except abundance. The temperatures for this species were comparatively low, ranging from 43-100 K. The best-fit source sizes were between 0.5″ (at B1) and 0.8″ at G35.03. The range of column densities is 0.3-7.6 x 10^{15} cm^{-2}.

2.D.5 Vibrationally excited transitions

High energy transitions were modeled uncoupled to the main state as those in our sources are observed to emit from a much smaller area than lower energy transitions (see Figures 2.3 and 2.4) and many are not observed in B1 or B2. Vibrationally excited emission from HC_3N is only found toward cores A and B3 and weakly toward B1. See Figure 2.8.

- Methanol (CH_3OH) - The v_{12}=1 and v_{12}=2 excited states were modeled separately on the assumption that the different excited states are emitted in different gas, since the spatial extent of each excited state grows more compact with increased energy (see section 2.3 and Sánchez-Monge et al. (2014) Figure 6). The source sizes for the v_{12}=2 are more compact than the v_{12}=1 states and generally have a higher temperature. The range of column densities between the two states are similar at 0.3-4.8 x 10^{18} cm^{-2} for v_{12}=1 and 1.9-5.1 x 10^{18} cm^{-2} for v_{12}=2.

- Cyanoacetylene (HC_3N) - Each of the vibrational states (ν_6=1, ν_7=1, ν_7=2) were modeled separately and the source size was more

compact with higher excitation. No vibrationally excited states were modeled for B2, as they were not detected in the observations and only the ν_7=1 state was modeled for B1 and G35.03. The ν_6=1 state was modeled for A and B3 and was coupled with HCC^{13}CN with the ^{12}C/^{13}C isotope ratio fixed at 50. The resulting temperatures based on these 2-3 transitions was 200 K at A and 365 K at B3 with source sizes of 0.6 and 0.4″. Both peaks had similar column densities at 3.1 and 2.7 x 10^{15} cm^{-2}, only slightly more than those of the ν=0 state. The ν_7=1 state was also modeled coupled with the three different ^{13}C isotopologues for A and B3 with the isotope ratio fixed at 50. The ν_7=1 source size is more compact for all modeled sources, but still somewhat extended at 0.8-1.0″. The excitation temperatures are 25-80 K higher than the ν=0 state, ranging from 194 K at G35.03 to 283 K for both A and B3. The abundances of the ν_7=1 state are similar to those of the ν=0 state, but for A, the abundance is about 0.45; for B1 and B3 the abundances are almost equal, and for G35.03, the ν_7=1 abundance is about twice the abundance of the ν=0 state. The ν_7=2 state was only modeled for A and B3 where the emission becomes very compact, i.e., 0.1 and 0.3″, the temperature is very hot, i.e., 420-450 K, and the abundances are 1.3 and 0.7 times higher than the ν=0 state.

- Methyl cyanide - CH_3CN v_8=1 was modeled separately since its spatial distribution was significantly different from that of the ν=0 transitions. The v_8=1 emission was not modeled for region B2 since it was not detected to a significant degree. Temperatures for this species are generally high, ranging from 215-360 K with compact source sizes of 0.3-0.6″. The column densities for this excited species are 0.4-3.6 x 10^{16} cm^{-2} , which are similar to those of the ν=0 state.

- Acetaldehyde (CH_3CHO) - The ν_{15}=1 and ν_{15}=2 excited states were modeled as more compact emission sources than the ν=0 state. Fits were made for the ν_{15}=1 state for all sources except B2, but only for A and B3 for the ν_{15}=2 state. In all sources the temperature increases with increasing excitation and the source size decreases. The column densities for both excited states range

from 3.5-9.8 x 10^{15} cm^{-2} though the column density for the ν_{15}=2 state at B3 is 5.2 x 10^{16} cm^{-2}.

2.D.6 Isotopologues and deuteration

- Formaldehyde (H_2CO) - Only the isotopologues HDCO, D_2CO, and $H_2C^{18}O$ were in the spectral range of these observations. These were modeled separately where the $H_2C^{18}O$ fit was based on six transitions and the HDCO fit was based on a single transition. For $H_2C^{18}O$ the size ranges from 0.24-0.75″ and the temperatures are 26 K for B2 to 275 K for A. The range of column densities is 0.4-4.6 x 10^{15} cm^{-2}. The abundances for HDCO are also on the order of 0.15-1.6 x 10^{15} cm^{-2} at 50 K and 0.3-16 x 10^{14} cm^{-2} at 100 K with the source size fixed at 1.5″. D_2CO was not fitted as only single weak lines were detected.

- Methanol - $CH_3{}^{18}OH$ and $^{13}CH_3OH$ were modeled uncoupled to the main isotopologue because their spatial extents differ somewhat from the main isotopologue. The isotope ratios reached were 20-80 for $CH_3OH/{}^{13}CH_3OH$ and 180-320 for $CH_3OH/CH_3{}^{18}OH$ at peaks B2, B3, and G35.03. The isotope ratios are less ideal for G35.30N A and B1 at 40 and 80, respectively, but the source size is also significantly different. Deuterated methanol (CH_2DOH) was not modeled because it was not in the XCLASS database, so analysis for this species was completed using Cassis.

- Methyl cyanide - $CH_3{}^{13}CN$, and CH_2DCN were modeled separately from the ν=0 emission because of their differing spatial distribution. The CH_2DCN was not modeled for region B2 since it was not detected to a significant degree.

- Ethyl cyanide - CH_3CHDCN was only detected at G35.20 A and was modeled for that location.

Appendix 2.E Line ID xclass fits

Presented below are the spectra of each peak with the original data, the full XCLASS fit, and fits of selected species alone in different colors.

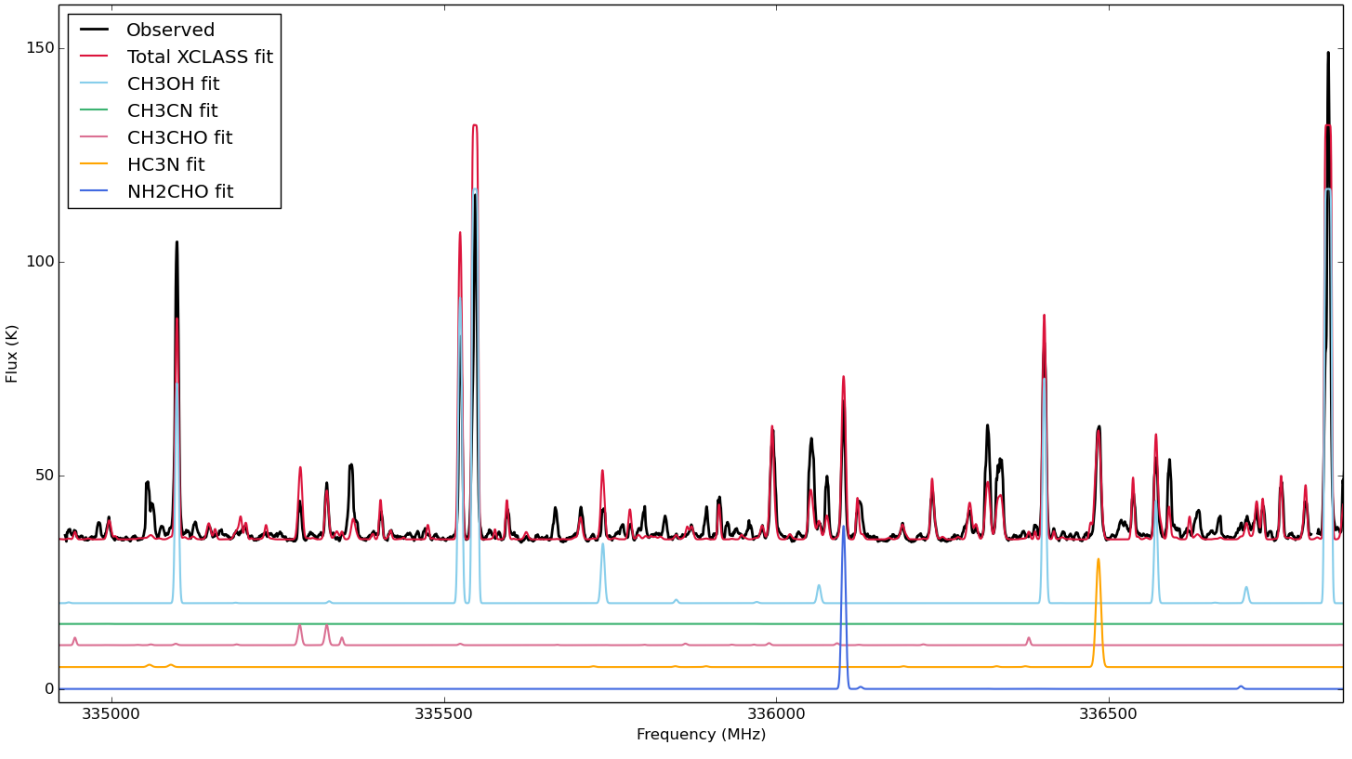

Figure 2.E.1: G35.20 peak A spectral window 1 (334.9-336.8 GHz), XCLASS total fit, plus selected species.

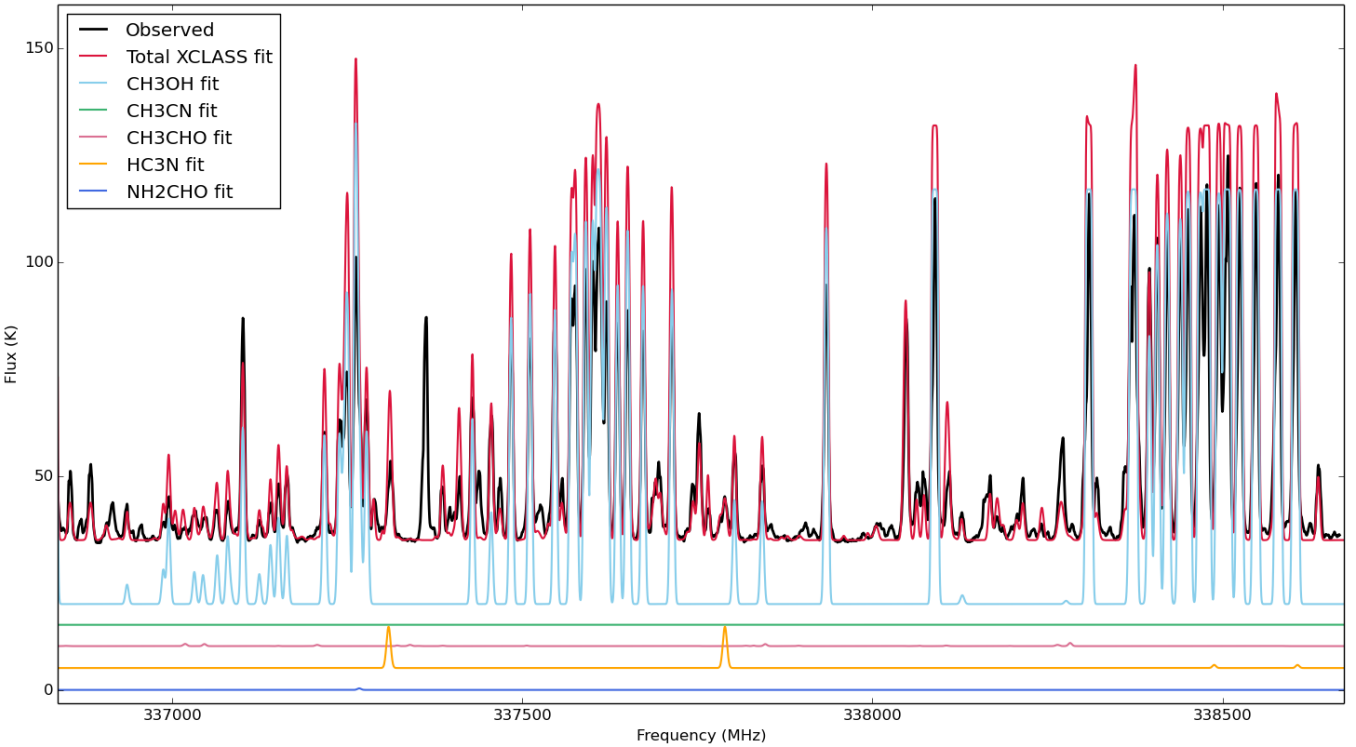

Figure 2.E.2: G35.20 peak A spectral window 0 (336.8-338.7 GHz), XCLASS total fit, plus selected species.

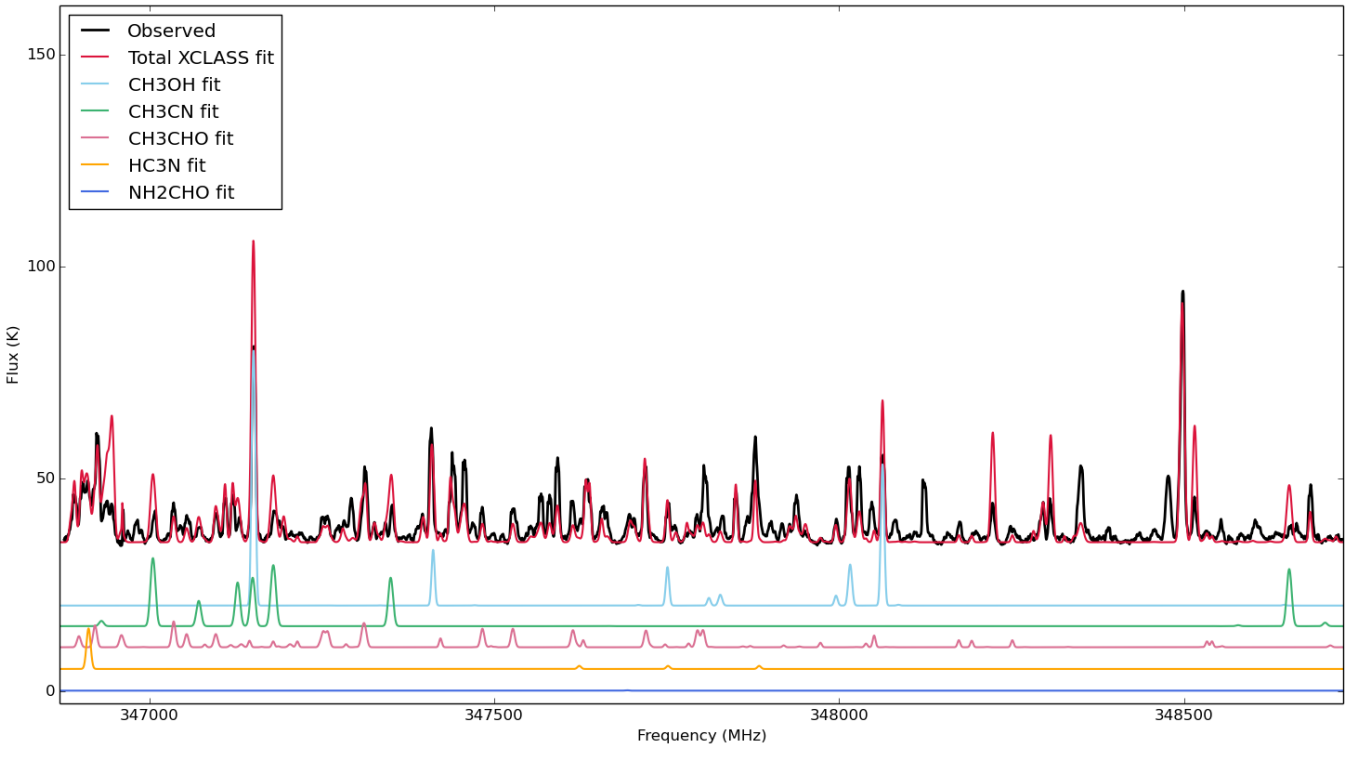

Figure 2.E.3: G35.20 peak A spectral window 3 (346.9-348.7 GHz), XCLASS total fit, plus selected species.

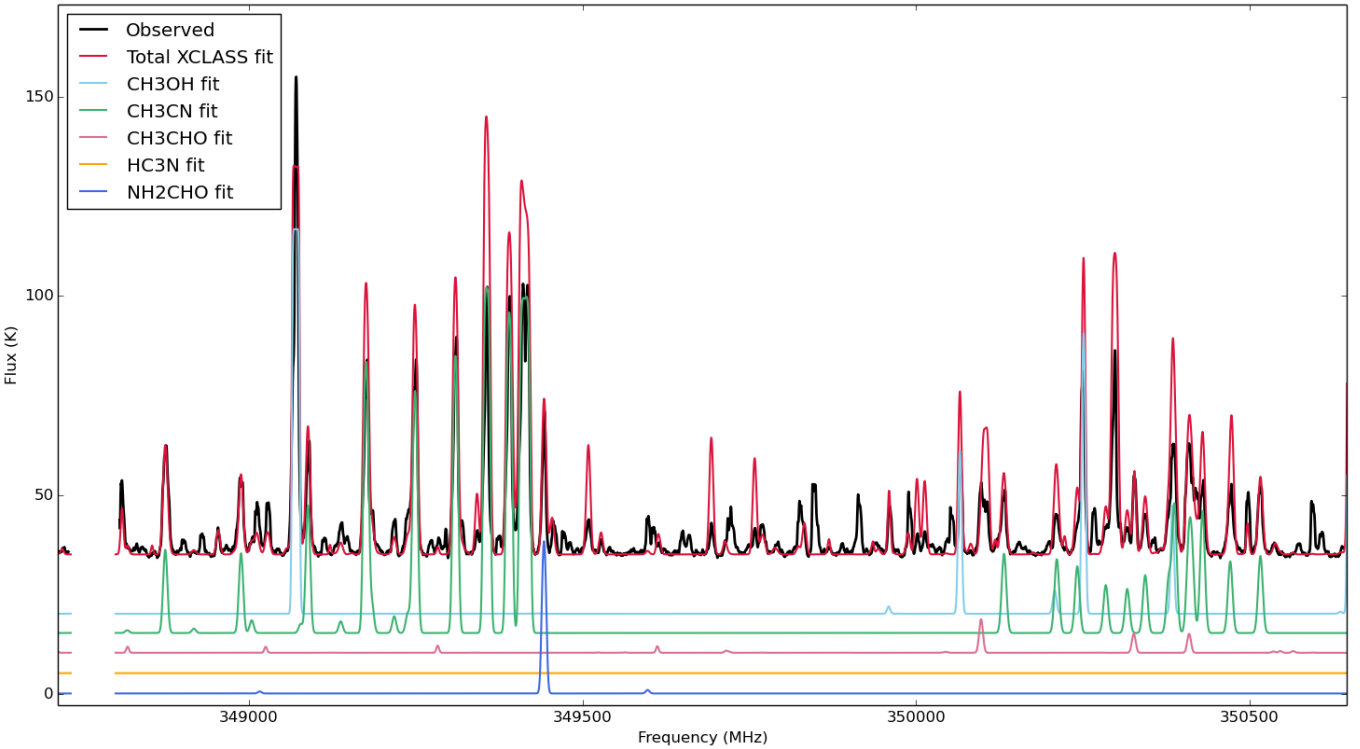

Figure 2.E.4: G35.20 peak A spectral window 2 (348.8-350.7 GHz), XCLASS total fit, plus selected species.

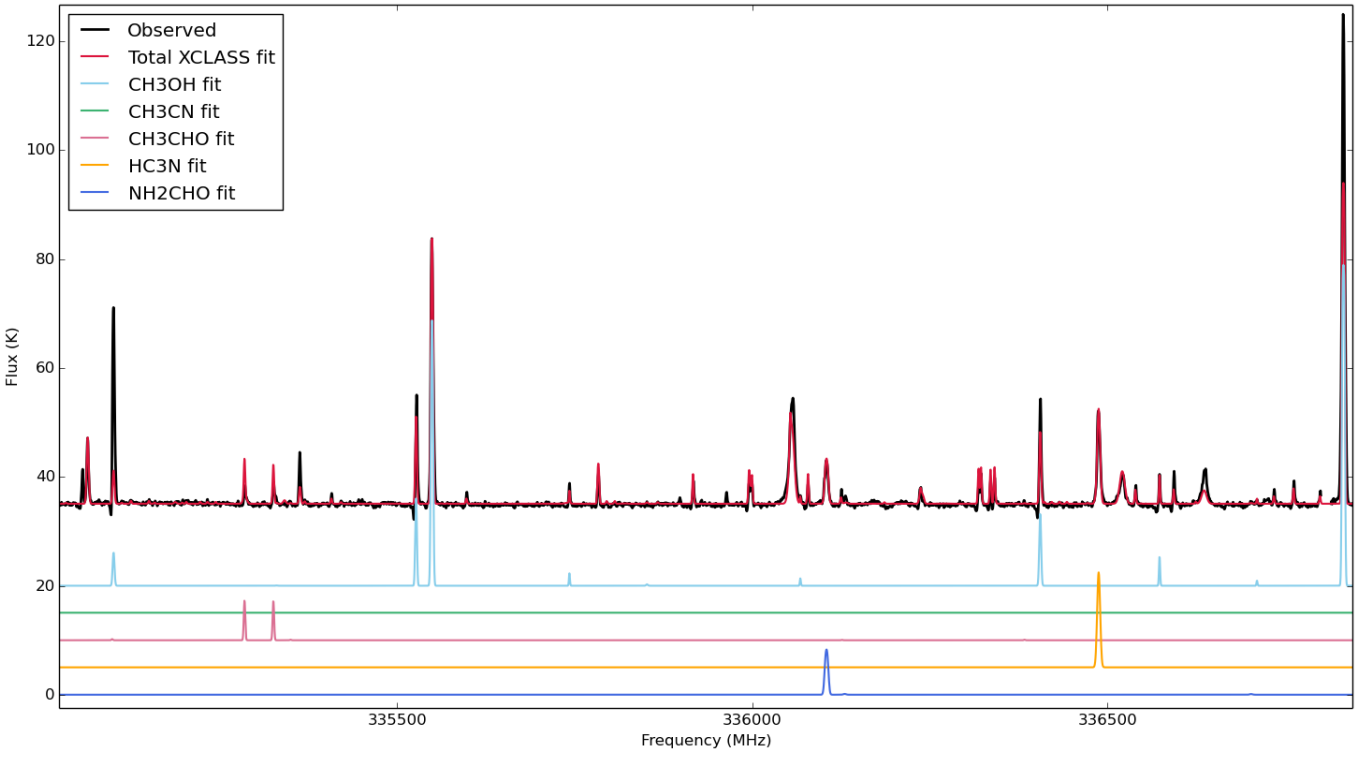

Figure 2.E.5: G35.20 peak B1 spectral window 1 (334.9-336.8 GHz), XCLASS total fit, plus selected species.

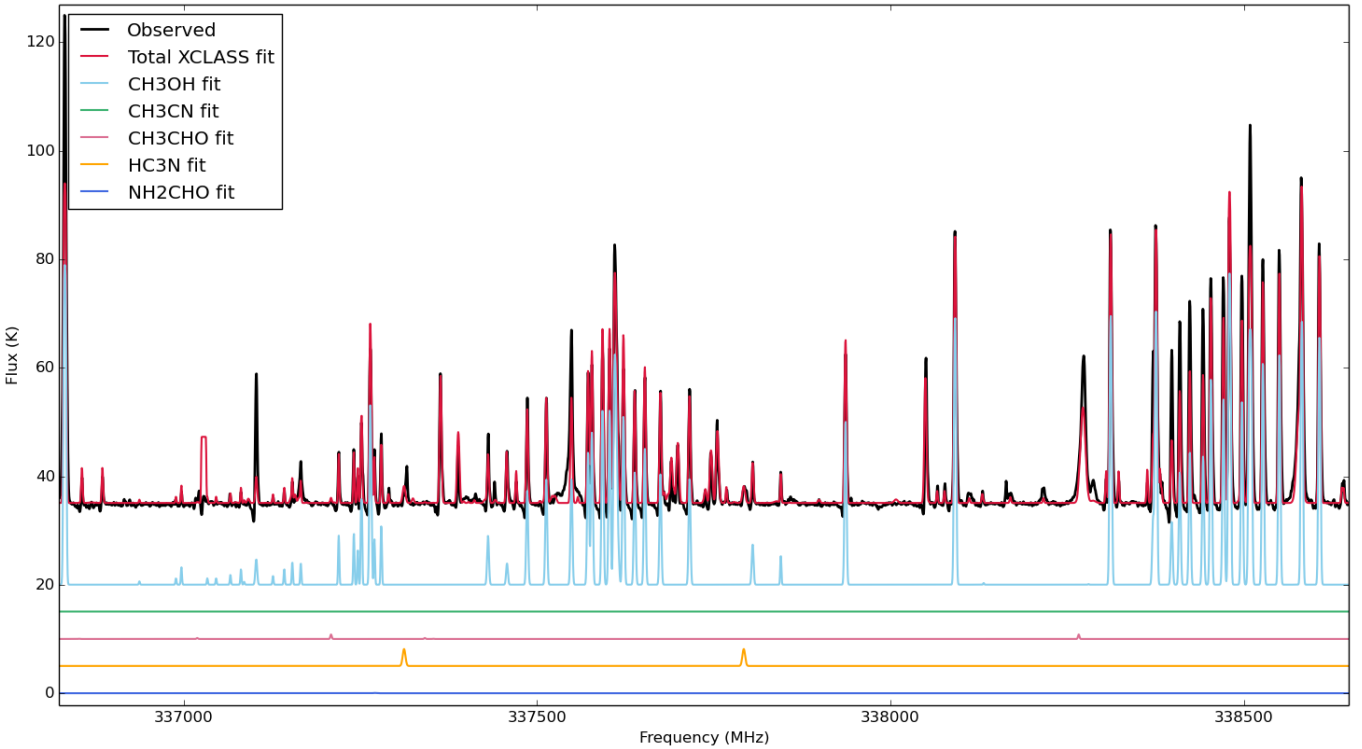

Figure 2.E.6: G35.20 peak B1 spectral window 0 (336.8-338.7 GHz), XCLASS total fit, plus selected species.

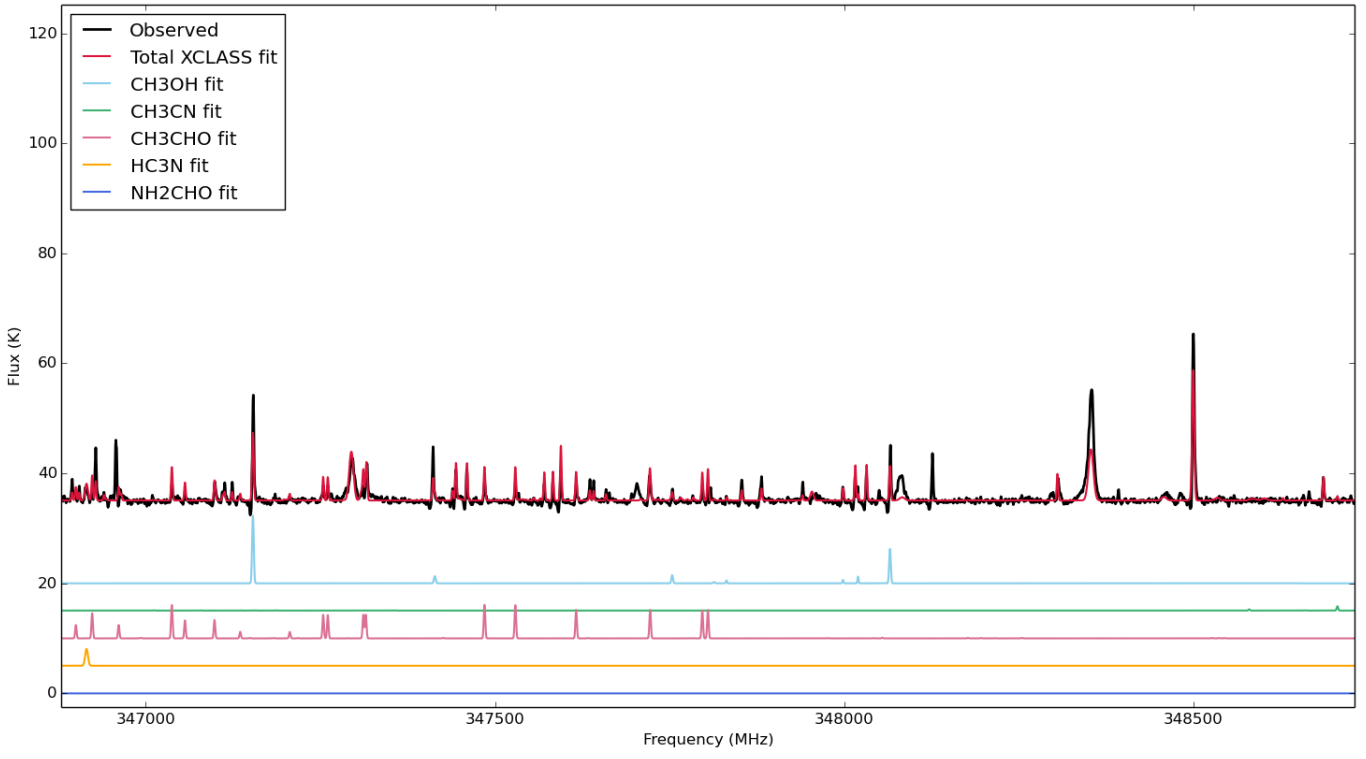

Figure 2.E.7: G35.20 peak B1 spectral window 3 (346.9-348.7 GHz), XCLASS total fit, plus selected species.

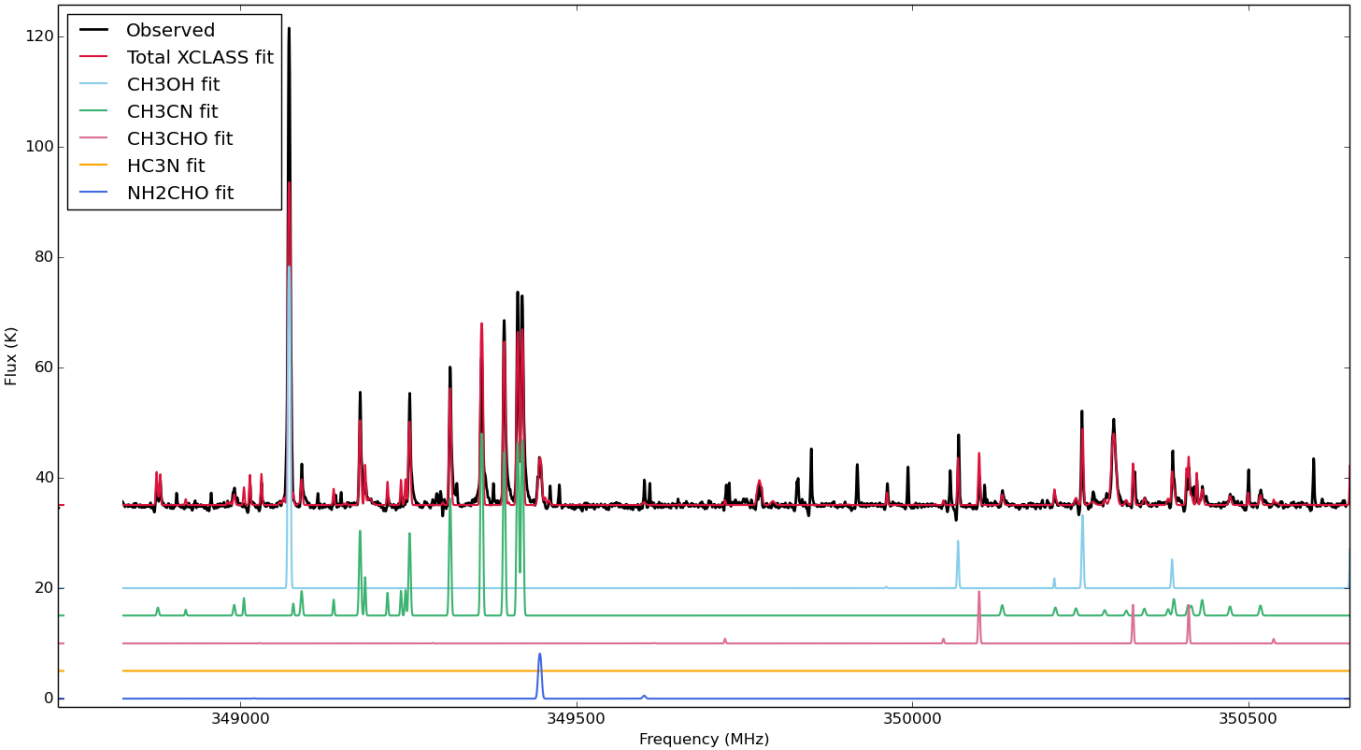

Figure 2.E.8: G35.20 peak B1 spectral window 2 (348.8-350.7 GHz), XCLASS total fit, plus selected species.

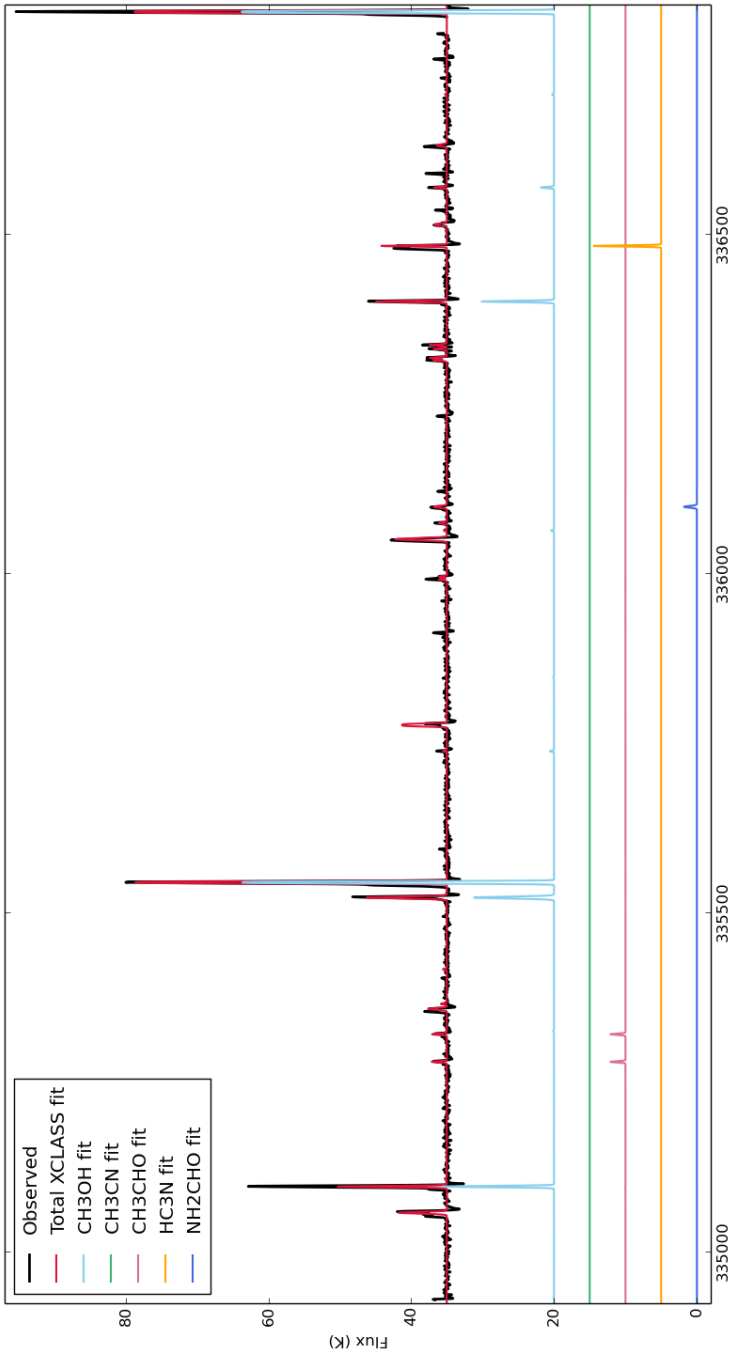

Figure 2.E.9: G35.20 peak B2 spectral window 1 (334.9-336.8 GHz), XCLASS total fit, plus selected species.

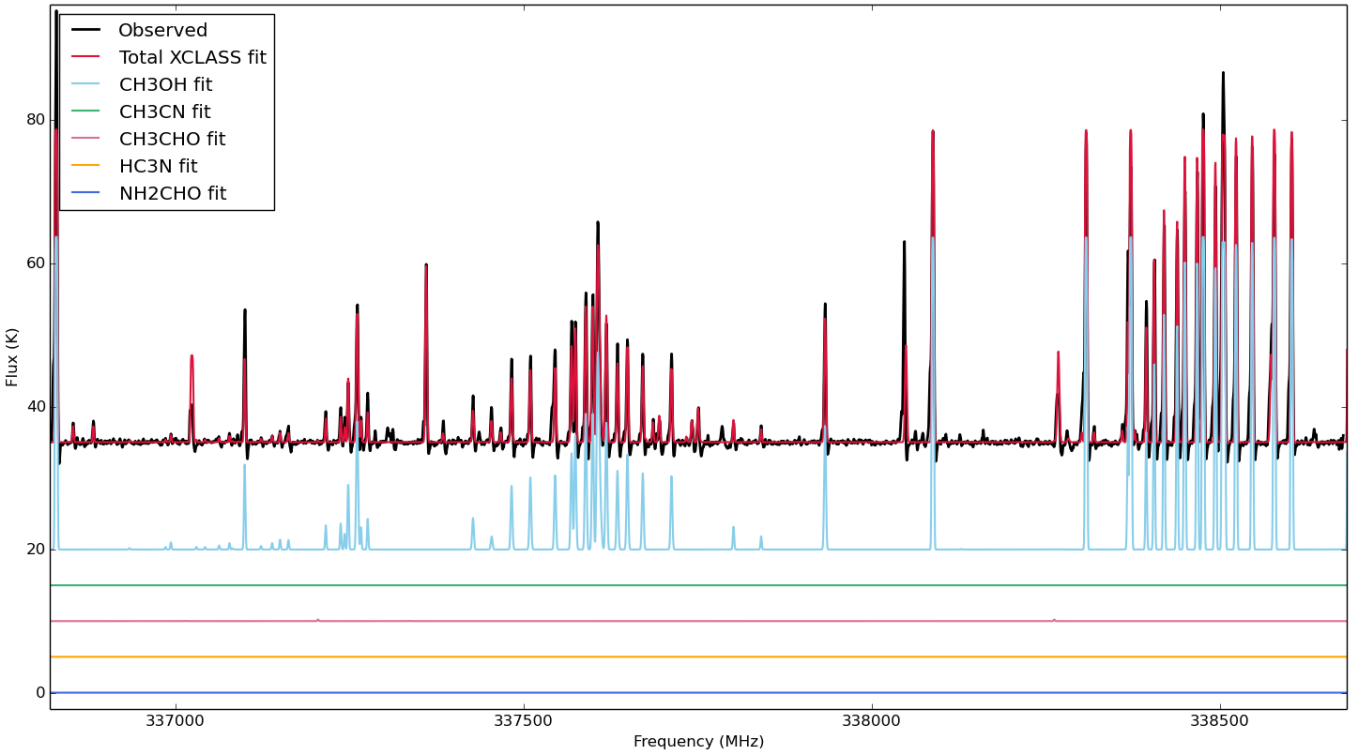

Figure 2.E.10: G35.20 peak B2 spectral window 0 (336.8-338.7 GHz), XCLASS total fit, plus selected species.

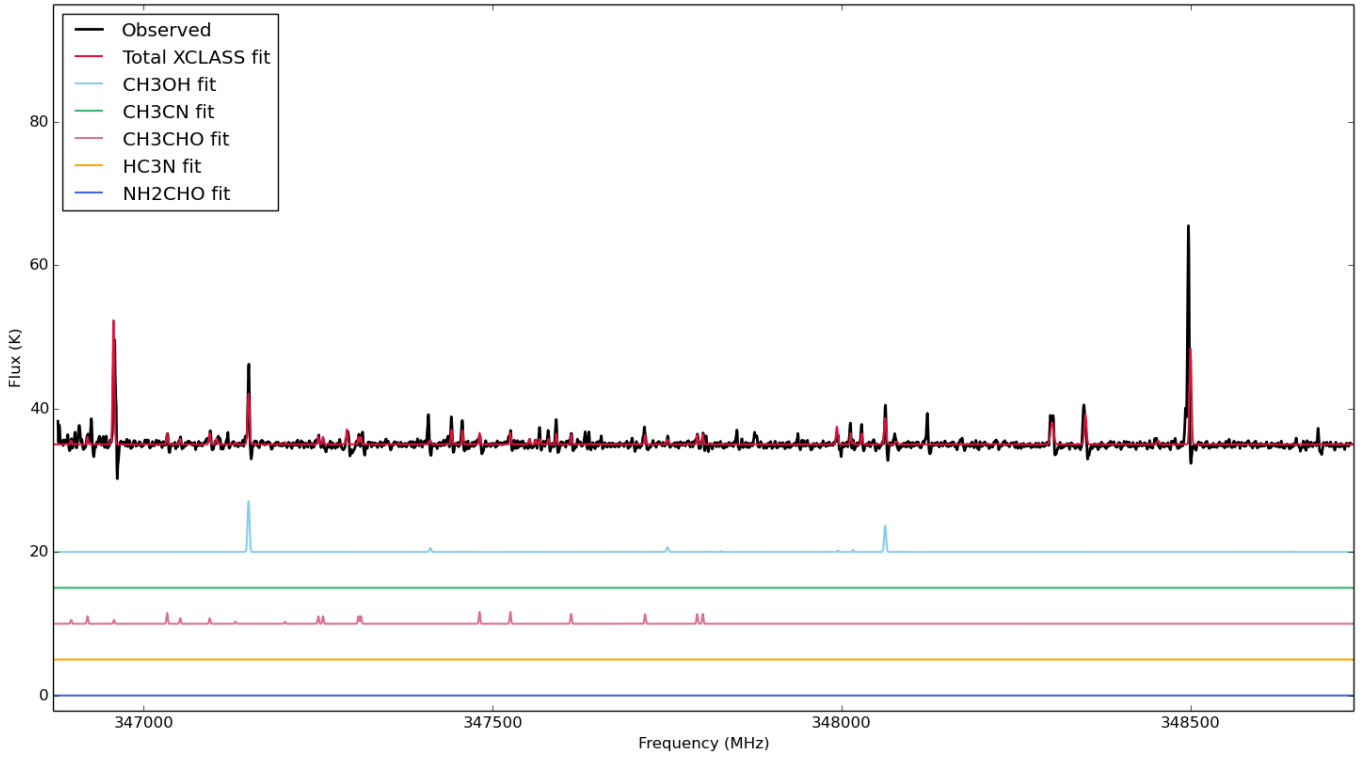

Figure 2.E.11: G35.20 peak B2 spectral window 3 (346.9-348.7 GHz), XCLASS total fit, plus selected species.

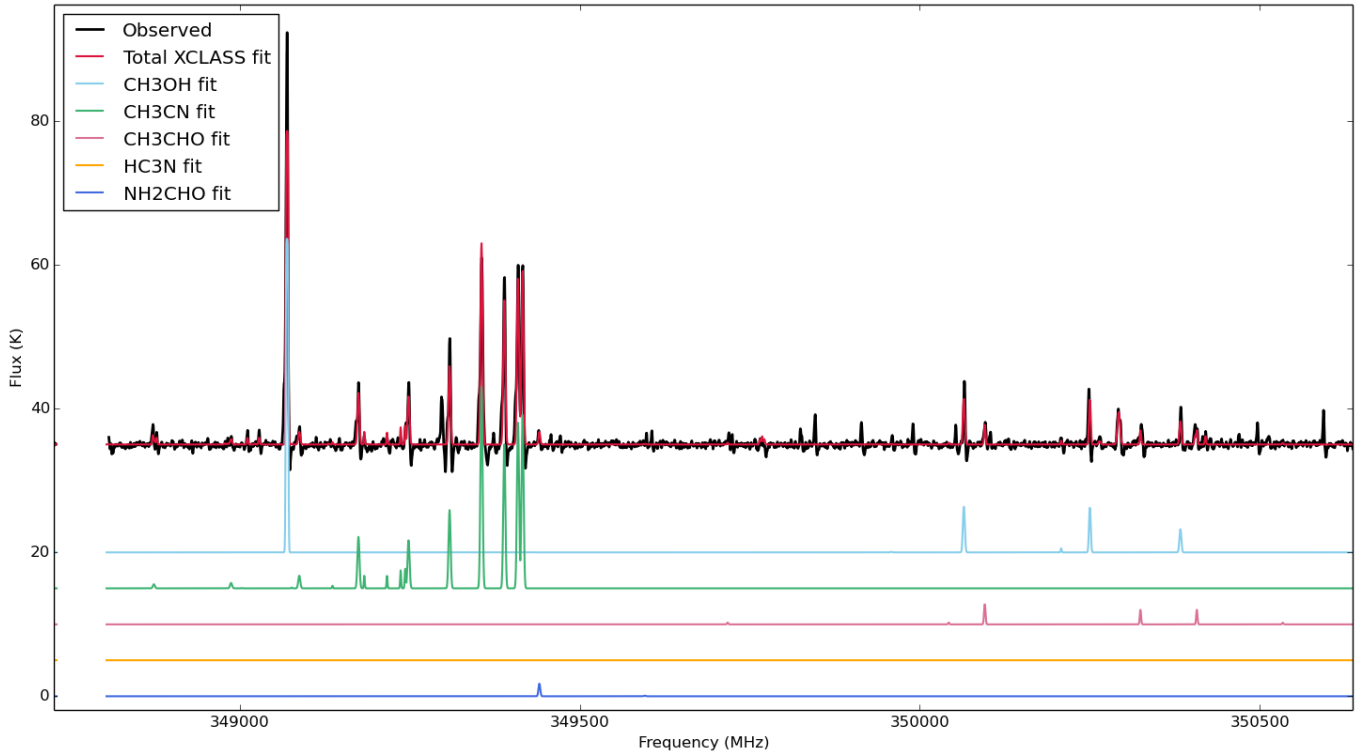

Figure 2.E.12: G35.20 peak B2 spectral window 2 (348.8-350.7 GHz), XCLASS total fit, plus selected species.

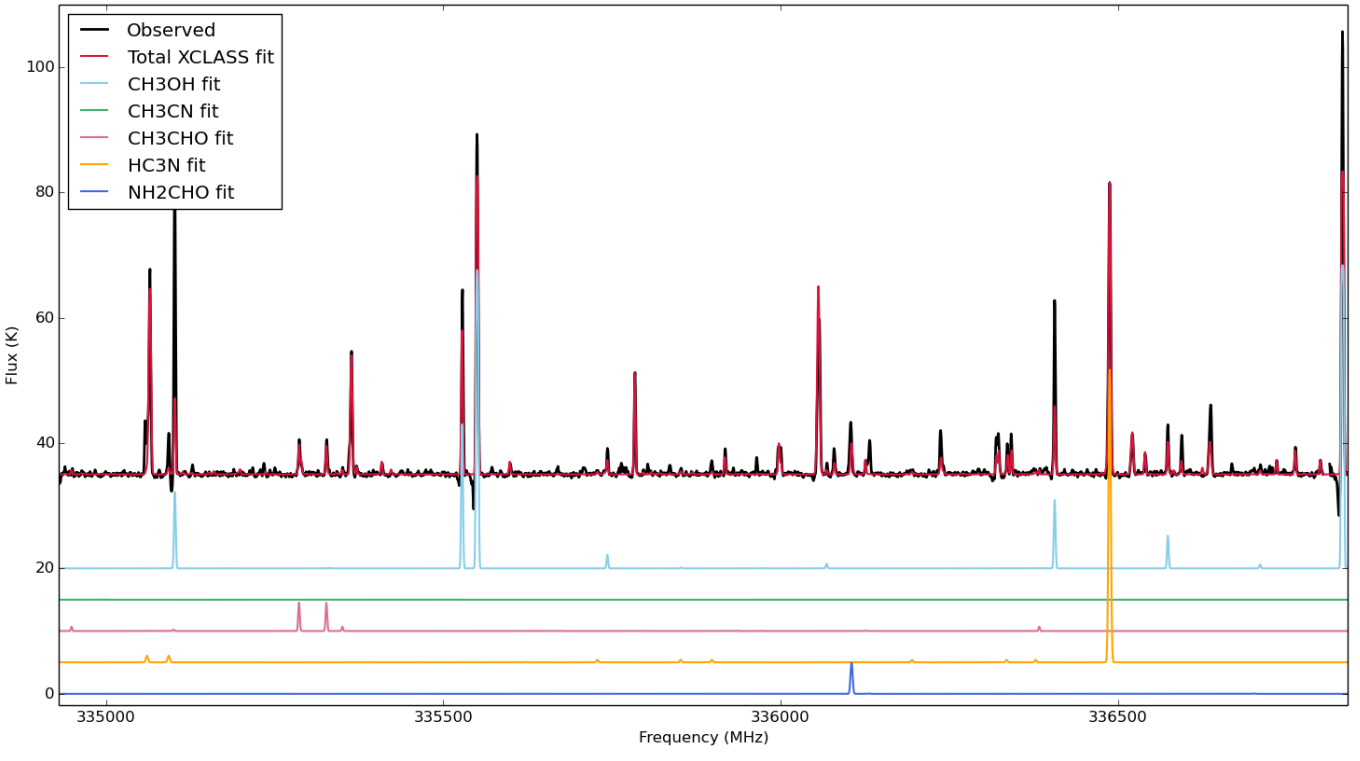

Figure 2.E.13: G35.20 peak B3 spectral window 1 (334.9-336.8 GHz), XCLASS total fit, plus selected species.

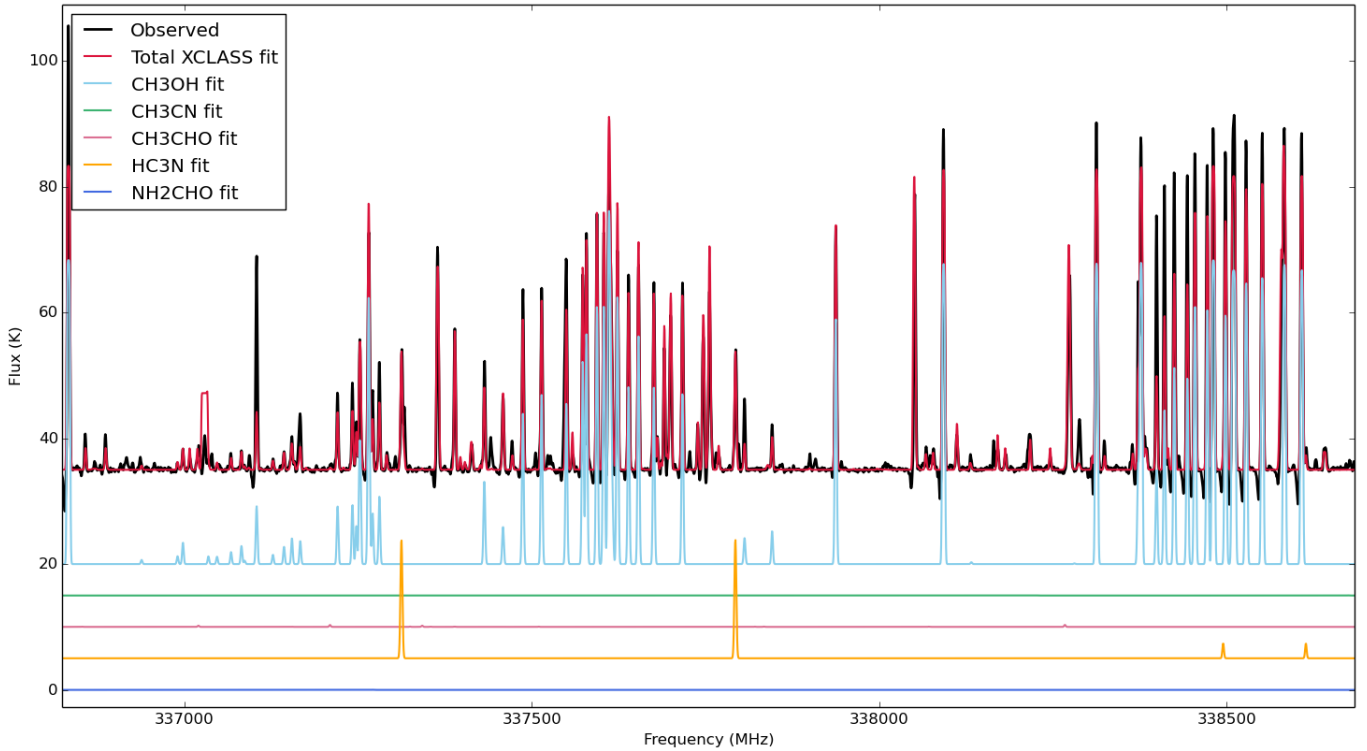

Figure 2.E.14: G35.20 peak B3 spectral window 0 (336.8-338.7 GHz), XCLASS total fit, plus selected species.

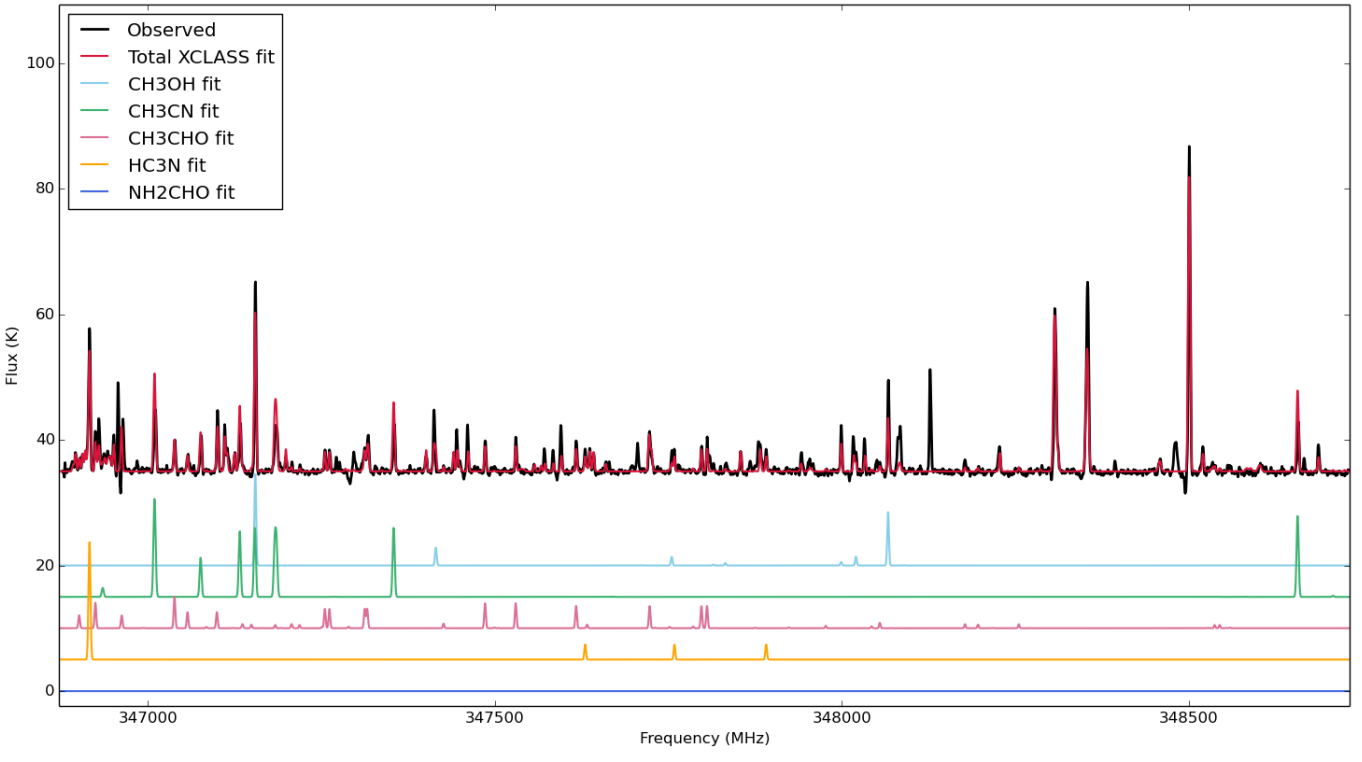

Figure 2.E.15: G35.20 peak B3 spectral window 3 (346.9-348.7 GHz), XCLASS total fit, plus selected species.

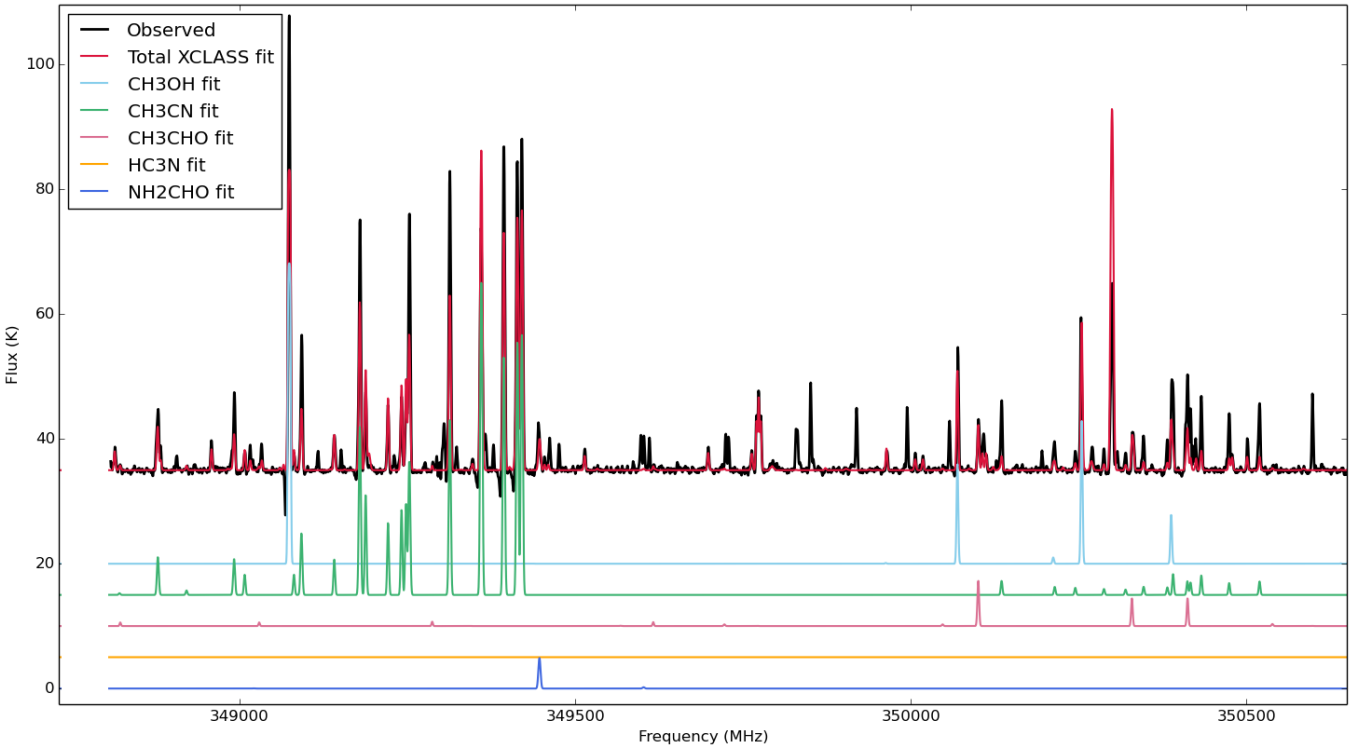

Figure 2.E.16: G35.20 peak B3 spectral window 2 (348.8-350.7 GHz), XCLASS total fit, plus selected species.

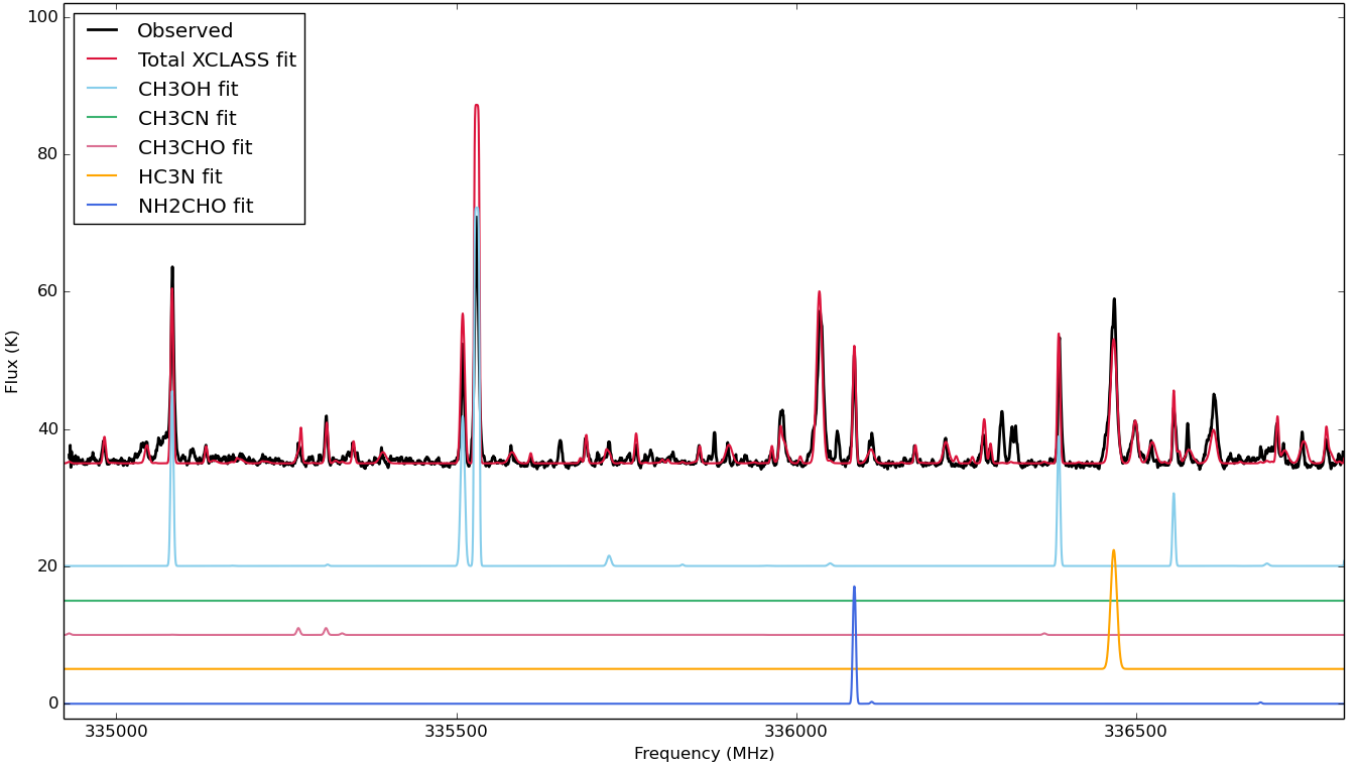

Figure 2.E.17: G3503 spectral window 1 (334.9-336.8 GHz), XCLASS total fit, plus selected species.

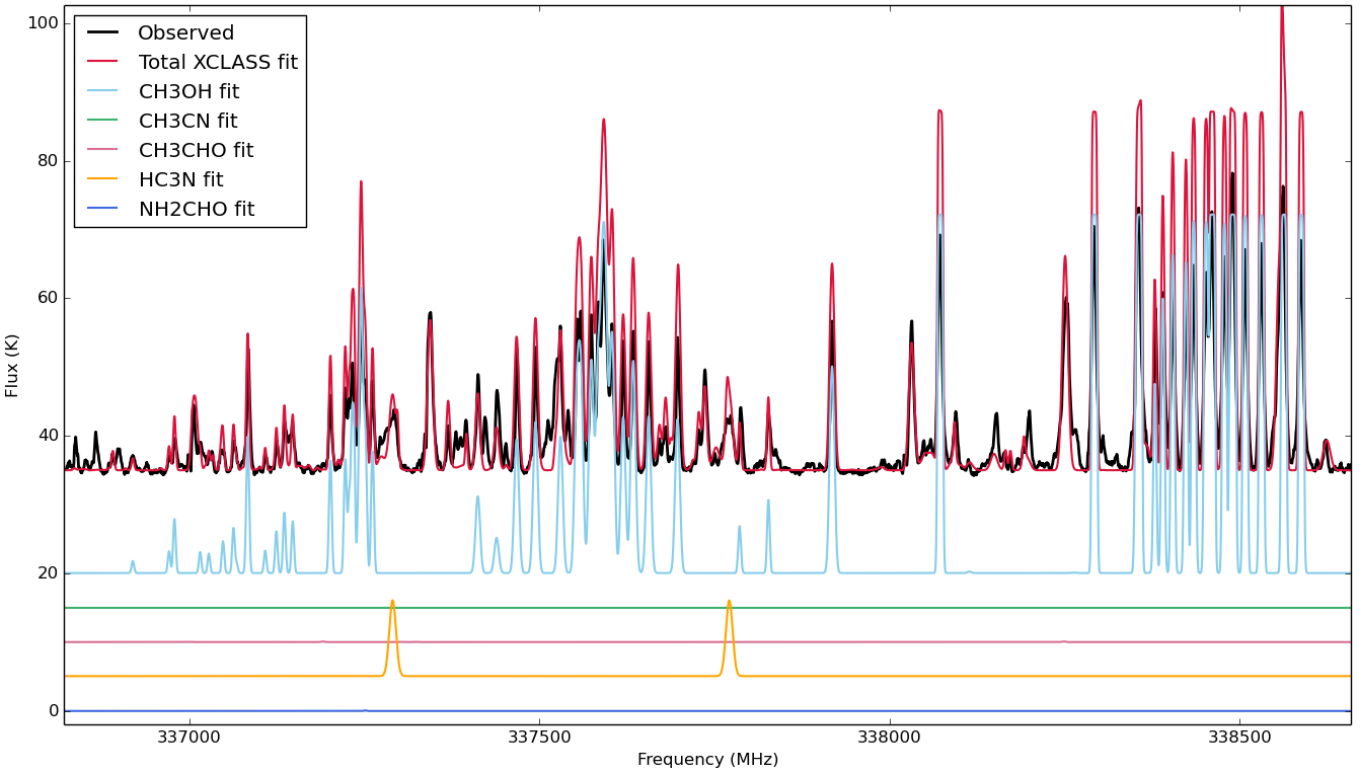

Figure 2.E.18: G3503 spectral window 0 (336.8-338.7 GHz), XCLASS total fit, plus selected species.

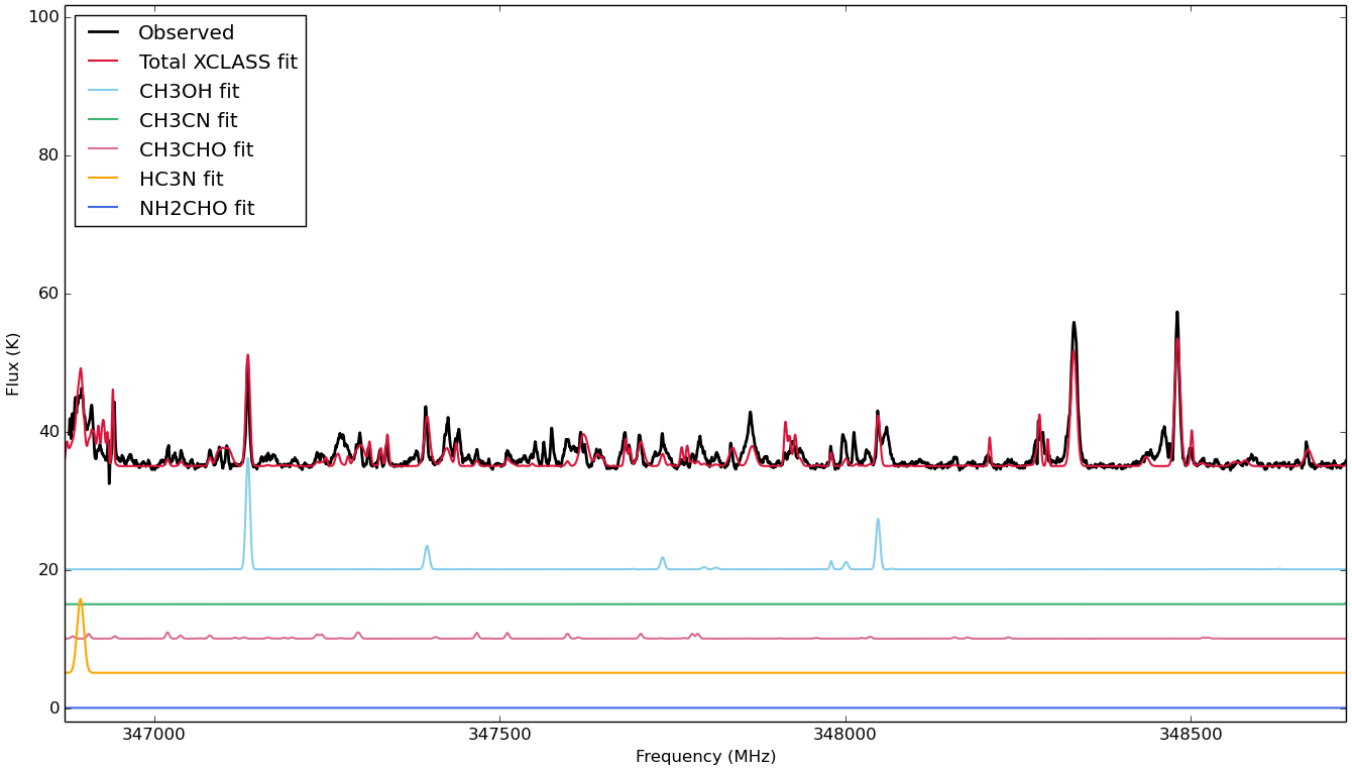

Figure 2.E.19: G3503 spectral window 0 (336.8-338.7 GHz), XCLASS total fit, plus selected species.

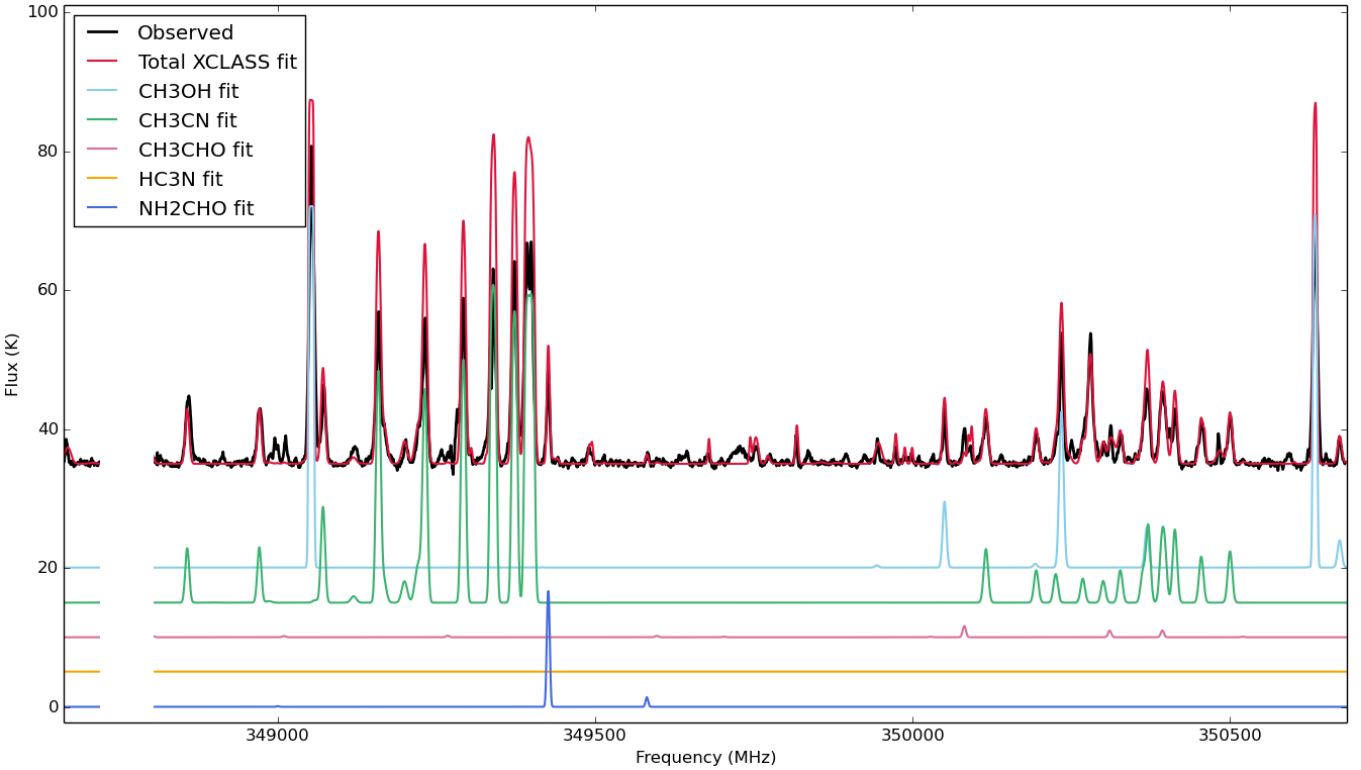

Figure 2.E.20: G35.03 spectral window 2 (348.8-350.7 GHz), XCLASS total fit, plus selected species.